

**University of Alberta**

**DESIGN AND OPTIMIZATION OF ANALOG AND DIGITAL IF FILTERS  
EMPLOYING A DIVERSITY CONTROLLED GENETIC ALGORITHM**

by

**Yifan Wu**



A thesis submitted to the Faculty of Graduate Studies and Research in partial fulfillment  
of the requirements for the degree of **Master of Science**.

Department of Electrical and Computer Engineering

Edmonton, Alberta

Fall 2008



Library and  
Archives Canada

Bibliothèque et  
Archives Canada

Published Heritage  
Branch

Direction du  
Patrimoine de l'édition

395 Wellington Street  
Ottawa ON K1A 0N4  
Canada

395, rue Wellington  
Ottawa ON K1A 0N4  
Canada

*Your file* *Votre référence*  
*ISBN: 978-0-494-47443-3*  
*Our file* *Notre référence*  
*ISBN: 978-0-494-47443-3*

**NOTICE:**

The author has granted a non-exclusive license allowing Library and Archives Canada to reproduce, publish, archive, preserve, conserve, communicate to the public by telecommunication or on the Internet, loan, distribute and sell theses worldwide, for commercial or non-commercial purposes, in microform, paper, electronic and/or any other formats.

The author retains copyright ownership and moral rights in this thesis. Neither the thesis nor substantial extracts from it may be printed or otherwise reproduced without the author's permission.

**AVIS:**

L'auteur a accordé une licence non exclusive permettant à la Bibliothèque et Archives Canada de reproduire, publier, archiver, sauvegarder, conserver, transmettre au public par télécommunication ou par l'Internet, prêter, distribuer et vendre des thèses partout dans le monde, à des fins commerciales ou autres, sur support microforme, papier, électronique et/ou autres formats.

L'auteur conserve la propriété du droit d'auteur et des droits moraux qui protègent cette thèse. Ni la thèse ni des extraits substantiels de celle-ci ne doivent être imprimés ou autrement reproduits sans son autorisation.

---

In compliance with the Canadian Privacy Act some supporting forms may have been removed from this thesis.

Conformément à la loi canadienne sur la protection de la vie privée, quelques formulaires secondaires ont été enlevés de cette thèse.

While these forms may be included in the document page count, their removal does not represent any loss of content from the thesis.

Bien que ces formulaires aient inclus dans la pagination, il n'y aura aucun contenu manquant.

  
**Canada**

# Abstract

Intermediate frequency (IF) filters find a variety of applications in modern communication systems. This thesis is concerned with the design and optimization of analog Operational Transconductance Amplifier-Capacitor and digital IF filters. Both designs are based on analog or digital realizations from analog passive filter circuits. The optimization is conducted by genetic algorithms (GAs). GAs represent IF filter by a bit-string chromosome and proceed from a population pool of candidate chromosomes to future generations in order to arrive at the desired IF filter satisfying the design specifications. In addition, diversity control has been employed to increase the diversity in the population pool and to avoid premature convergence. Moreover, a look-up table based approach is proposed to ensure that the digital IF filter offspring chromosomes are guaranteed BIBO stable. A fast convergence speed has been observed, which is an order of magnitude higher than that of the conventional GAs.

# Acknowledgements

The generous support and encouragement offered by Dr. Behrouz Nowrouzian has been most crucial in the successful completion of this thesis. I am deeply thankful to Dr. Nowrouzian for his patient advice and criticism during the period of my M.Sc studies. I would also like to thank Natural Sciences and Engineering Research Council of Canada (NSERC) under the Discovery Grant #A6715 to financially support this work.

Last but not the least, I would like to thank my parents for their support and love over my life. Without them, I would never have completed my study successfully.

# Contents

<b>1</b>	<b>Introduction</b>	<b>1</b>
<b>2</b>	<b>Overview of GA and DCGA Optimization Techniques</b>	<b>6</b>
2.1	Conventional GA Optimization Technique . . . . .	8
2.2	Improving Convergence Speed Based on DCGA . . . . .	11
2.3	Summary . . . . .	14
<b>3</b>	<b>Design and DCGA Optimization of OTA-C IF Filters</b>	<b>16</b>
3.1	Analog Filters . . . . .	16
3.2	Passive and Active Filters . . . . .	17
3.3	OTA-C Realization Technique . . . . .	20
3.3.1	Realization of resistor . . . . .	21
3.3.2	Realization of grounded inductor . . . . .	21
3.4	OTA-C Realization of the IF Filter . . . . .	23
3.4.1	OTA-C realization of the eighteenth-order IF filter . . . . .	23
3.4.2	OTA-C realization of a prototype sixth-order bandpass filter . . . . .	24
3.4.3	Stability of the OTA-C IF filter . . . . .	29
3.5	OTA-C IF Filter Optimization Employing DCGA . . . . .	30
3.6	Application Example . . . . .	34
3.7	Summary . . . . .	38
<b>4</b>	<b>Design and DCGA Optimization of Stable Digital IF filters Employing CSD</b>	

<b>Number Systems</b>	<b>40</b>
4.1 IIR and FIR Digital Filters . . . . .	40
4.2 Problem Associated with Direct Application of DCGA Optimization Technique . . . . .	42
4.3 Design of the Infinite-Precision Seed Digital IF Filter . . . . .	45
4.4 BIBO Stability Constraints for CSD Digital IF Filters . . . . .	51
4.5 Novel CSD LUTs for Guaranteed BIBO Stability . . . . .	55
4.6 Design Methodology for the Proposed DCGA Optimization . . . . .	57
4.6.1 Generation of the initial population pool . . . . .	57
4.6.2 Formation of the next generation population pool . . . . .	58
4.6.3 Fitness evaluation . . . . .	59
4.7 Application Examples . . . . .	59
4.7.1 Application example 1: . . . . .	59
4.7.2 Application example 2: . . . . .	61
4.8 Summary . . . . .	65
<b>5 Conclusion</b>	<b>74</b>
5.1 Conclusion . . . . .	74
5.2 Summary of Contributions . . . . .	75
5.3 Suggestions for Future Work . . . . .	77
<b>A Author's Contribution</b>	<b>78</b>
<b>B DCGA Optimization of FRM FIR Lowpass Digital Filters</b>	<b>80</b>
B.1 Overview of FRM FIR Lowpass Digital Filter Design Approach . . . . .	81
B.2 Design Methodology . . . . .	82
B.2.1 Generation of CSD LUT . . . . .	83
B.2.2 Generation of Initial Population Pool . . . . .	84
B.2.3 Formation of the Next Generation Population pool . . . . .	84
B.2.4 Fitness evaluation . . . . .	85

B.3 Application Example . . . . .	86
<b>C Generation of the Three LUTs</b>	<b>96</b>
<b>References</b>	<b>100</b>

# List of Tables

3.1	Numerator and Denominator Coefficients . . . . .	29
3.2	Back Transformed Passive Components . . . . .	31
3.3	Design Specifications for OTA-C IF Filter . . . . .	34
3.4	Initial Values of OTA-C IF Filter Transconductances [1] . . . . .	34
3.5	Optimized Transconductance Gains . . . . .	38
4.1	Infinite-Precision Multiplier Coefficients for $H_1(z)$ . . . . .	51
4.2	Infinite-Precision Multiplier Coefficients $H_2(z)$ . . . . .	52
4.3	Elements of Back-Transformed Series Arm Reactance $\hat{Z}_1(s)$ . . . . .	53
4.4	Elements of Back-Transformed Series Arm Reactance $\hat{Z}_2(s)$ . . . . .	54
4.5	Digital IF Filter Design Specifications for Example 1 . . . . .	69
4.6	Analog Element Values $C_{il_i}$ and $L_{il_i}$ for Example 1 . . . . .	69
4.7	Infinite-Precision Multiplier Coefficient Values for Example 1 . . . . .	70
4.8	Parameter values for Constructing the CSD LUTs for Example 1 . . . . .	70
4.9	Finite-Precision Multiplier Coefficient Values after DCGA Optimization for Example 1 . . . . .	71
4.10	Digital IF Filter Design Specifications for Application Example 2 . . . . .	71
4.11	Analog Element values $C_{il_i}$ and $L_{il_i}$ for Example 2 . . . . .	72
4.12	Infinite-Precision Multiplier Coefficient Values for Example 2 . . . . .	72
4.13	Parameter Values for LUTs in Example 2 . . . . .	72
4.14	Finite-Precision Multiplier Coefficient Values after DCGA for Example 2 . . . . .	73

B.1	Design Parameters for DCGA Optimization for FRM FIR Lowpass Digital Filter with a Passband Widths of $0.4\pi$ . . . . .	87
B.2	Additional Design Parameters for DCGA Optimization for FRM FIR Lowpass Digital Filter with a Passband Widths of $0.4\pi$ . . . . .	87

# List of Figures

1.1	Architecture of a Typical Superheterodyne Receiver . . . . .	2
2.1	Example of a Two-point Crossover Operation . . . . .	10
3.1	Simple Switched Capacitor Circuit Example . . . . .	19
3.2	Simple OTA Connection Example . . . . .	20
3.3	The Other OTA Connection Example . . . . .	21
3.4	OTA-C Reutilization of Grounded Resistor . . . . .	22
3.5	OTA-C Reutilization of Floating Resistor . . . . .	22
3.6	Equivalent VCCS Circuit of Grounded Inductor . . . . .	23
3.7	Realization of the Analog IF Filter By Cascading Three Identical Bandpass Filter $H_{A,BP}(s)$ Sections . . . . .	24
3.8	Sixth-Order Passive Bandpass Filter . . . . .	25
3.9	OTA-C Realization of the Floating/Grounded Resistors and Grounded In- ductors in Fig. 3.8 . . . . .	26
3.10	OTA-C Realization of the Floating Inductor and Capacitor in Fig. 3.8 . . .	27
3.11	OTA-C Realization of the Passive Bandpass Filter in Fig. 3.8 . . . . .	28
3.12	Back-transformed Passive Bandpass Filter Circuit . . . . .	30
3.13	OTA-C IF Filter Optimization Process Using DCGA . . . . .	32
3.14	OTA-C IF Filter Magnitude Frequency-Response Before DCGA . . . . .	35
3.15	Optimized OTA-C IF Filter Magnitude Frequency-Response after DCGA Application . . . . .	36
3.16	Optimized OTA-C IF Filter Group Delay after DCGA Application . . . . .	36

3.17	Convergence Speeds for Various $c$ -values . . . . .	37
3.18	Convergence Speeds for Various $\alpha$ -values . . . . .	37
4.1	Analog Prototype Reference Bandpass Filter Section . . . . .	47
4.2	Realization of the Reactance $Z_1(s)$ and $Z_2(s)$ . . . . .	47
4.3	Decomposition of $H(s)$ into $H_1(s)$ and $H_2(s)$ . . . . .	48
4.4	Realization of the Decomposed Transfer functions $H_i$ . . . . .	49
4.5	Bilinear-LDI Digital Realization of $H_1(s)$ . . . . .	49
4.6	Bilinear-LDI Digital Realization of $H_2(s)$ . . . . .	50
4.7	Bilinear-LDI Digital Realization of $H(s)$ . . . . .	50
4.8	Back-Transformed Analog Prototype Reference Bandpass Filter Section . .	53
4.9	Realization of Back-Transformed Reactance $\hat{Z}_1(s)$ and $\hat{Z}_2(s)$ . . . . .	62
4.10	Magnitude Frequency-Response of the Infinite-Precision Digital IF Filter in Example 1 . . . . .	62
4.11	Magnitude Frequency-Response of the Optimized Digital IF Filter for Ex- ample 1 . . . . .	63
4.12	Optimized Digital IF Filter Group Delay after DCGA Application in Ex- ample 1 . . . . .	63
4.13	Convergence Speeds for various $c$ -values in Example 1 . . . . .	64
4.14	Convergence Speeds for various $\alpha$ -values in Example 1 . . . . .	64
4.15	Magnitude Frequency-Response of the Infinite precision Digital IF Filter in Example 2 . . . . .	66
4.16	Magnitude Frequency-Response of the Optimized Digital IF Filter in Ex- ample 2 . . . . .	66
4.17	Optimized Digital IF Filter Group Delay after DCGA Application in Ex- ample 2 . . . . .	67
4.18	Convergence Speeds with various $c$ -values in Example 2 . . . . .	67
4.19	Convergence Speeds with various $\alpha$ -values in Example 2 . . . . .	73
B.1	Realization of an FIR Lowpass Digital Filter using the FRM Approach . . .	89

B.2	Magnitude Frequency-Response of the Bandedge-Shaping Digital Subfilter $H_a(e^{j\omega})$ . . . . .	89
B.3	Magnitude Frequency-Response of the Complementary Bandedge-Shaping Digital Subfilter $H_b(e^{j\omega})$ . . . . .	90
B.4	Magnitude Frequency-Response of $L$ -Interpolated Bandedge-Shaping Digital Subfilter $H_a(e^{jL\omega})$ . . . . .	90
B.5	Magnitude Frequency-Response of $L$ -Interpolated Complementary Bandedge-Shaping Digital Subfilter $H_b(e^{jL\omega})$ . . . . .	91
B.6	Magnitude Frequency-Response of Lowpass Masking Digital Subfilter $H_{ma}(e^{j\omega})$	91
B.7	Magnitude Frequency-Response of Lowpass Masking Digital Subfilter $H_{mb}(e^{j\omega})$	92
B.8	Magnitude Frequency-Response of Infinite-Precision FRM FIR Lowpass Digital Filter . . . . .	92
B.9	Magnitude Frequency-Response of FRM FIR Lowpass Digital Filter after Multiplier Coefficients Quantization . . . . .	93
B.10	Magnitude Frequency-Response of CSD FRM FIR Lowpass Digital Filter after DCGA Optimization . . . . .	93
B.11	Passband Magnitude Frequency-Response of CSD FRM FIR Lowpass Digital Filter after DCGA Optimization . . . . .	94
B.12	DCGA Convergence Speeds for FRM FIR Lowpass Digital Filter for Varying Values of the Shaping Parameter $c$ . . . . .	94
B.13	DCGA Convergence Speeds for FRM FIR Lowpass Digital Filter for Varying Values of the Exponent Parameter $\alpha$ . . . . .	95
C.1	Example of Possible Values for Multipliers $\hat{m}_{11}$ and $\hat{m}_{12}$ . . . . .	99

# Acronyms

<b>Acronyms</b>	<b>Definition</b>
AM	Amplitude Modulation
AMPS	American Mobile Telephone System
BIBO	Bounded-input Bounded-output
CDMA	Coded Division Multiple Access
CPSS	Cross Generational Probability Survival Selection
CSD	Canonical Signed Digit
DCGA	Diversity Controlled Genetic Algorithm
FIR	Finite Impulse Response
FM	Frequency Modulation
FRM	Frequency Response Masking
GA	Genetic Algorithm
IF	Intermediate Frequency
IIR	Infinite Impulse Response
LUT	Look-up Table
OTA-C	Operational Transconductance Amplifier-Capacitor
PLL	Phase Locked Loop
SA	Simulated Annealing
SPT	Signed Power of Two
VFO	Variable Frequency Oscillator

# List of Symbols

<b>Symbol</b>	<b>Definition</b>
$\alpha$	DCGA exponent coefficient
$\varepsilon$	Finite precision slack variable
$\varepsilon_p$	Maximum error in the passband
$\varepsilon_s$	Maximum error in the stopband
$\varepsilon_t$	Maximum error in the transition band
$\Omega_p$	Passband frequency points
$\Omega_s$	Stopband frequency points
$\Omega_t$	Transition band frequency points
$b_\zeta$	Block of bits in the chromosome
$c$	DCGA shape coefficient
$C_{OTA}$	Operational transconductance amplifier capacitance
$C_{sc}$	Switched capacitor capacitance
$f_{clock}$	Clock frequency of switched capacitor
$fitness$	Fitness value of a chromosome
$fitness_1$	Fitness value of a chromosome without a penalty component
$fitness_2$	Fitness value of a chromosome with a penalty component
$g_m$	Operational transconductance amplifier transconductances
$h$	Hamming distance between two chromosomes
$H(s)$	Sixth-order digital prototype passive RLC bandpass filter transfer function
$H(z)$	Sixth-order digital bandpass filter transfer function

$H_A(s)$	Analog IF filter transfer function
$H_{A,BP}(s)$	Sixth-order analog prototype passive RLC bandpass filter transfer function
$H_a(z)$	Band-edge shaping digital sub-filter
$H_a(z^L)$	L interpolated band-edge shaping digital sub-filter
$H_{am}(z)$	Lowpass masking digital sub-filter for $H_a(z^L)$
$H_b(z)$	Complementary band-edge shaping digital sub-filter
$H_b(z^L)$	L interpolated complementary band-edge shaping digital sub-filter
$H_{bm}(z)$	Lowpass masking digital sub-filter for $H_b(z^L)$
$H_D(z)$	Digital IF filter transfer function
$H_F(z)$	Lowpass FRM FIR digital filter
$H_i(s)$	Decomposed analog bandpass filter transfer function
$H_i(z)$	Decomposed digital bandpass filter transfer function
$I_{OTA}$	Operational transconductance amplifier current
$L$	Chromosome length
$L_g$	Ground inductor
$m_{ik_i}$	Infinite-precision digital IF filter multiplier coefficients
$\hat{m}_{ik_i}$	Finite precision digital IF filter multiplier coefficients in CSD format
$N$	Population pool size
$N_{mating}$	Number of chromosomes in mating pool
$P$	Total number of stopband penalty points
$\hat{P}(t)$	Enlarged population pool
$p_F$	Fixed probability for complementing bits in the chromosome
$p_s$	Probability of selecting a chromosome
$P(t)$	Current population pool
$P(t+1)$	Next generation population pool
$R_f$	Floating source resistor
$R_g$	Ground resistor
$s$	Continuous time complex frequency variable
$T$	Sampling period

$V_{OTA}$	Operational transconductance amplifier input voltage
$V_{OTA,1}$	Operational transconductance amplifier output voltage
$V_{OTA,2}$	Operational transconductance amplifier output voltage connected in reverse order
$W$	Finite-precision digital IF filter multiplier coefficient wordlength
$w$	Maximum number of non-zero digits in CSD digital IF filter multiplier coefficient
$W_F$	CSD multiplier coefficient fractional part wordlength
$W_I$	CSD multiplier coefficient integer part wordlength
$W_p$	Passband weighting factor
$W_s$	Stopband weighting factor
$W_t$	Transition band weighting factor
$z$	Discrete time complex frequency variable
$Z_1(s)$	Series arm reactance
$Z_2(s)$	Lattice arm reactance

# Chapter 1

## Introduction

Intermediate frequency (IF) filters are applied widely in the superheterodyne receivers in modern communication systems. The linear-phase wide-passband IF filters are used extensively in radio and television broadcast networks, American Mobile Telephone System (IS-54) (AMPS) [2] cellular communications and other wireless digital communication systems such as CDMA (IS-95) [3].

The architecture of a typical superheterodyne receiver is as shown in Fig. 1.1. The RF signal at variable frequency  $f_s$  received from the antenna is usually first passed through a lowpass filter to reduce the interference introduced from other stations. Before any further detection, the incoming signal is converted to IF signal. This is achieved by mixing the incoming signal with a signal of frequency  $f_{LO}$  generated from a local oscillator. Then, this IF signal is passed through a sharp bandpass filter with a central frequency of  $f_{IF}$ , which is called the IF filter. The IF filters are required to satisfy strict frequency-selective bandpass magnitude frequency-response characteristics so that only those RF signals with  $f_{IF} = |f_s - f_{LO}|$  could pass through. Therefore, the IF filter allows to select the signal from desired channel while attenuating the signal associated with all the other unwanted channels. It should be pointed out that the local oscillators in most superheterodyne receivers are usually widely tunable devices, such as a variable frequency oscillator (VFO) to allow tuning at different frequency stations. Finally, the signal is demodulated by a detector and

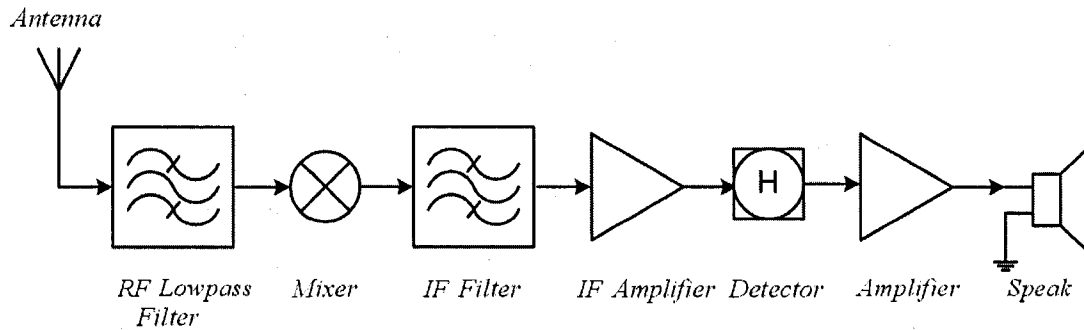


Fig. 1.1. Architecture of a Typical Superheterodyne Receiver

amplified to the speaker [4].

The superheterodyne receivers implemented with the IF filter is well known for the following advantages:

- It reduces the signal from very high frequencies to low frequencies. For example, in amplitude modulation (AM) receivers, the IF frequency is usually 455 kHz, for frequency modulation (FM) receivers, it is usually 10.7 MHz and for televisions, it is 45 MHz [4]. Consequently, lower frequency components can be used in the receiver which brings the cost of the equipment down as opposed to using high frequency components.
- Superheterodyne receivers have superior advantages in frequency stability and sensitivity to reject the incoming signal's sidebands and allow for single signal reception. Compared to the alternative design of a tuneable filter, the tuneable oscillator in the superheterodyne receiver is much easier to stabilize, especially with modern frequency synthesizer technology [5].
- Frequency selecting of different channels can be made very flexible by simply varying the local oscillator frequency  $f_{LO}$  to pick up the desired signal and isolate the unwanted stations.

The key component in the superheterodyne receiver is to realize the stringent bandpass IF filter frequency-response transfer function, which in practical circumstances, can be

realized in hardware by a combination of analog operational transconductance amplifiers (OTAs) and capacitors (Cs). For example, in [2], an eighteenth-order low noise IF filter for AMPS cellular phone applications is presented. The filter is based on three identical leapfrog stages each implemented by 13 OTAs. In addition, IF filters can also be implemented as digital filters using digital multipliers and adders as an alternative to the analog counterpart. For example, in [6], a twelfth-order digital IF filter is presented based on the wave digital filter technique.

The salient feature of the digital IF filters is that they can be integrated with other parts of the overall communication system on the same chip based on the emerging CMOS hardware implementation technologies. Moreover, they permit high yields, involve small chip areas, and entail lower power consumptions as compared to the corresponding systems incorporating analog IF filters [6]. However, the digital IF filters require the use of Analog-to-Digital (A/D) and Digital-to-Analog (D/A) converters, which introduces additional hardware and implementation costs. Therefore, depending on the application purposes, whether it is intended to deal with analog or digital signals, different realization approaches of the IF filters can be applied.

In both the OTA-C analog and digital (based on multipliers and adders) realization of IF filters, one has to determine the proper values of OTA transconductances or the multiplier coefficients in order to satisfy the required magnitude frequency-response specifications. This can be achieved by the existing conventional gradient-based optimization approaches or by using the evolutionary computing algorithms such as the genetic algorithms (GAs).

It is well known that GAs provide a promising approach to discrete optimization problems due to the fact that they are capable of automatically finding near optimum solutions while keeping the computational complexity of the optimization moderately low [7].

Recently, GAs have emerged as an efficient alternative for the optimization of finite impulse response (FIR) and infinite impulse response (IIR) digital filters [8]. These algorithms encode the digital filter properly into a chromosome, and proceed towards an optimal solution through the evolution of a population of potential candidate chromosomes from one generation to the next. However, it is well known that the conventional GAs do not search

the solution space robustly since they lack mechanisms through which entrapment at local optima can be successfully avoided [9]. It was demonstrated in [10] that diversity control (DC) can be applied to help to improve the convergence speed of the conventional GAs. The main principle behind DCGAs is to increase the diversity of the population pool through the incorporation of additional non-elite chromosomes as chosen based on a pair of external control parameters. It is shown in [9] that DCGAs are capable of increasing the convergence speeds of conventional GAs around an order of magnitude.

This thesis is concerned with the design and optimization of analog and digital IF filters using DCGA optimization technique. The optimization parameters are the OTA transconductances for analog IF filters and the multiplier coefficient values for the digital filters. Both of those parameters are first approximately determined as infinite-precision quantities using either conventional gradient-based optimization techniques or from the existing literature and filter design handbooks. It is important to point out that due to subsequent DCGA optimization, the infinite-precision parameters are expected to satisfy the given magnitude frequency-response design specifications only approximately [11].

The parameters are subsequently quantized and converted into binary-strings so that they can be concatenated to represent the IF filter as a chromosome. The optimization process begins with combining a number of candidate chromosomes together to form a population pool. Then, by using GA reproduction (e.g. crossover and mutation) operations, the chromosomes in the current population pool are manipulated to produce their offspring. Both the parents and their offspring are evaluated and ranked based on their fitness values (i.e. the degree to which they satisfy the design specifications). Next, the constituent chromosomes are chosen based on DCGA selection schemes to form the next generation population pool. DCGA optimization proceeds from one generation to the next, ending up with the best performing chromosome (i.e. the chromosome with the highest rank), which represents the desired IF filter.

The remainder of this thesis is organized as follows: Chapter 2 gives an overview of GA and DCGA optimization techniques. GA is a very effective optimization technique that searches for the optimal solution in parallel directions and DCGA can further be applied to

improve the convergence speed of conventional GA by an order of magnitude.

Chapter 3 is concerned with the design and DCGA optimization of analog IF filters. The realization of the analog IF filter is based on the replacement of analog resistors and inductors by OTAs and capacitors from a doubly resistivity terminated passive RLC band-pass circuit. The salient feature of the resulting OTA-C IF filter is that it is an automatically bounded-input bounded-output (BIBO) stable filter regardless of the OTA transconductances values. The proposed approach is illustrated through its application to the optimization of an OTA-C IF filter consisting of 39 OTAs for operation around a center frequency at 455 kHz.

Chapter 4 presents the design and DCGA optimization of stable digital IF filters employing Canonical Signed Digit (CSD) number systems. This optimization technique exploits the bilinear-LDI lattice digital filter design approach for the realization of the required initial infinite-precision seed digital IF filter chromosome. However, a direct application of DCGA technique to the digital IF filters may give rise to two separate problems. One is that the operations of crossover and mutation in the course of DCGA optimization may produce chromosomes which no longer conform to the CSD number format. The other is that DCGA optimization may produce a solution chromosome which may lead to a digital IIR IF filter that is not BIBO stable. A look-up table (LUT) based approach has been proposed to circumvent the above two problems by using the indices of the resulting multiplier coefficient in the LUTs as opposed to their values to represent digital IF filter chromosomes for DCGA optimization. The chapter presents the application of the proposed DCGA optimization to the design of a pair of digital IF filters for two different design specifications. Finally, Chapter 5 summarizes the entire thesis and draws a conclusion.

## Chapter 2

### Overview of GA and DCGA

### Optimization Techniques

This chapter is an detailed overview of GA and DCGA optimization techniques for discrete optimization of analog and digital IF filters. Broadly speaking, there are two different optimization approaches available for this purpose, one approach is based on the conventional gradient-based optimization techniques, while the other is based on the evolutionary optimization algorithms.

The gradient-based optimization techniques are applied to solve continuous optimization problems (where the optimization parameters are continuous variables) based on the gradient of the objective function for guiding the direction of search (e.g. the Newton's method). However, when the objective function has many local optimal points (usually defined as multimodal problems), such optimization techniques lack the mechanism to progress further from the first found local optimal point to the global optimal solution [12].

On the other hand, if the derivative of the objective function cannot be computed, which is the case for most optimization problems (when the optimization variables are discrete), one has to use evolutionary optimization techniques, e.g. GAs. GAs take the inspiration from natural selection and survival of the fittest in the biological world. Their main difference from the traditional gradient-based optimizations technique is that they involve a par-

allel search from a population of candidate solutions, rather than from a single candidate. It is well known that GAs are very efficient in solving complex multimodal optimization problems.

For example in [13], a nonlinear programming approach was developed for the optimization of FRM FIR digital filters over the SPT multiplier coefficients space. In [14], GAs were applied to the same FRM FIR digital filter optimization problem, leading to FIR digital filters with superior magnitude frequency-response characteristics. In addition, it was shown that the use of GAs overcomes the inherent drawback of the hitherto linear programming techniques which require the separate optimization of the constituent FIR digital sub-filters.

There are other discrete optimization techniques but they do not have the wide scope of applications as GAs. Simulated annealing (SA), for example, is another discrete optimization technique which starts from a random point in the search space. In SA, the search is made by a random move from the starting point. If the move leads to a better result, it is accepted (considered as a positive move). However, if it leads to a worse result (considered as a negative move), it is accepted only with a probability. This probability begins close to 1, but gradually reduces towards 0. In other words, initially in SA, any move is accepted, but as the optimization goes on, the probability of accepting a negative move is lowered. The reason for accepting negative moves is that they are sometimes essentially the key for escaping from the local optimal. However, too many negative moves will obviously lead the optimization away from the best solution [12].

As opposed to GA, where the search is performed by a number of candidate solutions at a time, SA only deals with one candidate at a time, and therefore does not build up an overall picture of the search space. In this way, SA can only be applied to very complicated problems when the use of GA is not possible because parallel search increases the computation and time complexity beyond reasonable limits.

## 2.1 Conventional GA Optimization Technique

GA was first introduced in books by Fraser and Burnell [7] in the 1970s and became popular from then on. GA is an optimization technique based on the natural selection and reproduction process that simulates the process of biological evolution. GAs have been successfully applied to find optimal solutions to discrete optimization problems by simultaneously searching along all directions in the search space. In general, GAs are proceeded in the following steps:

- Initialization: A seed chromosome is formed by concatenating the design parameters converted into bit-strings. Subsequently, an initial population pool consisting of  $N$  chromosomes is generated by randomly complementing bits of the seed chromosome [15].
- Evaluation: Each chromosome in the population pool is evaluated based on a particular fitness function which represents the degree to which the design specifications are satisfied. Subsequently, the chromosomes in the pool are ranked based on the values of their fitness [15].
- Generation of mating pool: In order to produce future generations, a mating pool is constructed by selecting  $N_{mating}$  ( $N_{mating} \leq N$ ) chromosomes from the population pool based on some stochastic functions after ranking the chromosomes in the population pool in accordance with their fitness values. The stochastic functions applied usually have a tendency in which the chromosome with a higher fitness value is more likely to be selected. However, it is both necessary and sufficient to include a few non-elite chromosomes (chromosomes with low fitness values) to increase diversity in the mating pool. In this way, the offspring of a non-elite chromosome and an elite one may outperform its parents. One example of the stochastic function used in [16] is based on the following Bernoulli distribution :

$$p(x) = t^{1-x}Z^x \quad (2.1)$$

where

$$t = \left(\frac{Z^N}{0.001}\right)^{1/(N-1)} \quad (2.2)$$

where  $Z$  has a fixed value of 0.8, and  $x$  represents the fitness rank of the particular chromosome in the population pool. This chromosome will be selected to be a member in the mating pool if  $p(x)$  is greater than a uniformly generated random number.

- Parent selection:  $N/2$  pairs of parents are selected from the mating pool to generate offspring by using the conventional roulette wheel selection or the correlative roulette wheel selection method [16].
- Formation of next generation population pool: The next generation population pool of total size  $N$  chromosomes is formed by:
  - Crossover operation: The  $N/2$  parent chromosome pairs in the mating pool undergo a two-point crossover operation, producing two offspring per parent pair. An example of a typical two-point crossover operation is as shown in Fig. 2.1. The resulting  $N$  chromosomes will become members of the next generation population pool after mutation operation.
  - Mutation operation: The  $N$  offspring undergo mutation operation, where mutation involves a very small probability that an arbitrary bit in the chromosome will be flipped (either from '0' to '1', or from '1' to '0').

The crossover operation generates a new chromosome which typically shares many of the desirable characteristics of its parents, and the mutation operation will explore entirely new searching areas, increasing the diversity of the population pool. Consequently, the next generation population pool is expected to have an average fitness value usually greater than the current generation since only the best solutions from the current generation are selected for reproduction (along with a small proportion of less fit members).

- Termination: The above process is repeated from the initial generation of the population pool to the next generation until a pre-specified termination condition is met.

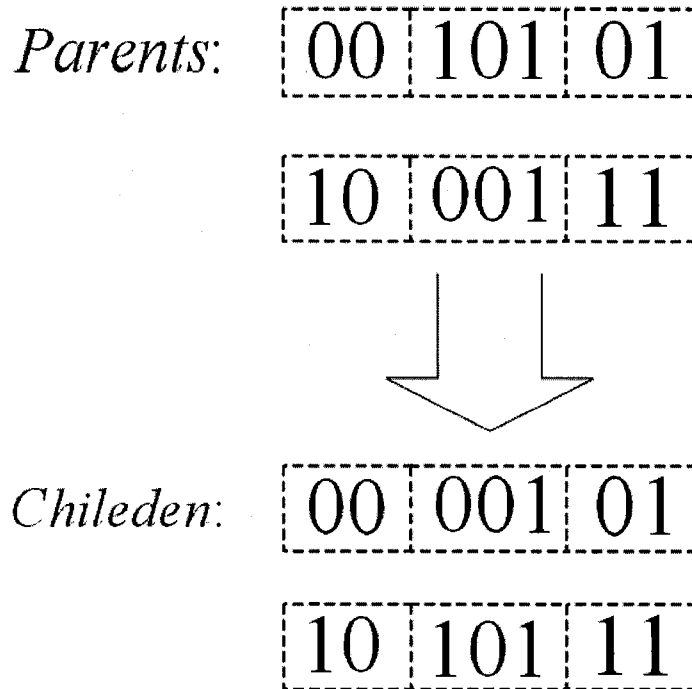


Fig. 2.1. Example of a Two-point Crossover Operation

This condition is either that the required design specifications are met or that the maximum number of iterations is reached where further generations of the population pool do not produce any better results [8].

The main advantages of GAs over the conventional optimization techniques are [15]:

- GAs manipulate the design variables at the bit level as opposed to a direct manipulation of the variables themselves.
- GAs can perform a parallel search using a population pool of potential candidate chromosomes, making them very efficient in finding optimum solutions to complex, multimodal optimization problems.
- GAs do not require any gradient information to perform the optimization.

Despite the above advantages of GAs, they are also well known to suffer from low convergence speed problems (usually called premature convergence), rendering them in-

efficient. This is because a few comparatively highly fit (but not globally optimal chromosomes) may rapidly dominate the population pool, causing GA to converge to a local maximum point. As a result, there will be a rapid decline in diversity of the population pool from one generation to the next, making the future generations very similar and curtailing the ability of GAs to continue to search for better solutions. Therefore, GAs usually have a tendency to get stuck at local optima points (instead of reaching the global optimum solution), resulting in a slow convergence.

## **2.2 Improving Convergence Speed Based on DCGA**

It is observed that the reason for quick decline in diversity in the population pool of conventional GA is because a small group of better performing individuals usually produce multiple offspring. On the other hand, other chromosomes with lower fitness values contribute less or even no offspring at all. Therefore, a dominant local optimum chromosome can increase rapidly and eventually dominate the population [10].

There have been many methods developed to improve the diversity of GAs, based on using a different fitness function, increasing the rate of mutation, or using selection techniques that maintain a diverse population pool. For instance, Srinivas [17] proposed the use of adaptive probabilities for crossover and mutation to maintain the diversity of the GA, where the probabilities of crossover and mutation are varied depending on the variation of the fitness values. [18] introduced simulate annealing (SA) to prevent GA from premature convergence. The overall optimization process is based on GA; however, SA comes into play by randomly flipping bits of the best performing chromosome when consecutive generations of the GA have the same best performing chromosome. Shimodaira [10] proposed DCGA where a cross generational probability survival selection (CPSS) scheme is used to choose candidate chromosomes for the next generation to successfully explore the solution space, and escape away from local optimum points.

Among all the methods proposed, DCGA technique is proven to strike a good balance between maintaining a diverse population pool among GA and reasonable time complexity.

The steps of DCGA are listed as follows [8]:

- In DCGA, the members of a current population pool  $P(t)$  of size  $N$  and their offspring chromosomes (obtained from crossover and mutation at a constant rate) are combined to form an enlarged population pool  $\hat{P}(t)$  of  $2N$  chromosomes, where  $t$  represents the generation number (initially  $t = 0$ ).
- The chromosomes in the enlarged population pool  $\hat{P}(t)$  are ranked by evaluating their fitness values. In addition, duplicate chromosomes in  $\hat{P}(t)$  are eliminated.
- The best chromosome in  $\hat{P}(t)$  is allowed to be a member of the next-generation population pool  $P(t + 1)$ .
- The remaining  $N - 1$  chromosomes in the population pool  $P(t + 1)$  are selected from the enlarged population pool  $\hat{P}(t)$  based on the following CPSS probability relation

$$p_s = [(1 - c)h/L + c]^\alpha \quad (2.3)$$

where  $h$  represents the hamming distance (i.e. the number of bit locations at which a given chromosome is different from the other chromosome)<sup>1</sup> between a candidate chromosome and the best chromosome in  $\hat{P}(t)$ ,  $L$  represents the bit-length of the individual chromosomes, and  $c$  and  $\alpha$  denote the shape coefficient and the exponent parameter, respectively. In this way, the selected chromosome is chosen as a candidate for the next generation population pool if  $p_s$  is greater than a locally generated uniform random number. It should be pointed out that according to Eqn. 2.3, chromosomes with a large hamming distance from the chromosome with the best fitness value will have a large chance to be selected to be members for the next generation. In other words, the more similar the structure of one chromosome is compared to the best fit one, the less the chance it will be selected.

---

<sup>1</sup>If two binary sequences of the same length differ in  $k$  places, the hamming distance between the two is  $k$ , e.g. the hamming distance between 000 and 010 is 1, the hamming distance between 0011 and 1100 is 4.

- The CPSS scheme is repeated until  $N$  chromosomes are identified for the next generation population pool  $P(t + 1)$ . However, in situations when CPSS leads to less than  $N$  chromosomes, the remaining chromosomes are formed by randomly complementing bits in the chromosome with the highest fitness value.

It should be pointed out that there are no analytical solutions available for selecting the shape coefficient  $c$  and the exponent parameter  $\alpha$ . Therefore, the values of these parameters must be selected empirically. The speed of convergence to an optimal solution is, in general, a function of both  $c$  and  $\alpha$  values. Therefore, empirical investigation is best conducted over a range of values for  $c$  and  $\alpha$  to identify the corresponding rapid convergence values. The appropriate values have to be explored by trial and error according to the optimization problem at hand [8].

The DCGA technique is considered of having the following advantages compared to the conventional GAs and other methods in [17, 18]:

- The chromosome with the best fitness value will always become the member of the next generation population pool. Thus, in the cases where it is in the region containing the global optimum solution, the global optimization result can be easily explored within only a few iterations. In the conventional GAs, however, crossover and mutation may have the side effect of destroying the chromosome with the highest fitness value.
- In cases where the chromosome with the best fitness value is in the region containing a local optimum, further offspring of this chromosome will result in premature convergence in GAs. In DCGA, on the other hand, since selection probability is based on the hamming distance of a chromosome from the best fit one, the offspring of the best fitness value is less likely to be similar to itself and thus the problem of getting trapped at local optimum points can successfully be avoided [10].
- On the other hand, chromosomes with low fitness values have a high chance to survive. Obviously such chromosomes have a large hamming distances to the chromo-

some with the highest fitness value, giving them the opportunity to produce offspring with a fitness values near the global optimum solution.

- By choosing the values of  $c$  and  $\alpha$  appropriately, DCGAs permit the desired external control of the diversity in the population pool for rapid convergence to an optimal solution. Through empirical investigations, it has been observed that if the fitness function has a few local optima only, then by using a high value of  $c$  and/or a small value of  $\alpha$ , one can achieve a rapid convergence to an optimal solution. On the other hand, when the fitness function is multimodal, lower values of  $c$  and/or higher values of  $\alpha$  can be chosen to increase the probability of selecting chromosomes which are different from the chromosome with the highest fitness value [8].
- The amount of computations in DCGA and conventional GAs are almost the same. On the other hand, the computational time of DCGA is much less than the that of the joint optimization technique employing SA in [18] and the variable crossover and mutation rate method in [17].

By comparing DCGA to the corresponding conventional GA for the optimization of bandpass frequency response-masking (FRM) FIR digital filters (see further discussions in the Appendix), it has been observed that DCGA leads to convergence speeds which are around an order of magnitude higher than those of the conventional GA. For example, by using the conventional GA, it took 1000 generations to arrive at a bandpass FRM FIR digital filter, whereas the proposed DCGA took only 144 generations for satisfying the same design specifications [15].

## 2.3 Summary

This chapter is concerned with two discrete evolutionary optimization techniques, GA and DCGA. GA is an effective discrete optimization technique that simulates the process of natural selection and biological evolution. It performs a parallel search using a population pool of potential candidate solutions to find optimal solutions (from one generation to the

next). However, GA is well known for suffering from premature convergence problems. They usually have a high tendency to converge towards a local optimal point (rather than the global optimal) because of the rapid decline in diversity of the population pool from one generation to the next.

DCGA, on the other hand, has been proposed recently that employs diversity control to increase the convergence speed of GA. The reason for using DCGA is because it has the advantage of increasing the diversity of the population pool through the incorporation of additional non-elite chromosomes. Those non-elite ones are chosen based on their hamming distances from the chromosome with the best fitness value. It is observed that DCGA increases the convergence speed of GA by an order of magnitude.

## **Chapter 3**

# **Design and DCGA Optimization of OTA-C IF Filters**

In chapter 2, it was discussed how GAs can be applied to solve complex and discontinues multimodal optimization problems, and how DC can be employed to increase the convergence speed of conventional GAs (usually by an order of magnitude). In this chapter, DCGA is applied to optimize the magnitude frequency-response of OTA-C IF filters with the optimization parameters being the transconductance gains of the constituent OTAs. The capacitors in OTA-C IF filters are usually assigned fixed values throughout the course of optimization [19].

### **3.1 Analog Filters**

Filters are electrical/electronic devices that are designed to manipulate the spectrum of signals in the frequency domain. They are used in particular to attenuate the unwanted frequency components (in the stopband region of the filter) and to amplify the wanted frequency components (in the passband region of the filter). Basically, one can distinguish between five different categories of filters based on their frequency-response characteristics as follows [15]:

- **Lowpass filters:** Filters that pass only low frequency components of the signal but attenuate high frequency components.
- **Highpass filters:** Filters that operate in the opposite way compared to lowpass filters, by passing only high frequency components and attenuating low frequency components.
- **Bandpass filters:** Filters that only allow frequency components between two pre-specified intermediate frequency points to pass through and attenuate the remaining frequency components.
- **Bandstop filters:** Filters that operate in the opposite way compared to bandpass filters, by attenuating frequency components between two pre-specified intermediate frequency points and passing all the remaining frequency components.
- **Allpass filters:** Filters that pass all frequency components equally, but may change the phase of various frequency components.

Depending on the type of input signals, filters can be broadly categorized as analog filters and digital filters. Analog filters deal with input signals that are continuous-time infinite precision quantities such as a voltage or a current, whereas digital filters deal with signals which are discrete-time finite precision quantities, e.g. a voltage that is sampled and quantized.

## 3.2 Passive and Active Filters

In general, analog filters can be classified by the type of components that realize them [20]:

- **Passive filters:** Filters which are implemented by using resistors, capacitors and inductors. Passive filters have the advantage of guaranteed BIBO stability. However, they cannot be manufactured on Integrated circuits (ICs) due to difficulties in integrating the constituent inductors.

- Active filters: Filters which are implemented by using the active components instead of inductors, lending themselves to IC fabrications. Active filters are usually realized by the following components:
  - Active-RC filters: These type of filters use operational amplifiers (OP-AMPs) and capacitors to replace the inductors in the corresponding passive prototype filter circuits. However, the active-RC filters are not suitable for IC implementations due to the difficulty of building resistors with accurate resistances <sup>1</sup>.
  - Switched-capacitor (SC) filters: These type of filters employ two discrete switches and one capacitor to replace the resistor in the corresponding active-RC filters as shown in Fig. 3.1, where  $\Psi_1$  and  $\Psi_2$  represent two-phase non-overlapping clocks. A net charge  $q$  is accumulated at the capacitor  $C_{sc}$  at the clock cycle when  $\Psi_1$  is open and  $\Psi_2$  is closed, where  $q = C_{sc}V_{sc}$ . In the next clock cycle when  $\Psi_1$  is closed and  $\Psi_2$  is open, the charge stored in  $C_{sc}$  is transferred to the ground. In this way, for each sequential pair of switch closures, a quantum charge  $q$  is moved from  $V_{sc}$  to the ground. When this process is repeated in a small amount of time duration  $T$ , a continuous current  $I_{sc}$  is moving from  $V_{sc}$  to the ground, where:

$$I_{sc} = \frac{C_{sc}V_{sc}}{T} = V_{sc}C_{sc}f_{clock} \quad (3.1)$$

The SC circuit represents a resistor with resistance of  $R_{sc} = \frac{1}{C_{sc}f_{clock}}$ , where  $f_{clock} = \frac{1}{T}$  is the frequency of the clock at the switches. There are two advantages behind the SC filters. First, resistors usually consume a large amount of area in IC layout. Second, it is extremely difficult to build a resistor with accurate resistance due to CMOS manufacturing errors. However, the frequency-response of the SC filters depends on the ratios of capacitors, which can be made very accurate in IC fabrications [21].

- OTA-C filters: OTA-C filters consist of operational transconductance amplifiers and capacitors only. The OTA-C filters do not require traditional OP-AMPs

---

<sup>1</sup>This renders, in turn, the time-constant of the filter inaccurate.

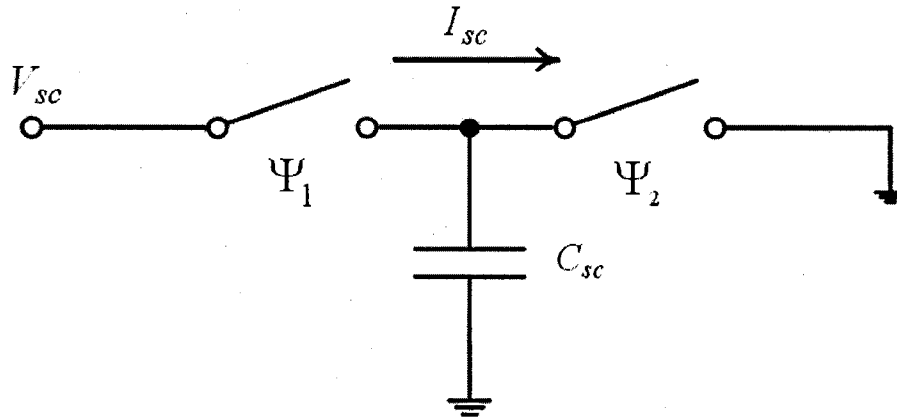


Fig. 3.1. Simple Switched Capacitor Circuit Example

as in the active-RC filters and additional external clock frequencies as in the SC filters. The frequency-response of OTA-C filters usually depends on the respective ratio of  $\frac{g_m}{C}$ , where  $g_m$  represents the transconductance gain.

In actual hardware realization, OTA-C filters are not as accurate as the SC filters since each transconductance could vary as much as 10 percent from its normal value due to temperature and manufacturing errors. To circumvent this problem, frequency turning techniques can be applied to correct for such errors by using phase locked loops (PLLs). In PLLs, the control voltage which forces the voltage controlled oscillator (VCO) to lock onto the reference frequency also sets the bias current in the OTA-C IF filter. It is well known that the transconductance of the OTA can be accurately tuned by the bias current, implying that the transconductance in the analog filter can be well adjusted to the desired value by properly setting up the reference frequency in the PLLs [21].

The SCs and the OTA-Cs provide the two most popular realization techniques for analog filters in current CMOS technologies. However, the SC realizations have been limited to the audio range, as sensitivity and stability problems will occur when the input signal frequency is increased. Therefore, the OTA-C realizations are the the choice of implementation for today's high-frequency filtering applications [21].

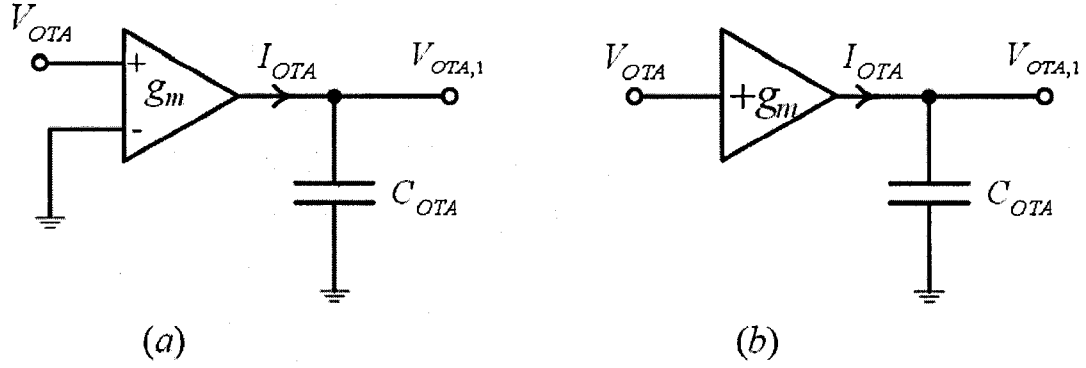


Fig. 3.2. Simple OTA Connection Example

### 3.3 OTA-C Realization Technique

Let us consider a simple OTA-C circuit as shown in Fig. 3.2a. Usually, one input of the OTA is connected to the ground, and the other is connected to an input voltage  $V_{OTA}$ . The output current from the OTA is therefore  $I_{OTA} = g_m \times V_{OTA}$ , where  $g_m$  represents the transconductance gain of the OTA<sup>2</sup>. By considering a capacitor  $C_{OTA}$  at the output of the OTA, one can write

$$V_{OTA,1} = V_{OTA} \times \frac{g_m}{sC_{OTA}}, \quad (3.2)$$

where  $V_{OTA,1}$  represents the output voltage associated with the OTA-C circuit [19]. In order to simplify matters for further discussions, the OTA configuration in Fig. 3.2a is simplified by that in Fig. 3.2b

In actual hardware implementation, there is a similar OTA-C configuration as shown in Fig. 3.3a, where the voltage  $V_{OTA}$  is tied to the inverting input of the OTA. In this configuration, one has

$$V_{OTA,2} = V_{OTA} \times \frac{-g_m}{sC_{OTA}}, \quad (3.3)$$

Again, to simply representations for further discussions, the OTA in Fig. 3.3a is simplified by the configuration shown in Fig. 3.3b, where  $-g_m$  denotes a negative transconductance gain.

<sup>2</sup>The unit of  $g_m$  is the siemens, with the symbol S (1 siemens = 1 ampere per volt).

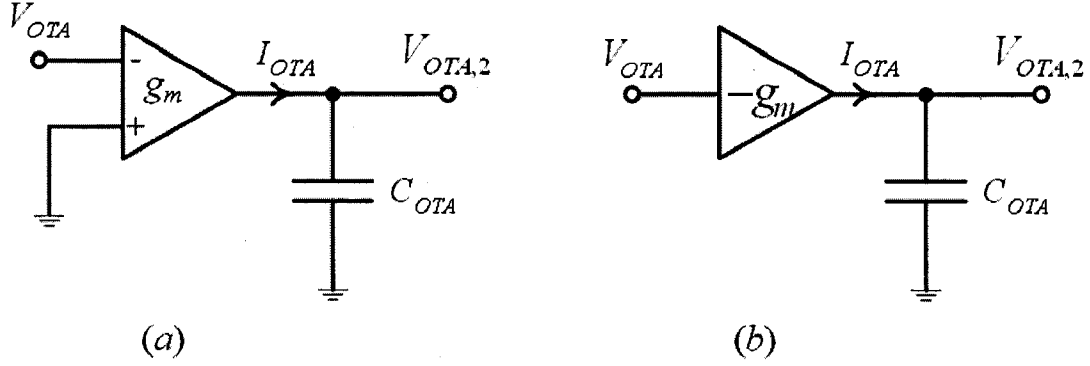


Fig. 3.3. The Other OTA Connection Example

In the following, OTAs and capacitors are employed to realize grounded or floating resistors and inductors in a passive analog prototype filter circuit (capacitors remains the same).

### 3.3.1 Realization of resistor

A grounded resistor  $R_g$  shown in Fig. 3.4a can be realized by using a single OTA as shown in Fig. 3.4b [21]. The relationship between the input voltage and the input current in Fig. 3.4b is given by:

$$V_R = \frac{1}{g_m} \times I_R \quad (3.4)$$

leading to an equivalent resistor with a resistance of  $R_g = \frac{1}{g_m}$ .

Similarly, a floating resistor  $R_f$  shown in Fig. 3.5a can be realized by using a pair of OTAs as shown in Fig. 3.5b, where  $R_f = \frac{1}{g_m}$  [21].

### 3.3.2 Realization of grounded inductor

A grounded inductor circuit as shown in Fig. 3.6a can be realized indirectly by an equivalent circuit consisting of two voltage controlled current sources (VCCSs)  $g_{m1}$  and  $g_{m2}$  as shown in Fig. 3.6b. The voltage-current relationship for the equivalent circuit in Fig. 3.6b is given by:

$$I_L = g_{m1} \times V_x \quad (3.5)$$

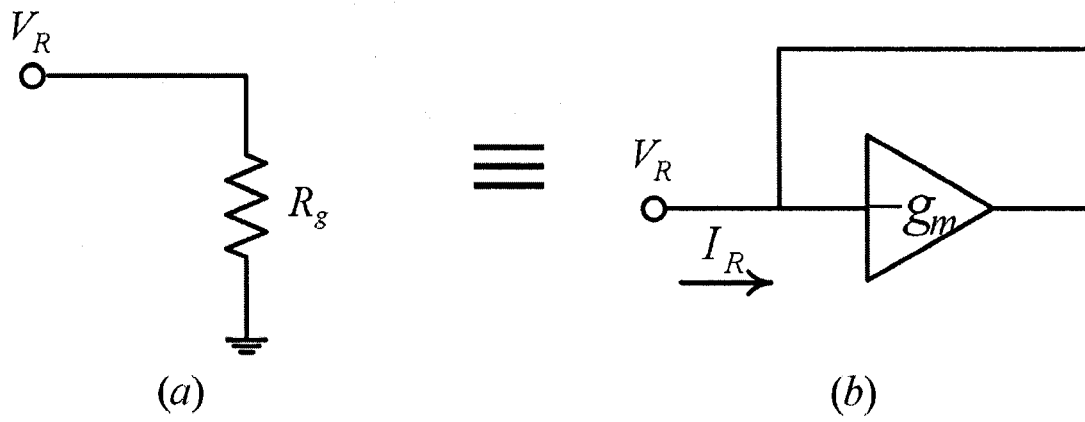


Fig. 3.4. OTA-C Reutilization of Grounded Resistor

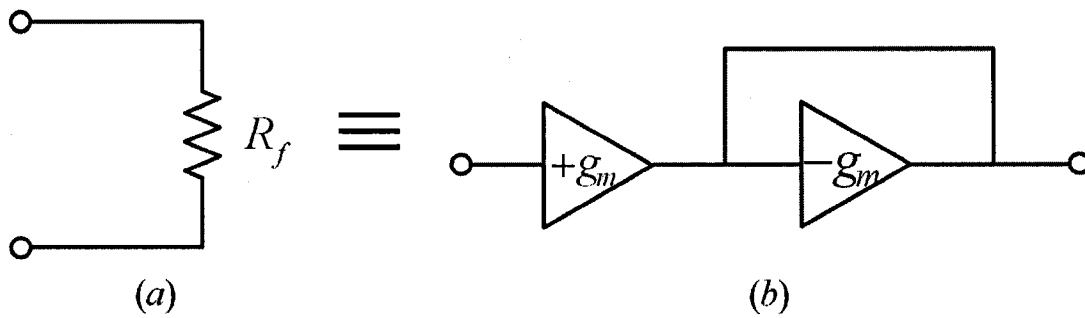


Fig. 3.5. OTA-C Reutilization of Floating Resistor

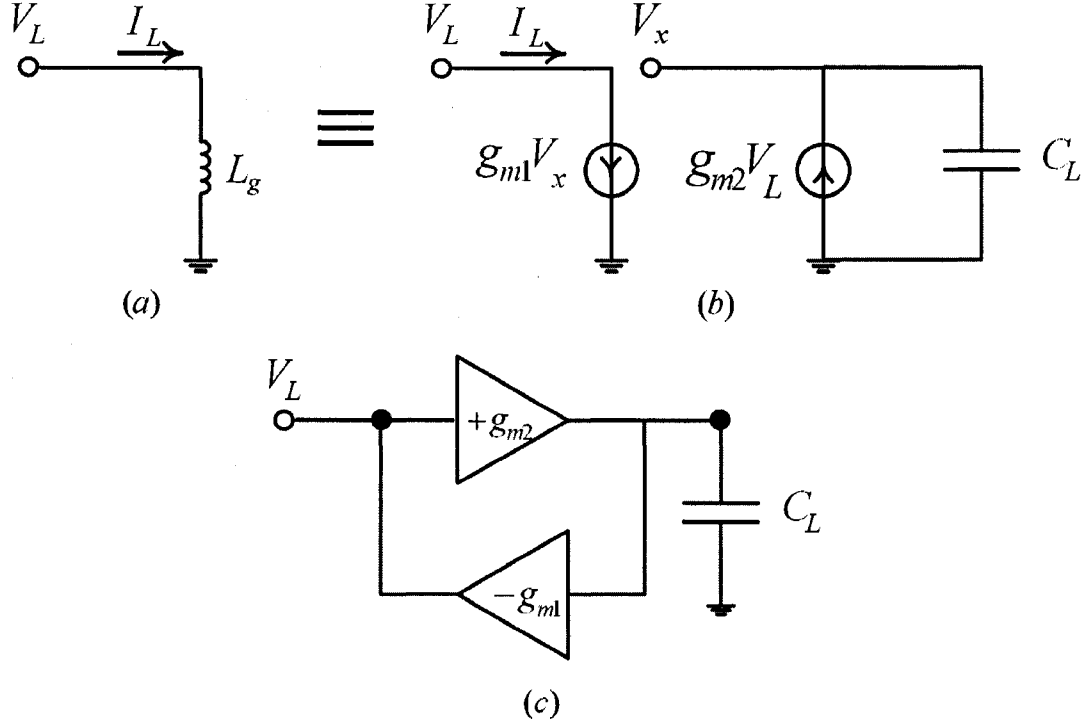


Fig. 3.6. Equivalent VCCS Circuit of Grounded Inductor

$$g_{m2} \times V_L = sC_L \times V_x \quad (3.6)$$

Then, by realizing  $g_{m1}$  and  $g_{m2}$  in terms of OTAs, one can obtain the following OTA-C realization of grounded inductor as shown in Fig. 3.6c. The voltage-current relationship for the resulting OTA-C realization is given by:

$$V_L = s \times \frac{C_L}{g_{m1} \times g_{m2}} I_L \quad (3.7)$$

leading to an equivalent inductor with inductance  $L_g = \frac{C_L}{g_{m1} \times g_{m2}}$  [21].

## 3.4 OTA-C Realization of the IF Filter

### 3.4.1 OTA-C realization of the eighteenth-order IF filter

It was proposed in [22] that an OTA-C IF filter can be realized by a cascade combination of three identical OTA-C bandpass filters each having a transfer function of a sixth-order pas-

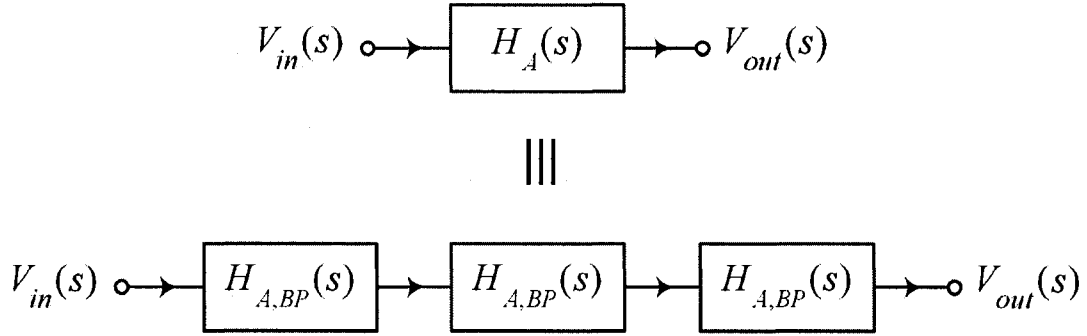


Fig. 3.7. Realization of the Analog IF Filter By Cascading Three Identical Bandpass Filter  $H_{A,BP}(s)$  Sections

sive RLC filter. The same technique [22] is adopted in this thesis for the OTA-C realization of the IF filters as shown in Fig. 3.7, where the transfer function of the IF filter is

$$H_A(s) = [H_{A,BP}(s)]^3, \quad (3.8)$$

where  $H_{A,BP}(s)$  is the transfer function of a sixth-order OTA-C bandpass filter realized in the following discussion.

### 3.4.2 OTA-C realization of a prototype sixth-order bandpass filter

In accordance with the above discussion, one can realize a passive prototype filter circuit in terms of an equivalent OTA-C filter circuit by replacing the constituent resistors and inductors by their OTA-C counterparts in accordance with the discussions in Section 3.3.1 and Section 3.3.2.

To this end, let us consider a sixth-order prototype bandpass passive filter as shown in Fig. 3.8. The corresponding OTA-C realization of this passive filter circuit is carried out in a step-by-step manner as follows:

- The floating source resistor  $R_1$  can be replaced by OTA  $A_1$  and  $Q_1$  as shown in Fig. 3.9a, where:

$$R_1 = \frac{1}{Q_1} \quad (3.9)$$

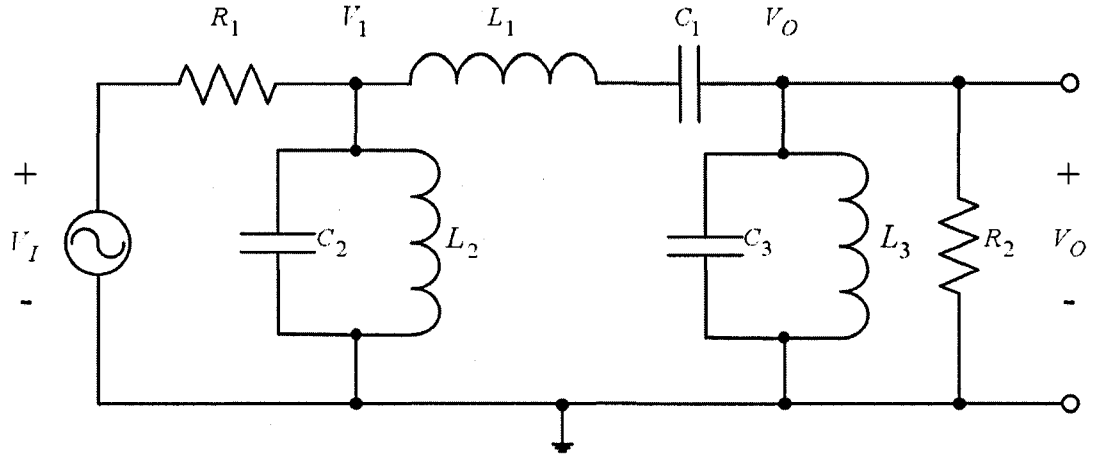


Fig. 3.8. Sixth-Order Passive Bandpass Filter

- The grounded inductor  $L_2$  is replaced by OTAs  $W_1, W_2$  and capacitor  $C_{p2}$  in Fig. 3.9a, where:

$$L_2 = \frac{C_{p2}}{W_1 W_2} \quad (3.10)$$

- The Capacitor  $C_2$  is replaced by the capacitor  $C_{p1}$  in Fig. 3.9a, where:

$$C_2 = C_{p1} \quad (3.11)$$

- The grounded inductor  $L_3$  is replaced by OTAs  $W_5$  and  $W_6$  and capacitor  $C_{p6}$  in Fig. 3.9b, where:

$$L_3 = \frac{C_{p6}}{W_5 W_6} \quad (3.12)$$

- The grounded resistor  $R_2$  is replaced by OTA  $Q_6$  in Fig. 3.9b, where:

$$R_2 = \frac{1}{Q_6} \quad (3.13)$$

- In addition, capacitor  $C_3$  in Fig. 3.8 is replaced by  $C_{p5}$  in Fig. 3.9b, where:

$$C_3 = C_{p5} \quad (3.14)$$

- The remaining active elements, namely, the floating inductor  $L_1$  and floating capacitor  $C_1$  are realized as discussed in an indirect manner. Since there is no direct method

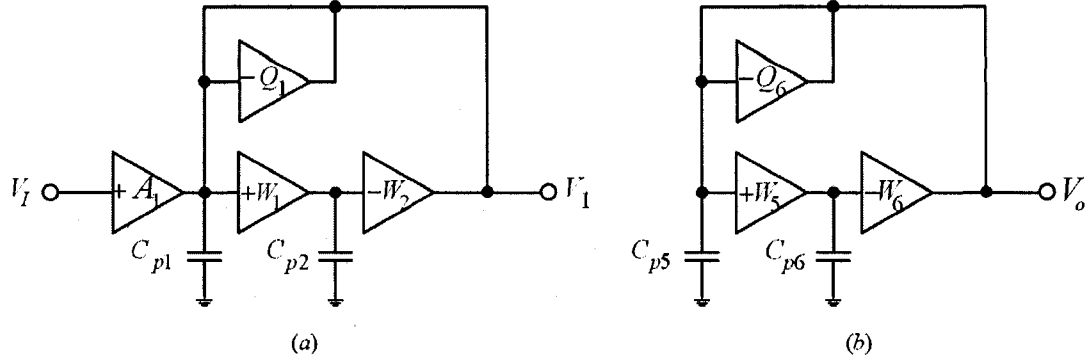


Fig. 3.9. OTA-C Realization of the Floating/Grounded Resistors and Grounded Inductors in Fig. 3.8

available to realize floating passive elements (c.f. Section 3.3.1 and 3.3.2), transformation techniques have to be employed. Let us consider only the LC resonator consisting of  $L_1$  and  $C_1$  as shown in Fig. 3.10a. The equivalent circuit for the same voltage-current relationship is as shown in Fig. 3.10b.  $L_1$  is realized by the grounded capacitor  $C_{p3}$  and two VCCSs  $Q_2$  and  $Q_3$ , where  $L_1 = \frac{C_{p3}}{Q_2 Q_3}$ . Similarly,  $C_1$  is realized by the grounded inductor  $L_{p1}$  and two VCCSs  $Q_4$  and  $Q_5$ , where  $C_1 = L_{p1} Q_4 Q_5$ .

Finally, one can realize the four VCCSs in terms of OTAs  $Q_2$ ,  $Q_3$ ,  $Q_4$ , and  $Q_5$ , and realize the grounded inductor  $L_{p1}$  in terms of OTAs  $W_3$ ,  $W_4$  and capacitor  $C_{p4}$  (the capacitor  $C_{p3}$  remains the same). The above OTA-C realization of  $L_1$  and  $C_1$  gives:

$$L_1 = \frac{C_{p3}}{Q_2 Q_3} \quad (3.15)$$

$$C_1 = \frac{C_{p4}}{W_3 W_4} Q_4 Q_5 \quad (3.16)$$

In accordance with the above discussion, one can finally obtain the OTA-C realization of the passive bandpass filter circuit in Fig. 3.11, which consists of 13 OTAs and 6 capacitors. The transfer function of the OTA-C filter in Fig. 3.11 is (assume that all the capacitors have the same capacitance denoted by  $c$ ).

$$H_{A,BP}(s) = \frac{V_O}{V_I} = \frac{a_3 c^3 s^3}{c^6 s^6 + b_5 c^5 s^5 + b_4 c^4 s^4 + b_3 c^3 s^3 + b_2 c^2 s^2 + b_1 c s + b_0} \quad (3.17)$$

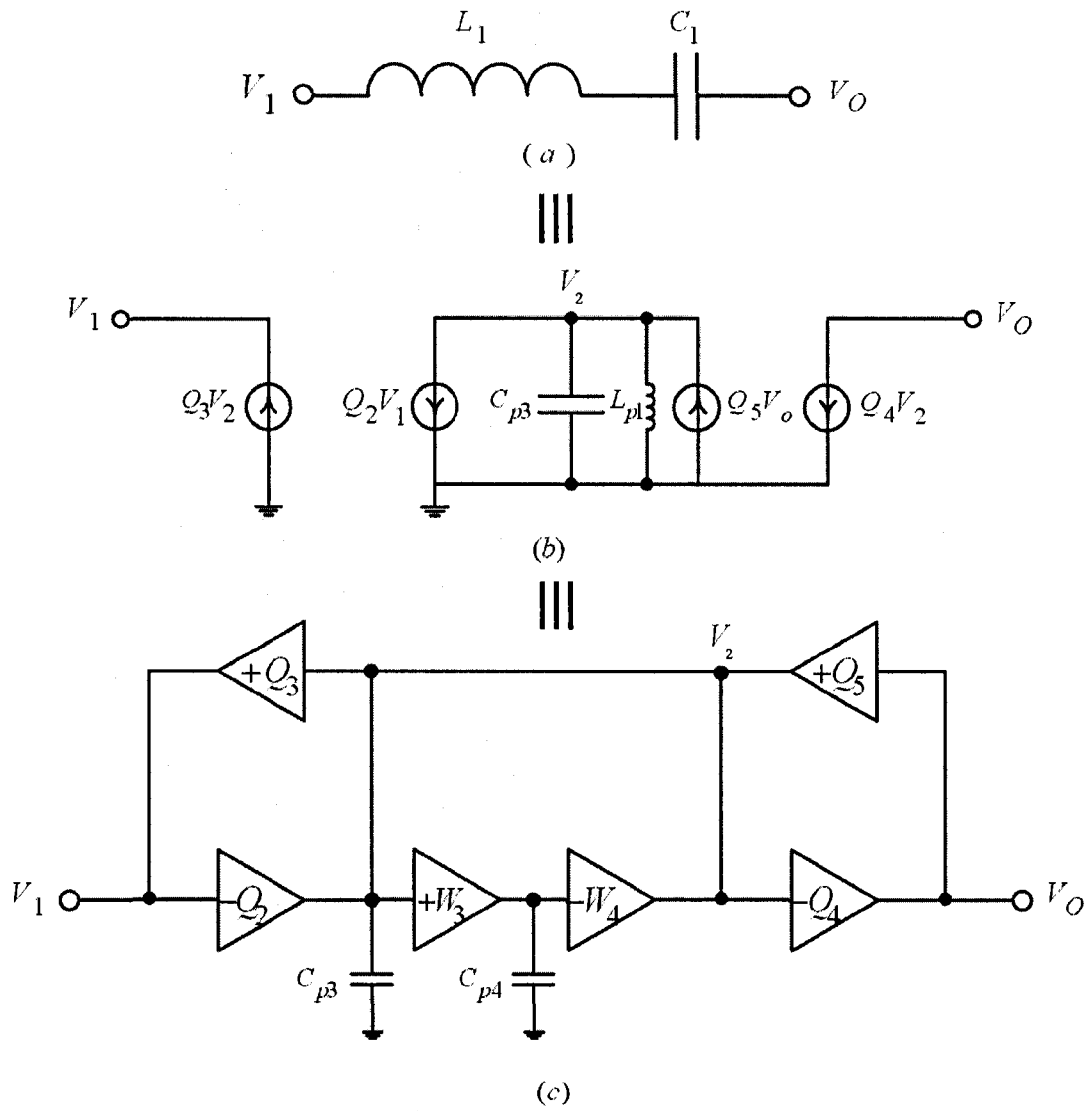


Fig. 3.10. OTA-C Realization of the Floating Inductor and Capacitor in Fig. 3.8

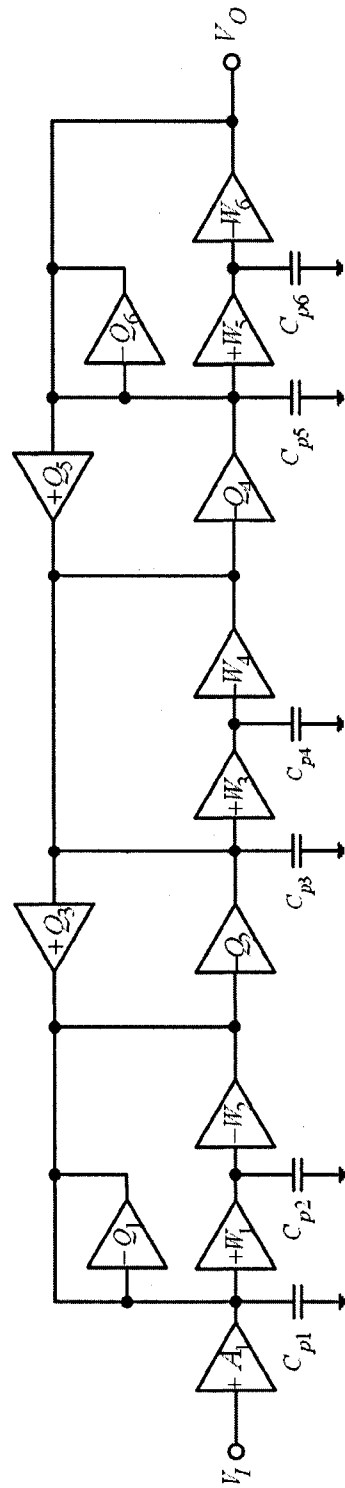


Fig. 3.11. OTA-C Realization of the Passive Bandpass Filter in Fig. 3.8

where the numerator coefficient  $a_3$ , and the denominator coefficients  $b_k$  (for  $k = 0, 1, 2, \dots, 5$ ) are as given in Table 3.1. In this way, the denominator coefficients  $b_k$  are all positive, permitting a BIBO stable transfer function  $H_{A,BP}(s)$ .

TABLE 3.1  
Numerator and Denominator Coefficients

$a_3$	$A_1 Q_2 Q_4$
$b_5$	$Q_6 + Q_1$
$b_4$	$Q_4 Q_5 + Q_2 Q_3 + Q_1 Q_6 +$ $W_5 W_6 + W_3 W_4 + W_1 W_2$
$b_3$	$Q_4 Q_1 Q_5 + Q_2 Q_3 Q_6 + Q_1 W_3 W_4 +$ $Q_1 W_5 W_6 + Q_6 W_1 W_2 + Q_6 W_3 W_4$
$b_2$	$Q_4 Q_5 W_1 W_2 + Q_2 Q_3 W_5 W_6 + Q_1 Q_6 W_3 W_4 +$ $W_3 W_4 W_5 W_6 + W_1 W_2 W_3 W_4 + W_1 W_2 W_5 W_6$
$b_1$	$Q_1 W_3 W_4 W_5 W_6 +$ $Q_6 W_1 W_2 W_3 W_4$
$b_0$	$W_1 W_2 W_3 W_4 W_5 W_6$

### 3.4.3 Stability of the OTA-C IF filter

In order to make the OTA-C realization of the sixth-order bandpass filter BIBO stable, the denominator of Eqn. 3.17 must have all its poles on the left hand side of the complex  $s$ -plane. To determine stability for the above bandpass filter section, one can apply the Routh-Hurwitz stability criterion [23]. For higher order denominator polynomials, one need to form the Routh-Hurwitz table. The number of sign changes in the first column of this table gives the number of unstable poles in Eqn. 3.17. However, it is impractical to use this method because  $b_k$  in the table do not have numerical values at this movement and it is difficult to find whether the elements in the table is positive or negative.

Alternatively, one can transform the OTA-C filter circuit back to the corresponding passive filter circuit as shown in Fig. 3.12. Then the values of the elements of the back-transformed filter circuit can be determined in accordance with the analytical equations in Table 3.2 (in terms of the transconductances and capacitances). In this way, the back-transformed filter circuit is guaranteed BIBO stable if all the elements have positive values. Therefore, to make the sixth-order OTA-C filter circuit BIBO stable, it is both necessary and sufficient to have  $Q_i > 0, W_i > 0$  and  $C_{pi} > 0$ , for  $i = 1, 2, \dots, 6$ .

Since the OTA-C IF filter is obtained by cascading three identical sections of the band-pass OTA-C filter circuit, as long as all the transconductances are positive, the OTA-C IF filter is BIBO stable.

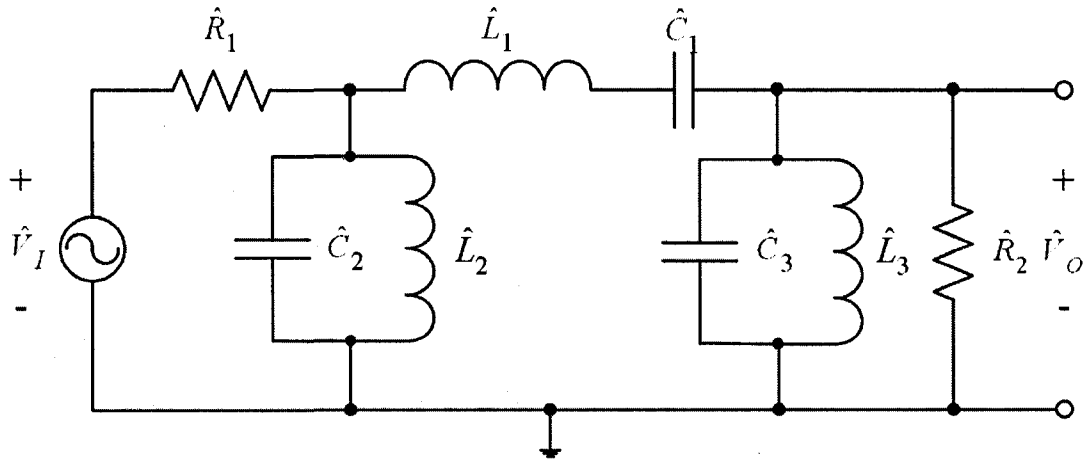


Fig. 3.12. Back-transformed Passive Bandpass Filter Circuit

### 3.5 OTA-C IF Filter Optimization Employing DCGA

By employing the above mentioned OTA-C IF realization technique, one can implement and optimize the IF filter based on the transconductance parameters of the constituent OTAs in an attempt to satisfy the IF filter design specifications. The proposed optimization principle is illustrated in Fig. 3.13, with the optimization parameters including the 13 OTA transconductances,  $Q_i, W_i$ , and  $A_1$ . The capacitors  $C_{pi}$  are usually assigned fixed values at

the outset and throughout the course of optimization. It should be pointed out that the optimization of OTA-C IF filter does not suffer from BIBO stability problems since all the 13 transconductances are assumed to be positive by design.

The transconductance values ( $g_{mi}$ ) can take infinite-precision (positive) numbers as their values. However, in order to encode them into bit-string representations for DCGA optimization, one has to truncate their values to the nearest binary counterpart ( $\hat{g}_{mi}$ ) as given by <sup>3</sup>:

$$\hat{g}_{mi} = \sum_{n=1}^W D_{in} 2^{R-n} \quad (3.18)$$

where  $W$  represents a pre-fixed wordlength, and the integer  $R$  represents a radix-point in the range  $0 < R < W$  and  $D_{in} \in (0, 1)$ .

By using Eqn. 3.18, one can form an IF filter chromosome obtained by concatenating all the binary string representations of  $\hat{g}_{mi}$ . The total length of the chromosome is therefore  $13 \times W$ .

The optimization process begins with gathering a number of candidate chromosomes together to obtain a population pool. Then, by using the GA reproduction (e.g. crossover

<sup>3</sup>In practical, their values will ultimately become finite-precision.

TABLE 3.2  
Back Transformed Passive Components

$\hat{R}_1$	$\frac{1}{Q_1}$
$\hat{C}_1$	$\frac{C_{p4}}{W_3 W_4} Q_4 Q_5$
$\hat{L}_1$	$\frac{C_{p3}}{Q_2 Q_3}$
$\hat{R}_2$	$\frac{1}{Q_6}$
$\hat{C}_2$	$C_{p1}$
$\hat{L}_2$	$\frac{C_{p2}}{W_1 W_2}$
$\hat{C}_3$	$C_{p5}$
$\hat{L}_3$	$\frac{C_{p6}}{W_5 W_6}$

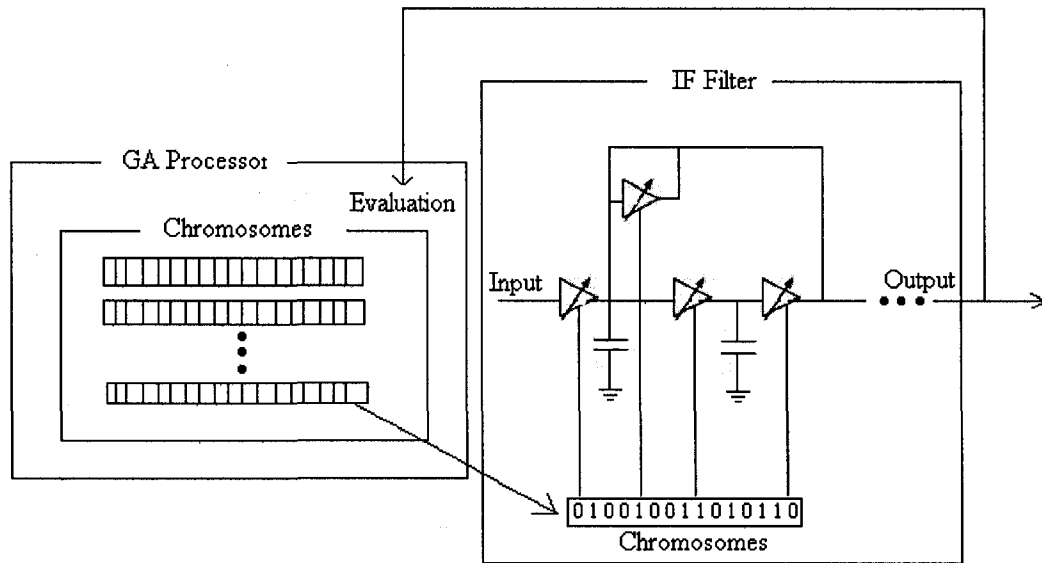


Fig. 3.13. OTA-C IF Filter Optimization Process Using DCGA

and mutation) operations, a next generation population pool is generated, and the constituent chromosomes are evaluated and ranked based on their fitness values. The GA optimization proceeds from one generation to the next, ending up with the best performing chromosome (i.e. the chromosome with the highest rank). The resulting chromosome represents the desired OTA-C IF filter. The design steps in DCGA are as follows [19]:

- Initialization: A seed chromosome is formed by concatenating the binary-string representations of the OTA transconductance values (usually obtained from conventional optimization techniques or from the literature). Then, the remaining members of the initial population pool are constructed by randomly complementing bits in the seed chromosome.
- Reproduction: Parent pairs are selected from the current population pool, and their offspring are formed after crossover and mutation operations.
- Evaluation: Population pool chromosomes are evaluated based on a pre-defined fit-

ness function. This fitness function can be formulated as

$$fitness = -20\log[\max(\varepsilon_p, \varepsilon_t, \varepsilon_s)] \quad (3.19)$$

where

$$\varepsilon_p = \underbrace{\max}_{\omega \in \Omega_p} [W_p |H(e^{j\omega}) - 1|] \quad (3.20)$$

with  $\Omega_p$  representing the passband frequency regions, and where

$$\varepsilon_t = \underbrace{\max}_{\omega \in \Omega_t} [W_t |H(e^{j\omega}) - 0.7079|] \quad (3.21)$$

with  $\Omega_t$  representing the 3dB attenuation frequencies points, and where

$$\varepsilon_s = \underbrace{\max}_{\omega \in \Omega_s} [W_s |H(e^{j\omega}) - 0.001|] \quad (3.22)$$

with  $\Omega_s$  representing the stopband attenuation frequencies points. Here,  $W_p$ ,  $W_t$ , and  $W_s$  represent the passband, transitionband, and stopband weighing factors, respectively (all set to be equal to 1).

- Next generation population pool: In order to form the next generation population pool, all (but one) duplicate chromosomes in the current population pool are eliminated. Then, the remaining chromosomes are ranked based on their fitness values. The chromosome with the highest fitness value is selected at the outset as a member of the next generation population pool. The remaining  $N - 1$  chromosomes are selected based on the CPSS scheme introduced in Section 2.2. The above iteration is repeated until an optimum OTA-C IF filter satisfying the design specifications is found.

In DCGA, the search is made effective by keeping track of current chromosomes which have low fitness values but have the potential of evolving to individuals with high fitness values in future generations. Moreover, chromosomes for the next-generation population pool are selected probabilistically on the basis of their hamming distances from the current chromosome having the highest fitness value [9]. The convergence speed of DCGA has been observed to be an order of magnitude higher than the conventional GAs.

### 3.6 Application Example

In this section, DCGA is applied to the the design of an OTA-C IF filter satisfying the design specifications given as follows in Table 3.3.

TABLE 3.3  
Design Specifications for OTA-C IF Filter

Center frequency	455 kHz
Bandwidth	21 kHz
3 dB attenuation frequency regions	
Lower passband (444 kHz, 445 kHz)	Upper passband (465 kHz, 466 kHz)
60 dB attenuation frequency regions	
Lower stopband (403 kHz, 407 kHz)	Upper stopband (503 kHz, 507 kHz)

From [1], the transconductance values for the initial chromosome are chosen as given in Table 3.4. The magnitude frequency-response associated with the initial chromosome is shown in Fig. 3.14. By inspection of Fig. 3.14, the 3dB attenuation frequency point is violated by 3 kHz and the 60 dB attenuation point is violated by 20 kHz.

TABLE 3.4  
Initial Values of OTA-C IF Filter Transconductances [1]

Transconductances	Value
$W_1, \dots, W_{18}$	$2858nS$
$Q_1, \dots, Q_{18}$	$130nS$
$a_1, a_2, a_3$	$260nS$
	$c = 1pF$

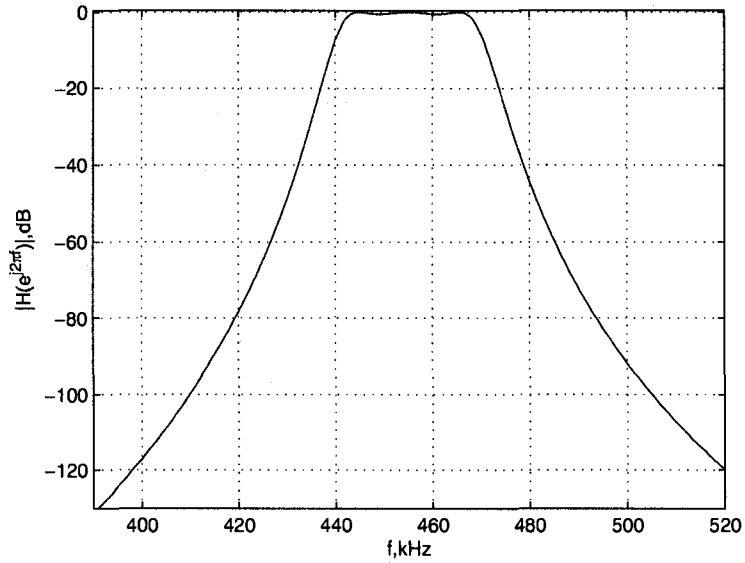


Fig. 3.14. OTA-C IF Filter Magnitude Frequency-Response Before DCGA

By applying the proposed DCGA optimization to the initial chromosome, and after 341 generations, an optimal OTA-C IF filter is obtained to have the transconductance values given in Table 3.5. The magnitude frequency-response of the resulting OTA-C IF filter is as shown in Fig. 3.15. By inspection of Fig. 3.15, the 3 dB attenuation frequency is at 444.6 kHz and 465.8kHz, and the 60 dB attenuation frequency point is at 403.1 kHz and 503.5 kHz. The group delay of the resulting OTA-C IF filter is as shown in Fig. 3.16.

The convergence speed for the above DCGA optimization for various values of the shape coefficient parameter  $0.6 \leq c \leq 0.95$  for a fixed  $\alpha$ -value of 0.6 is as shown in Fig. 3.17, with a best convergence within 208 generations when  $c = 0.8$ . In Fig. 3.18, the convergence speed is shown for various values of the exponent parameter  $0.1 \leq \alpha \leq 0.7$  for a fixed  $c$ -value of 0.8, leading to a best convergence within 167 generations when  $\alpha = 0.5$ .

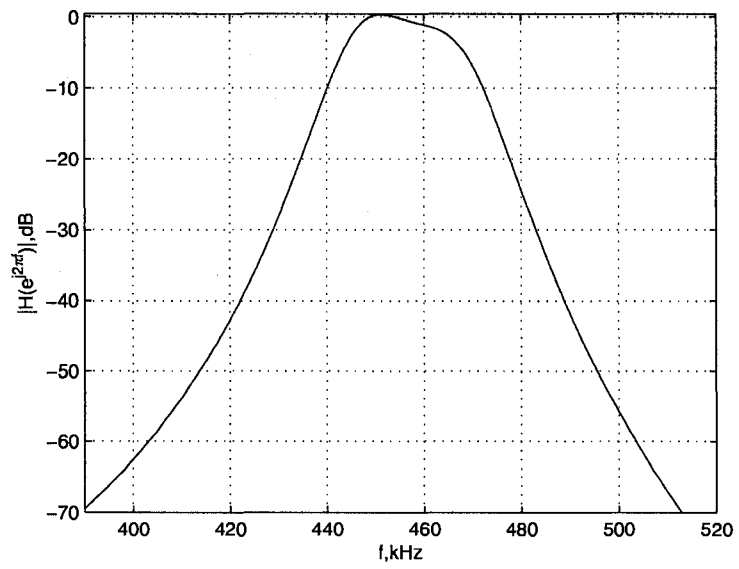


Fig. 3.15. Optimized OTA-C IF Filter Magnitude Frequency-Response after DCGA Application

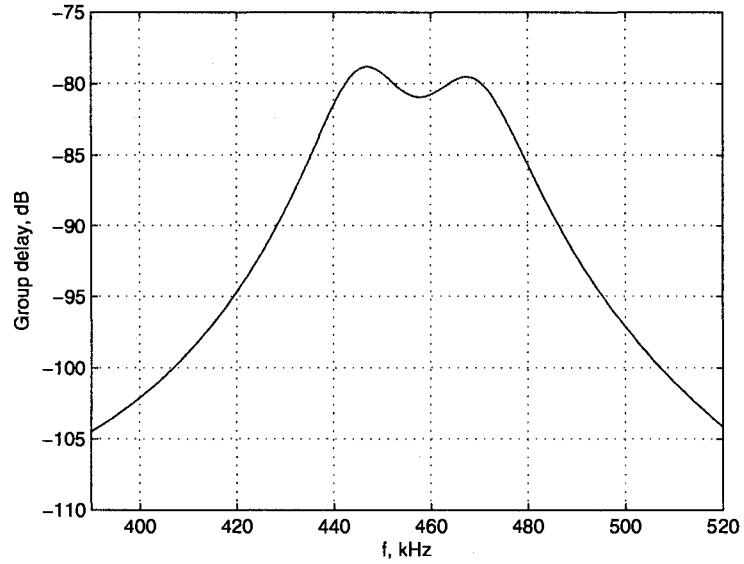


Fig. 3.16. Optimized OTA-C IF Filter Group Delay after DCGA Application

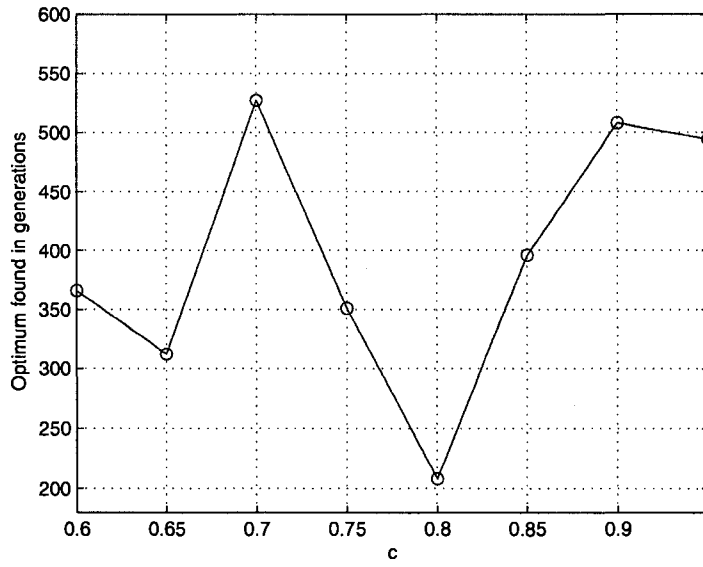


Fig. 3.17. Convergence Speeds for Various  $c$ -values

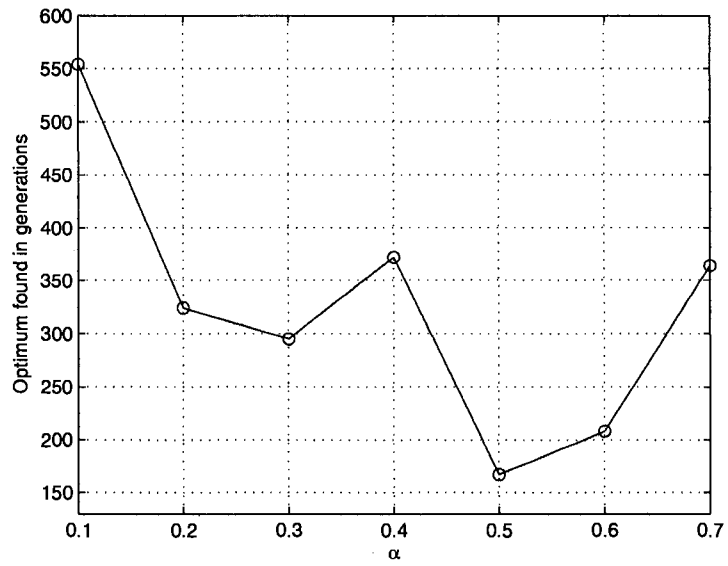


Fig. 3.18. Convergence Speeds for Various  $\alpha$ -values

### 3.7 Summary

This chapter has been concerned with the design and discrete optimization of analog OTA-C IF filters. The design starts from a prototype passive RLC bandpass filter section and by replacing resistors and inductors in the prototype bandpass filter with their respective OTA-C combinations, the desired OTA-C bandpass filter is obtained. A cascaded combination of three such identical OTA-C bandpass filters gives rise to an eighteenth-order OTA-C IF filter consisting of 39 OTAs and 18 capacitors. The resulting OTA-C IF filter is automatically BIBO stable by design.

In the optimization of OTA-C IF filter, the 39 OTA transconductance gains have been

TABLE 3.5  
Optimized Transconductance Gains

Transconductances	Values
$W_1, W_7, W_{13}$	$2823nS$
$W_2, W_8, W_{14}$	$2928nS$
$W_3, W_9, W_{15}$	$3415nS$
$W_4, W_{10}, W_{16}$	$2354nS$
$W_5, W_{11}, W_{17}$	$1870nS$
$W_6, W_{12}, W_{18}$	$1795nS$
$Q_1, Q_7, Q_{13}$	$271nS$
$Q_2, Q_8, Q_{14}$	$373nS$
$Q_3, Q_9, Q_{15}$	$102nS$
$Q_4, Q_{10}, Q_{16}$	$480nS$
$Q_5, Q_{11}, Q_{17}$	$256nS$
$Q_6, Q_{12}, Q_{18}$	$120nS$
$A_1, A_2, A_3$	$368nS$
	$c = 1pF$

quantized to their nearest binary counterparts and encoded into a chromosome, while all the capacitors are usually assigned with fixed capacitance values. DCGA starts from a population pool of candidate chromosomes and proceeds from one generation to the next in an attempt to find the desired IF filter satisfying the required design specifications. Application example has been presented for an OTA-C AMPS IF filter operating around a center frequency of 455 kHz. Through investigation over a region of the DCGA external control parameters, a fastest convergence of 167 generations has been reached when  $c = 0.8$  and  $\alpha = 0.5$ .

## **Chapter 4**

# **Design and DCGA Optimization of Stable Digital IF filters Employing CSD Number Systems**

It was discussed in section 3.1 that there were two important classes of filters, namely, analog filters and digital filters. Digital filters use multipliers and adders to perform numerical manipulations on sampled values of the signal. In order to convert the signal from analog to digital or conversely from digital to analog, it is required to use A/D convertors and D/A convertors, respectively. Digital filters offer many advantages over the analog counterparts, including programmability, adaptability, high stability with respect to aging, temperatures changes, and manufacturing errors. In addition, with the impact of silicon technology scaling, digital filters can be successfully implemented for high-frequency applications with increased speeds, smaller chip areas and lower power consumptions [15].

### **4.1 IIR and FIR Digital Filters**

Digital filters can be broadly classified by the length of their impulse response. Digital filters with infinite impulse response length are called IIR filters. On the other hand, digital

filters with finite impulse response length are called FIR filters. The IIR filters usually have the following input to output difference equation:

$$y(n) = b_0x(n) + b_1x(n-1) + \dots + b_Mx(n-M) - a_1y(n-1) - a_2y(n-2) - \dots - a_Ny(n-N) \quad (4.1)$$

where  $x(n)$  represents the input signal and  $y(n)$  represents the output signal of the filter. The transfer function of IIR filters  $H(z)$  (subject to zero initial conditions) can be derived by taking the z-transform of Eqn. 4.1:

$$H(z) = \frac{Y(z)}{X(z)} = \frac{b_0 + b_1z^{-1} + \dots + b_Mz^{-M}}{1 + a_1z^{-1} + a_2z^{-2} + \dots + a_Nz^{-N}} \quad (4.2)$$

In contrast to IIR filters, the FIR filters have the following difference equation:

$$y(n) = b_0x(n) + b_1x(n-1) + \dots + b_Mx(n-M) \quad (4.3)$$

The transfer function of FIR filters is of the form:

$$H(z) = \frac{Y(z)}{X(z)} = b_0 + b_1z^{-1} + b_2z^{-2} + \dots + b_Mz^{-M} \quad (4.4)$$

In order to realize IIR filters, one need to start from the corresponding analog prototype filters and transform the filter transfer function from analog domain to digital domain using the bilinear transformation technique [24] with the form:

$$s = \frac{2}{T} \frac{z-1}{z+1} \quad (4.5)$$

to obtain the desired IIR filter here,  $s$  ( $z$ , respectively) represents the continuous-time (discrete-time, respectively) complex frequency variable, and  $T$  represents the sampling period. Alternatively, one can apply the wave digital filter technique [6] to transform the filter structure from analog to digital. Compared to the later technique, the bilinear transformation technique is well known for preserving the BIBO stability and sensitivity properties of the analog prototype reference filter. However, in both these two techniques, one must design carefully to avoid any delay free loops. Moreover, IIR filters usually suffer from BIBO stability problems because of the existence of feedback loops (IIR filters are stable if

all the poles are inside the unit circle of the complex  $z$  plane). They also require a secondary allpass filter in order to compensate for phase distortions.

On the other hand, FIR filters do not have the above problems. They are always BIBO stable and can be designed with the exact linear phase. Conventionally, FIR filters are designed by truncating an infinite duration impulse response sequence using windowing techniques (e.g. Rectangular window, Bartlett window, Kaiser window) to obtain the desired finite impulse response. However, at a cost for BIBO stability and linear phase, FIR filters are generally more complex and involve larger number of multipliers than IIR filters. As a result, IIR filters can achieve a given filtering characteristic using less memory and shorter filter order than a similar FIR filter design. This chapter is concerned with the design and DCGA optimization of digital IIR IF filters based on an analog prototype band-pass filter. Section 4.2 discusses the two problems associated with a direct application of the DCGA optimization technique. Section 4.3 is concerned with the design of the initial infinite-precision seed digital IF filter. Section 4.4 discusses the BIBO stability constraints for digital IF filters. Section 4.5 suggests a novel LUT-based technique for DCGA optimization for guaranteed BIBO stable digital IF filter. Section 4.6 summarizes the design methodology for the proposed DCGA optimization technique and section 4.7 gives two design examples. Finally, section 4.8 summarizes the entire chapter.

## **4.2 Problem Associated with Direct Application of DCGA Optimization Technique**

DCGA was successfully applied to optimize the magnitude frequency-responses of analog OTA-C IF filters in chapter 3 by taking its advantages of parallel searching and high convergence speed. The same technique can be applied to optimize digital IF filters with the optimization parameters being the value of the constituent multiplier coefficients. These infinite-precision coefficients can be first approximated by using filter design handbooks and tables based on the magnitude frequency-response design specifications [25]. Then,

DCGA can be applied to further optimize them to satisfy the design specifications. As discussed in Section 2.1, the multiplier coefficient values have to be quantized to their nearest binary counterparts to allow bit-string representations as chromosomes.

From a practical point of view, particularly in the hardware implementation of the digital filters, there is every incentive to represent the constituent multiplier coefficient values in more computationally-efficient number system (e.g. the signed-power-of-two (SPT) [26] or the canonical signed-digit (CSD) systems [27]) while still satisfying all the design specifications. This is mainly because such number systems permit the representations of the multiplier coefficients in terms of a few non-zero digits within the coefficient wordlength, eventually reducing the corresponding multiplication into a few shift and add operations [14].

Let us consider a digital IF filter having floating radix-point CSD<sup>1</sup> multiplier coefficients  $\hat{m}_{ik_i} \in CSD(W, w)$  (for  $i = 1, 2$  and  $k_1 = 1, k_2 = 1, 2, 3, 4$ ), where  $CSD \in (W, w)$  represents the set of all possible CSD numbers having a wordlength of  $W$  digits and a maximum number of  $w$  nonzero digits. In this way, the CSD multiplier coefficients  $\hat{m}_{ik_i}$  can be expressed in the general form

$$\hat{m}_{ik_i} = \sum_{n=1}^W (D_{ik_i})_n 2^{R-n} \quad (4.6)$$

with

$$\sum_{k=1}^W |(D_{ik_i})_n| \leq w \quad (4.7)$$

where  $0 < R < W$  represents a floating radix-point. Moreover, due to the CSD number system constraints,

$$(D_{ik_i})_n \in \{1, -1, 0\} \quad (4.8)$$

$$(D_{ik_i})_n \times (D_{ik_i})_{n+1} = 0 \quad (4.9)$$

Let the total wordlength  $W$  be represented as  $W = W_I + W_F$ , where  $W_I$  represents the wordlength associated with the integer part, and where  $W_F$  represents the wordlength associated with the fractional part of the CSD multiplier coefficients numbers. In practical

---

<sup>1</sup>The CSD number system is a special case of the SPT number system, where a given number has a unique CSD representation as opposed to more than one representations in the SPT number system.

situations, the integer wordlength  $W_I$  is chosen to accommodate the representation of the maximum integer values of the infinite-precision multiplier coefficients  $m_{ik_i}$ , and the fractional wordlength  $W_F$  is chosen based on the precision requirements. The resulting CSD multiplier coefficients  $\hat{m}_{ik_i} \in CSD(W, w)$  usually turn out to be very sparse, permitting computationally efficient hardware implementation of the corresponding multiplication operations in terms of a limited number of shift and add operations.

However, a direct application of the DCGA optimization technique to the digital IF filters may give rise to two separate problems as follows:

- The operations of crossover and mutation in the course of DCGA optimization to obtain next generation offspring may produce chromosomes which no longer conform to the CSD number format.
- The DCGA optimization may produce a solution chromosome which satisfies the given magnitude frequency-response design specifications, however, the resulting digital IIR IF filter is not BIBO stable.

In accordance with the above discussions, GAs lack inherent built-in mechanisms to ensure that the optimized IIR digital IF filters conform to the CSD number format, and that they are also BIBO stable. This chapter presents a novel approach to the design and DCGA optimization of BIBO stable digital IF filters over the CSD multiplier coefficient space. The salient feature of the proposed approach is its computational efficiency. This is achieved by ensuring that the resulting digital IF filter chromosomes not only conform to the CSD number format but also are BIBO stable automatically throughout the course of DCGA optimization [11].

The first problem was successfully resolved in the context of the DCGA optimization of FRM [26] FIR digital filters [8] by employing an indexed look-up table (LUT) consisting of only permissible (with pre-specified wordlengths and pre-specified maximum number of nonzero digits) CSD multiplier coefficient values and by employing the indices of the resulting multiplier coefficient values (as opposed to their values) to represent FRM FIR digital filter chromosomes. The key point in generating the CSD LUTs is to ensure that

the constituent indices form a closed set under the operations of crossover and mutation (or other similar operations) in the course of the underlying DCGA optimization so as to preserve adherence to the CSD number format [11].

In this chapter, the two problems mentioned earlier are resolved by resorting to a set of three LUTs, which can be used to find a set of permissible CSD multiplier coefficient values to represent digital IF filter chromosomes which are guaranteed to be BIBO stable. Moreover, the LUTs consist of CSD multiplier coefficient values which satisfy the CSD number system under the operations of crossover and mutation in the course of DCGA optimization.

The proposed DCGA optimization starts from a seed digital IF filter consisting of infinite-precision multiplier coefficient values. The infinite-precision seed digital IF filter is derived from a corresponding analog prototype reference bandpass filter section by using the bilinear-LDI lattice digital filter realization technique [24] as discussed in the following section. In order to obtain a corresponding finite-precision digital IF filter chromosome, the infinite-precision multiplier coefficients are subsequently quantized to their closest CSD counterparts (within the pre-specified maximum number of non-zero digits and the pre-specified wordlengths). The resulting finite-precision CSD digital IF filter is subsequently used to form an initial population pool of IF filter chromosomes for further DCGA optimization [11].

### **4.3 Design of the Infinite-Precision Seed Digital IF Filter**

This section is concerned with the realization of an infinite-precision seed digital IF filter for subsequent DCGA optimization. The infinite-precision seed digital IF filter is obtained indirectly by applying the bilinear-LDI lattice digital filter realization technique [28] to a suitable analog prototype reference filter.

The salient features of the bilinear-LDI lattice digital filter realization technique are twofold [11]:

- It maintains the bilinear frequency transformation in Eqn. 4.5 for mapping be-

tween the discrete-time  $z$ -domain and the corresponding continuous-time  $s$ -domain frequency-response specifications.

However, a delay-free path may exist in the bilinear integrator due to the order of the numerator and denominator in Eqn. 4.5 being equal. This delay-free path in the bilinear integrator will give rise to delay-free loop in the final digital filter when the bilinear transformation is achieved by replacing the analog integrators in the signal flow graph (describing the analog network) with the digital bilinear integrators. Thus, the bilinear transformation is not physically realizable.

- The bilinear-LDI lattice digital filter realization technique employs the LDI frequency transformation

$$s = \frac{1}{T}(z^{\frac{1}{2}} - z^{-\frac{1}{2}}) \quad (4.10)$$

for digital filter realization, leading to a digital filter incorporating LDIs as the only frequency-dependent elements. Here,  $s$  ( $z$ , respectively) represents the continuous-time (discrete-time, respectively) complex frequency-variable, and  $T$  represents the sampling period.

The advantages of the resulting bilinear-LDI digital IF filters are [11] the following:

- They are minimal in the number of digital multiplication operations,
- they lend themselves to fast two-cycle parallel digital signal processing speeds, and
- they exhibit exceptionally low passband sensitivity to their multiplier coefficient values, permitting low coefficient wordlengths.

In accordance with the above discussion, we can proceed to obtain the desired digital IF filter circuit based on an analog prototype RLC reference filter by using the bilinear-LDI lattice digital filter realization technique. The analog prototype RLC reference filter is chosen from a cascaded combination of three identical passive bandpass filter sections [6]. The individual bandpass filter sections themselves are formed as equally resistively

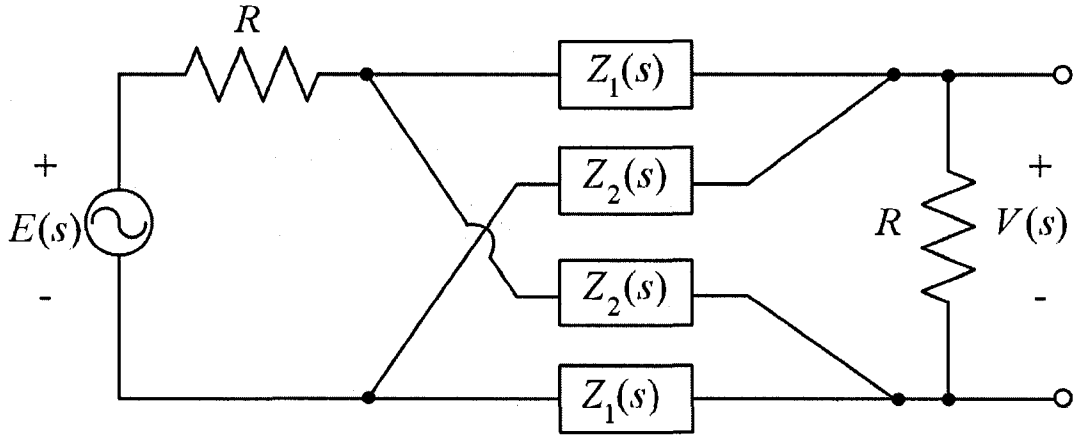


Fig. 4.1. Analog Prototype Reference Bandpass Filter Section

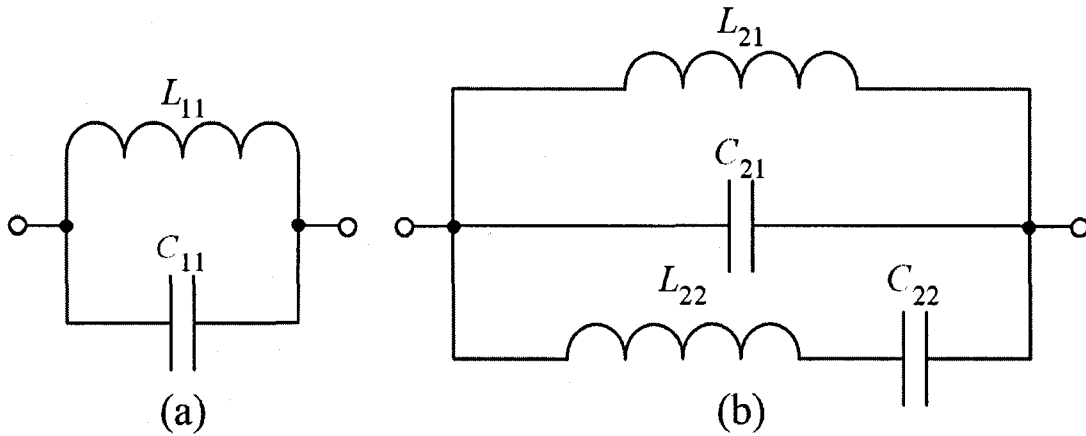


Fig. 4.2. Realization of the Reactance  $Z_1(s)$  and  $Z_2(s)$

terminated symmetrical lattice reactance two-port networks as shown in Fig. 4.1, where  $Z_1(s)$  and  $Z_2(s)$  represent the series and lattice arm reactance, respectively [11].

The bandpass filter section in Fig. 4.1 has a voltage transfer function:

$$H(s) = \frac{V(s)}{E(s)} = \frac{1}{2} \frac{Z_1(s) - Z_2(s)}{1 + Z_1(s) + Z_2(s) + Z_1(s)Z_2(s)} \quad (4.11)$$

By choosing the bandpass transfer function  $H(s)$  having an order of six, the series arm and the lattice reactance  $Z_1(s)$  and  $Z_2(s)$  can be realized as shown in Figs. 4.2a and 4.2b, respectively.

Based on Bartlett's bisection theorem, The transfer function  $H(s)$  in Eqn. 4.11 can

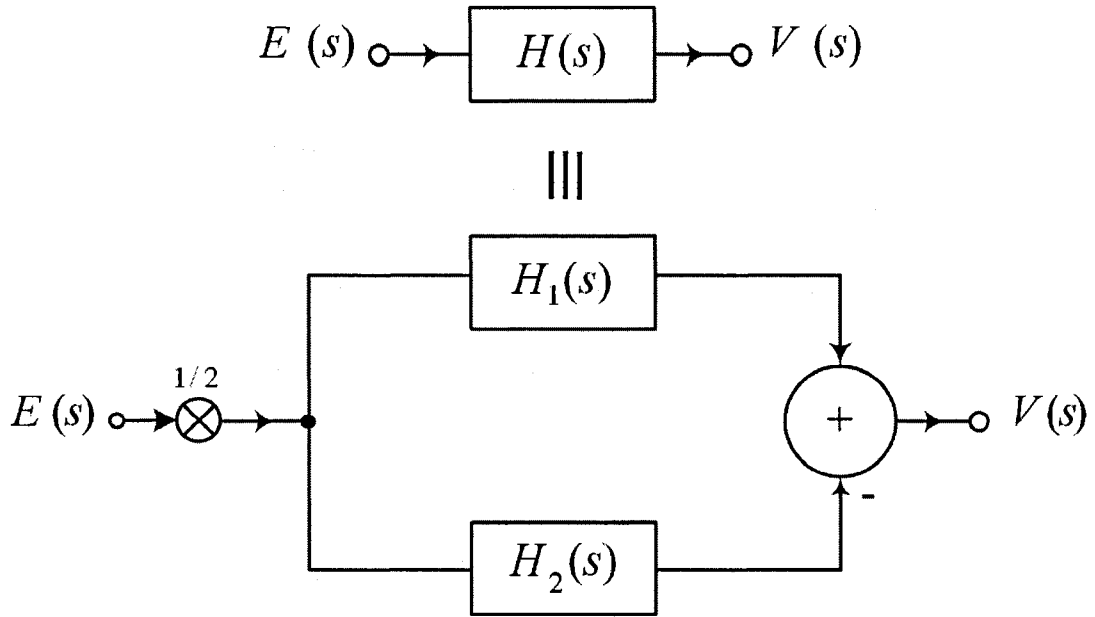


Fig. 4.3. Decomposition of  $H(s)$  into  $H_1(s)$  and  $H_2(s)$

be decomposed into a pair of transfer functions  $H_1(s)$  and  $H_2(s)$  as shown in Fig. 4.3 in accordance with

$$H(s) = \frac{1}{2}H_1(s) - \frac{1}{2}H_2(s) \quad (4.12)$$

where

$$H_i(s) = \frac{Z_i(s)}{1 + Z_i(s)} \quad (4.13)$$

for  $i = 1, 2$ . Consequently, the transfer functions  $H_i(s)$  can be realized in terms of the feedback systems shown in Fig. 4.4.

By employing the bilinear-LDI lattice digital filter realization technique [29], the discrete-time transfer functions

$$H_i(z) = H_i(s) \Big|_{s=\frac{2}{T} \frac{z-1}{z+1}} \quad (4.14)$$

can be realized in the digital domain as shown in Figs. 4.5 and 4.6 for  $i = 1$  and  $i = 2$ , respectively. Moreover, the values of the constituent multiplier coefficients  $m_{ik_l}$  can be obtained in terms of  $C_{il_l}$ ,  $L_{il_l}$  (for  $l_1 = 1$  and  $l_2 = 1, 2$ ) as given in Tables 4.1 and 4.2 [30].

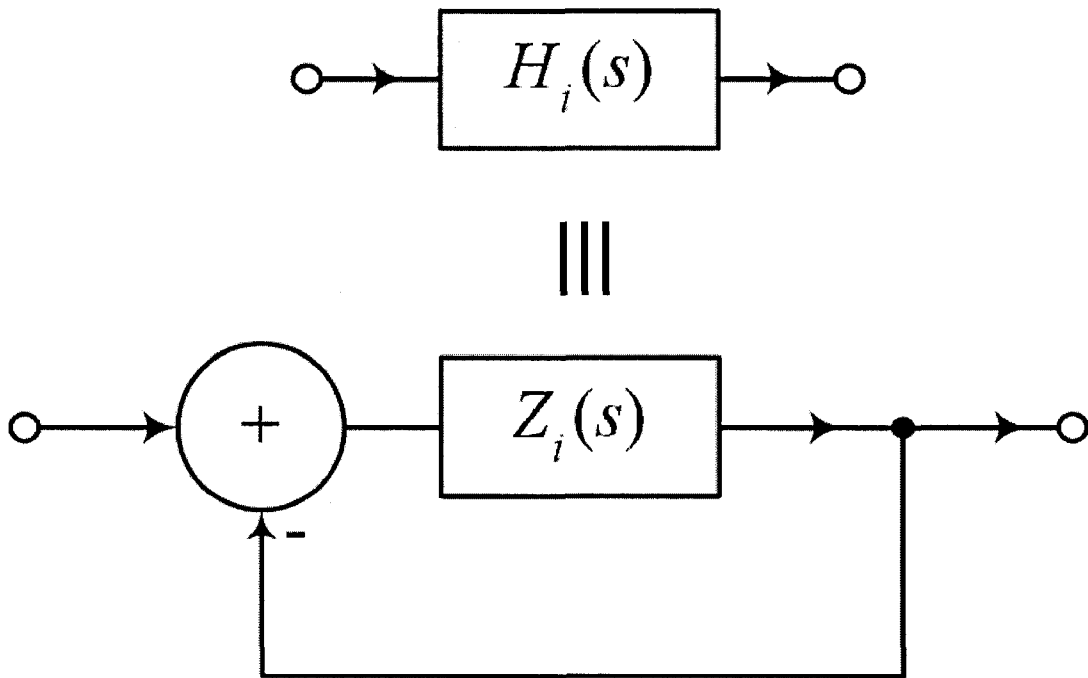


Fig. 4.4. Realization of the Decomposed Transfer functions  $H_i$

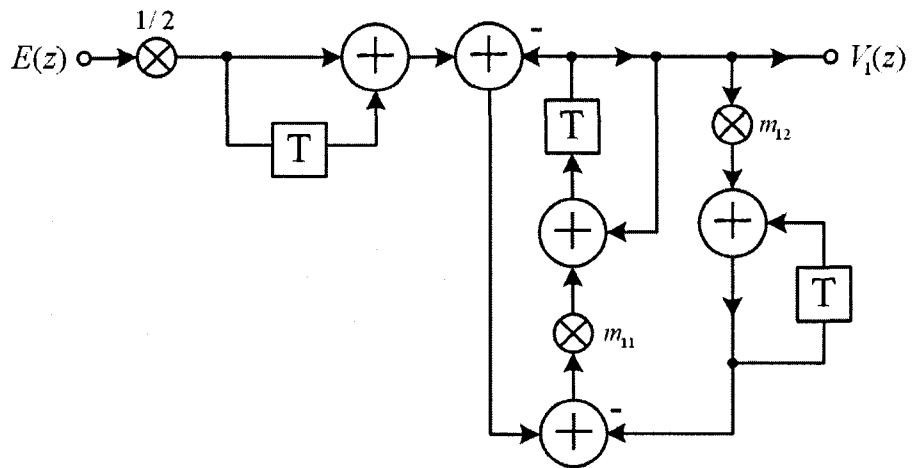


Fig. 4.5. Bilinear-LDI Digital Realization of  $H_1(s)$

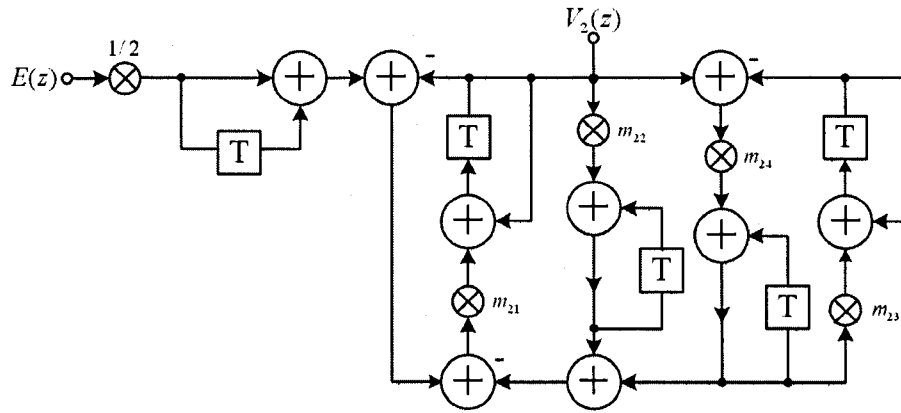


Fig. 4.6. Bilinear-LDI Digital Realization of  $H_2(s)$

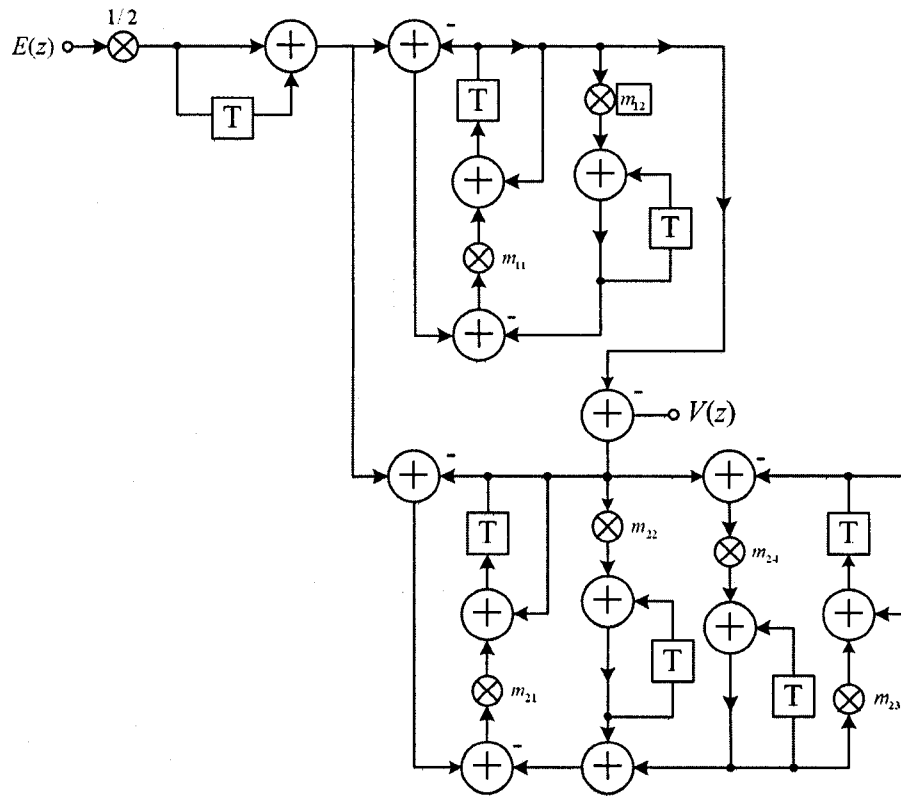


Fig. 4.7. Bilinear-LDI Digital Realization of  $H(s)$

In addition, the transfer function  $H(z)$  can then be realized in accordance with

$$H(z) = \frac{1}{2}H_1(z) - \frac{1}{2}H_2(z) \quad (4.15)$$

$$= H(s) \Big|_{s=\frac{2}{T} \frac{z-1}{z+1}} \quad (4.16)$$

The digital realization of  $H(z)$  is as shown in Fig. 4.7, which is consisted of six multipliers.

Finally, the desired digital IF filter is formed to have a transfer function

$$H_D(z) = [H(z)]^3, \quad (4.17)$$

achieved by a cascade combination of three identical bandpass filter sections each realizing a transfer function of  $H(z)$ .

The infinite-precision seed digital IF filter obtained above is subsequently replaced by a corresponding finite-precision digital IF filter by quantizing the values of the multiplier coefficients  $m_{ik_i}$  to their nearest CSD counterparts (constrained by the pre-specified wordlengths and maximum number of non-zero digits). The finite-precision digital IF filter is manipulated to form an initial population pool of candidate digital IF filter chromosomes by randomly flipping its bits for DCGA optimization.

## 4.4 BIBO Stability Constraints for CSD Digital IF Filters

This section is concerned with the development of appropriate constraints for the guaranteed BIBO stability of the bandpass digital IF filter section in Figs. 4.5 and 4.6 over the CSD multiplier coefficient number format.

TABLE 4.1

Infinite-Precision Multiplier Coefficients for  $H_1(z)$

$m_{11}$	$T / (C_{11} + \frac{T^2}{4L_{11}} + \frac{T}{2R})$
$m_{12}$	$T / L_{11}$

It is not possible to form a digital IF filter chromosome by just concatenating the CSD representation of the constituent multiplier coefficients  $\hat{m}_{ik_i}$  values since in the course of the underlying DCGA optimization, the crossover and mutation operations may lead to offspring digital IF filter chromosomes which no longer conform to the CSD number system constraints in Eqn. 4.8 and 4.9. [16] suggested to resolve this problem by employing an exhaustive indexed LUT of permissible CSD multiplier coefficient values in such a manner that the indices of the multiplier coefficient values form a closed set under crossover and mutation operations. By concatenating the LUT indices of the values of the CSD multiplier coefficients  $\hat{m}_{ik_i}$ , (instead of the values of the CSD multiplier coefficients  $\hat{m}_{ik_i}$  themselves) the offspring digital IF filter chromosomes automatically conform to the CSD number system throughout the course of genetic operations [11].

Having solved the first problem, there still remains the problem that the offspring digital IF filter chromosomes generated in various stages of the DCGA optimization may not be BIBO stable. A straightforward approach to circumvent this problem is to discard any offspring digital IF filter chromosomes which is not BIBO stable. However, this makes the DCGA optimization more time consuming than necessary, essentially rendering it inefficient. The following discussion presents a novel approach to the design and DCGA optimization of guaranteed BIBO stable digital IF filters over the CSD multiplier coefficient space (without generating any intermediate digital IF filter chromosomes which is not BIBO stable) [11].

TABLE 4.2

Infinite-Precision Multiplier Coefficients  $H_2(z)$

$m_{21}$	$T/[C_{21} + \frac{T^2}{4L_{21}} + \frac{T}{2R} + \frac{C_{22}}{(1+4C_{22}L_{22}/T^2)}]$
$m_{22}$	$T/L_{21}$
$m_{23}$	$T(1 + \frac{T^2}{4C_{22}L_{22}})/C_{22}$
$m_{24}$	$\frac{T}{L_3[(C_{22} + \frac{T^2}{4L_{22}})/C_{22}]^2}$

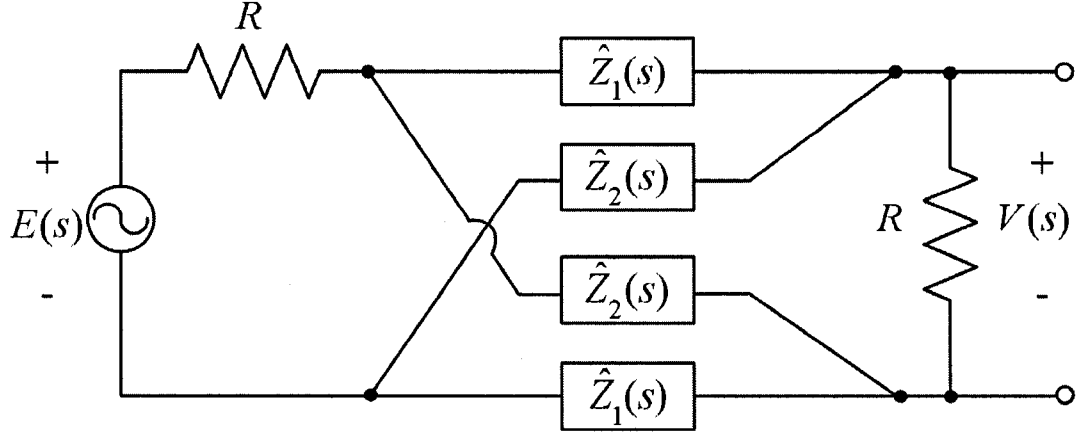


Fig. 4.8. Back-Transformed Analog Prototype Reference Bandpass Filter Section

By reversing the bilinear-LDI lattice digital filter realization technique, the CSD bandpass digital filter section can be back-transformed to an equally resistively terminated symmetrical lattice reactance two-port network as shown in Fig. 4.8. The series arm reactance  $\hat{Z}_1(s)$  and the lattice arm reactance  $\hat{Z}_2(s)$  are as shown in Figs. 4.9a and 4.9b, where  $\hat{C}_{il_i}$  and  $\hat{L}_{il_i}$  (for  $l_1 = 1$  and  $l_2 = 1, 2$ ) are as given in Tables 4.3 and 4.4, where the multiplier coefficients  $\hat{m}_{ik_i}$  represent the quantized CSD counterparts of the infinite-precision multiplier coefficients  $m_{ik_i}$ .

TABLE 4.3

Elements of Back-Transformed Series Arm Reactance  $\hat{Z}_1(s)$

$\hat{C}_{11}$	$-T(\hat{m}_{11}\hat{m}_{12} + 2\hat{m}_{11} - 4)/4\hat{m}_{11}$
$\hat{L}_{11}$	$T/\hat{m}_{12}$

Based on the properties of the bilinear analog-to-digital frequency transformation, in order for the bandpass digital filter section in Figs. 4.5 and 4.6 to be BIBO stable, it is both necessary and sufficient for the values of the elements  $\hat{C}_{il_i}$  and  $\hat{L}_{il_i}$  in Tables 4.3 and 4.4 to be positive. Based on this fact, one can guarantee the BIBO stability of the offspring digital IF filter chromosomes generated in various stages of the DCGA optimization indirectly, simply by ensuring that  $\hat{C}_{il_i} > 0$  and  $\hat{L}_{il_i} > 0$  (see also [31] for some related discussions)

TABLE 4.4

Elements of Back-Transformed Series Arm Reactance  $\hat{Z}_2(s)$ 

$\hat{C}_{21}$	$-T \left( \hat{m}_{22} + 2 - \frac{4}{\hat{m}_{21}} - \frac{4\hat{m}_{24}}{\hat{m}_{23}\hat{m}_{24} - 4} \right) / 4$
$\hat{L}_{21}$	$T / \hat{m}_{22}$
$\hat{C}_{22}$	$-4T / \hat{m}_{23}(\hat{m}_{23}\hat{m}_{24} - 4)$
$\hat{L}_{22}$	$T(\hat{m}_{23}\hat{m}_{24} - 4)^2 / 16\hat{m}_{24}$

[11].

From Table 4.3,

$$\hat{C}_{11} > 0 \Rightarrow -T(\hat{m}_{11}\hat{m}_{12} + 2\hat{m}_{11} - 4) / 4\hat{m}_{11} > 0 \quad (4.18)$$

$$\hat{L}_{11} > 0 \Rightarrow T / \hat{m}_{12} > 0 \quad (4.19)$$

and from Table 4.4,

$$\hat{C}_{21} > 0 \Rightarrow \frac{-T}{4} \left( \hat{m}_{22} + 2 - \frac{4}{\hat{m}_{21}} - \frac{4\hat{m}_{24}}{\hat{m}_{23}\hat{m}_{24} - 4} \right) > 0 \quad (4.20)$$

$$\hat{L}_{21} > 0 \Rightarrow T / \hat{m}_{22} > 0 \quad (4.21)$$

$$\hat{C}_{22} > 0 \Rightarrow \frac{-4T}{\hat{m}_{23}(\hat{m}_{23}\hat{m}_{24} - 4)} > 0 \quad (4.22)$$

$$\hat{L}_{22} > 0 \Rightarrow \frac{T(\hat{m}_{23}\hat{m}_{24} - 4)^2}{16\hat{m}_{24}} > 0 \quad (4.23)$$

In this way, the inequality constraint (4.19) implies

$$\hat{m}_{12} > 0 \quad (4.24)$$

and the inequalities (4.22) and (4.23) imply

$$\hat{m}_{22} > 0 \quad (4.25)$$

$$\hat{m}_{24} > 0 \quad (4.26)$$

Therefore, it remains to satisfy the inequality constraint (4.19), and the inequalities constraints (4.21) and (4.23). In order to simplify matters, it is expedient to assume that

the remaining multiplier coefficients  $\hat{m}_{11}$ , and  $\hat{m}_{21}$  and  $\hat{m}_{23}$  also have positive values <sup>2</sup>. Although this assumption precludes the DCGA optimization from obtaining other potential digital IF filters which may also satisfy the given design specifications, it has the advantage of reducing the size of the three LUTs, and consequently, lead to increased computational speed.

In accordance with the above assumption, the inequality constraint (4.19) can be simplified as

$$\hat{m}_{11}\hat{m}_{12} + 2\hat{m}_{11} - 4 < 0 \quad (4.27)$$

and the inequalities (4.21) and (4.23) can be simplified as

$$\hat{m}_{23}\hat{m}_{24} - 4 < 0 \quad (4.28)$$

$$\hat{m}_{22} + 2 - \frac{4}{\hat{m}_{21}} - \frac{4\hat{m}_{24}}{\hat{m}_{23}\hat{m}_{24} - 4} < 0 \quad (4.29)$$

In this way, in order to make the CSD bandpass digital filter section BIBO stable, it is both necessary and sufficient to choose the values of the multiplier coefficients  $\hat{m}_{ik_i} \in CSD(W, w)$  such that the inequality constraints (4.27), (4.28), and (C.8) are satisfied [11]. The aforementioned constraints are satisfied by employing a LUT-based approach as discussed in the next section.

## 4.5 Novel CSD LUTs for Guaranteed BIBO Stability

The proposed approach for DCGA optimization of BIBO stable digital IF filters over the CSD multiplier coefficient space is based on three independent indexed CSD LUTs, where the constituent indices form closed sets under the genetic operations of crossover and mutation. These LUTs are constructed as follows [11]:

- The first LUT is constructed to include all permissible values for the pair of multiplier coefficients ( $\hat{m}_{11} \in CSD(W, w), \hat{m}_{12} \in CSD(W, w)$ ) satisfying the inequality constraint in (4.27).

---

<sup>2</sup>The, the resulting bilinear-LDI digital IF filter realization becomes compatible with the original LDI digital filter realization technique

- The second LUT is constructed to include all permissible values for the pair of multiplier coefficients ( $\hat{m}_{23} \in CSD(W, w), \hat{m}_{24} \in CSD(W, w)$ ) satisfying the inequality constraint in (4.28).
- The third LUT is constructed to satisfy the inequality constraint (C.8). However, since this constraint concerns the values of four multiplier coefficients (as opposed to two multiplier coefficients for the previous two LUTs), different considerations have to be considered. Let us first replace the inequality constraint (C.8) by a corresponding equality constraint in accordance with

$$\tilde{m}_{22} = -\varepsilon + \frac{4\hat{m}_{24}}{\hat{m}_{23}\hat{m}_{24} - 4} + \frac{4}{\hat{m}_{21}} - 2 \quad (4.30)$$

where  $\varepsilon > 0$  is a positive (finite-precision) slack variable, and  $\tilde{m}_{22}$  is an infinite-precision multiplier coefficient.

It should be pointed out that since the finite-precision slack variable  $\varepsilon$  is always positive, the inequality constraint (4.28) is always satisfied. However, the remaining problem is to truncate the infinite-precision multiplier coefficient  $\tilde{m}_{22}$  properly so as to enable the resulting multiplier coefficient satisfying  $\hat{m}_{22} \in CSD(W, w)$ .

Based on the above discussion, a third LUT is constructed to include all permissible values for the monads  $\hat{m}_{21} \in CSD(W, w)$ . In this way, in the process of encoding the digital IF filter section into a corresponding chromosome, one can bypass any direct reference to the value of the multiplier coefficient  $\hat{m}_{22}$ . Instead, the value of the finite-precision slack variable  $\varepsilon$  can be incorporated as a gene in the construction of the digital IF filter chromosome. This is achieved by representing  $\varepsilon$  by a binary number having a suitable wordlength<sup>3</sup>. Finally,  $\hat{m}_{22} \in CSD(W, w)$  is determined by truncating the infinite-precision multiplier coefficient  $\tilde{m}_{22}$  to its nearest CSD counterpart in the respective LUT. This guarantees that  $\hat{m}_{22}$  conforms to the specified CSD format while satisfying the inequality constraint (C.8).

---

<sup>3</sup>The value of the wordlength is set empirically, starting with a large value which is reduced later so as not to slow down the DCGA optimization. In the ensuring application examples, it has been found that a wordlength of 16 bits is more than adequate for this purpose

In accordance with the above discussions, the bandpass digital IF filter chromosome is formed by an ordered concatenation of

- the first LUT indices referencing the values of the multiplier coefficient pair  $(\hat{m}_{11}, \hat{m}_{12})$
- the second LUT indices referencing the values of the multiplier coefficient pair  $(\hat{m}_{23}, \hat{m}_{24})$ ,
- the third LUT indices referencing the value of the multiplier coefficient monad  $\hat{m}_{21}$  together with the finite-precision slack variable  $\varepsilon$ .

If necessary, the above three CSD LUTs are reduced in size in such a manner that the  $\rho$ -th LUT (for  $\rho = 1, 2, 3$ ) incorporates  $2^{B_\rho}$  rows. As a result, the indices for the  $\rho$ -th LUT can be represented by  $B_\rho$ -bit binary numbers, and the resulting index sets become automatically closed under the operations of crossover and mutations in the course of the underlying DCGA optimization [11].

## 4.6 Design Methodology for the Proposed DCGA Optimization

After generating the CSD LUTs for optimizing digital IF filter, the design methodology for the proposed DCGA optimization of BIBO stable digital IF filters over the CSD multiplier coefficient space can be summarized as follows.

### 4.6.1 Generation of the initial population pool

The starting point in the proposed DCGA optimization is to obtain a corresponding initial infinite-precision seed digital IF filter by using the bilinear-LDI lattice digital filter realization technique as discussed in section 4.2. Then, the resulting infinite-precision multiplier coefficients  $m_{ik_i}$  are quantized to their nearest CSD counterparts to obtain the corresponding finite-precision multiplier coefficients  $\hat{m}_{ik_i}$ , where  $\hat{m}_{ik_i} \in CSD(W, w)$  [32].

Let the value of the finite-precision slack variable  $\varepsilon$  be represented as a  $B_4$ -bit binary number. Then, the initial digital IF filter seed chromosome is formed by successfully concatenating:

- the  $B_1$  block of bits representing the binary LUT index for the multiplier coefficient pair  $(\hat{m}_{11}, \hat{m}_{12})$ ,
- the  $B_2$  block of bits representing the binary LUT index for the multiplier coefficient pair  $(\hat{m}_{23}, \hat{m}_{24})$ ,
- the  $B_3$  block of bits representing the binary index for the multiplier coefficient  $\hat{m}_{21}$ , and
- the  $B_4$  block of bits representing the binary value of the slack variable  $\varepsilon$  [11].

In this way, the first three blocks of bits in the chromosome represent the binary indices of the CSD multiplier coefficient values  $\hat{m}_{11}$ ,  $\hat{m}_{12}$ ,  $\hat{m}_{21}$ ,  $\hat{m}_{23}$ , and  $\hat{m}_{24}$  in the three LUTs, whereas the fourth block of bits represents the binary value of the slack variable  $\varepsilon$ .

Finally, an initial population pool of  $N$  chromosomes is formed by scanning the digital IF filter seed chromosome successively at  $B_\zeta$  block of bits at a time (where  $\zeta = 1, 2, 3, 4$ ), and by randomly flipping bits in the  $\zeta$ -th block of bits in accordance with the probabilistic relationship  $p_F \times 0.5^{B_\zeta+1-b_\zeta}$  (where  $1 \leq b_\zeta \leq B_\zeta$ , and  $p_F$  is a fixed probability factor) from the least significant bit to the most significant one [11].

#### 4.6.2 Formation of the next generation population pool

Having obtained an initial population pool of  $N$  chromosomes, the current population pool  $P(t)$  is manipulated to generate  $N$  offspring through mutation and two-point crossover operations. Then, both the parents and their offspring are combined to form an enlarged population pool  $\hat{P}(t)$  of  $2N$  chromosomes. Duplicate chromosomes are then eliminated so as to maintain diversity and then the chromosomes in the enlarged population pool  $\hat{P}(t)$  are ranked by evaluating their fitness values (as discussed in the following subsection), and

the next generation population pool of  $P(t + 1)$  is subsequently formed by using the CPSS scheme (c.f. Eqn 2.3) [11].

### 4.6.3 Fitness evaluation

The fitness of each of the resulting digital IF filter chromosomes in the enlarged population pool  $\hat{P}(t)$  is evaluated in accordance with

$$fitness = -20 \log_{10}[\max(\epsilon_p, \epsilon_t, \epsilon_s)] \quad (4.31)$$

where

$$\epsilon_p = \max_{\omega \in \Omega_p} [W_p |H(e^{j\omega}) - 1|] \quad (4.32)$$

with  $\Omega_p$  representing the passband frequency regions, and where

$$\epsilon_t = \max_{\omega \in \Omega_t} [W_t |H(e^{j\omega}) - 0.7079|] \quad (4.33)$$

with  $\Omega_t$  representing the 3dB attenuation frequency points, and where

$$\epsilon_s = \max_{\omega \in \Omega_s} [W_s |H(e^{j\omega}) - 0.001|] \quad (4.34)$$

with  $\Omega_s$  representing the 60dB attenuation frequency points. Here,  $W_p$ ,  $W_t$ , and  $W_s$  represent the passband, transition band, and stopband weighing factors, respectively.

## 4.7 Application Examples

This section presents the application of the above DCGA optimization technique to the design of a pair of digital IF filters for two different sets of design specifications.

### 4.7.1 Application example 1:

In this subsection, the proposed DCGA optimization is applied to the design of a BIBO stable digital AMPS IF filter, where the design specifications consist of magnitude frequency-response constraints given in Table 4.5.

In accordance with the above frequency-response design specifications, the values for the elements  $C_{il_i}$  and  $L_{il_i}$  in the analog prototype reference bandpass filter section in Fig. 4.1 are obtained as given in Table 4.6. These element values are obtained:

- by using the bilinear analog-to-digital frequency transformation in Eqn. (4.5) to transform the discrete-time  $z$ -domain bandpass frequency response specifications in Table 4.5 to the corresponding continuous-time  $s$ -domain bandpass frequency-response specifications. This is achieved by replacing  $s$  by  $j\omega$  and  $z$  by  $e^{j\Omega T}$  in Eqn. 4.5 to get:

$$\omega = \frac{2}{T} \tan\left(\frac{\Omega T}{2}\right) \quad (4.35)$$

It should be pointed out that Eqn. 4.35 is a nonlinear mapping between the analog frequency  $\omega$  and digital frequency  $\Omega$ . This is known to give rise to frequency wrapping effect from analog to digital frequencies [31].

- by transforming the resulting  $s$ -domain bandpass frequency-response specifications to the corresponding  $s$ -domain lowpass frequency-response specifications [33],
- by realizing the corresponding analog prototype reference lowpass filter section using the filter design handbook in [25], and
- by transforming the analog prototype reference lowpass filter section back to the corresponding bandpass filter section in Fig. 4.1 using the lowpass to bandpass filter transformation to obtain  $C_{il_i}$  and  $L_{il_i}$ :

$$s = \frac{1}{B} \left( \hat{s} + \frac{\omega_0^2}{\hat{s}} \right) \quad (4.36)$$

where  $s$  is the bandpass filter frequency variable, and  $\hat{s}$  is the lowpass filter frequency variable,  $B$  is the bandwidth and  $\omega_0$  is the central frequency of the corresponding bandpass filter.

Finally, the values of the multiplier coefficients  $m_{ik_i}$  for the infinite-precision seed digital IF filter are obtained in terms of the values of  $C_{il_i}$  and  $L_{il_i}$  (c.f. Table 4.1 and 4.2) as shown in Table 4.7.

The magnitude frequency-response associated with the initial finite-precision seed digital IF filter is as shown in Fig. 4.10. It is observed that the 3dB attenuation frequency point is violated by 2 kHz, and that the 60 dB attenuation frequency point is violated by 27 kHz.

Based on the infinite-precision multiplier coefficients values  $m_{ik_i}$  in Table 4.7, the CSD LUTs for the proposed DCGA optimization are constructed by choosing the remaining design parameters as shown in Table 4.8.

By employing the proposed DCGA optimization technique, the values of the quantized multiplier coefficients  $\hat{m}_{ik_i}$  are obtained as given in Table 4.9 (where the overhat digit  $\hat{1}$  is used to represent  $-1$ ). The magnitude frequency-response of the resulting digital IF filter is as shown in Fig. 4.11. By inspection of Fig. 4.11, the 60dB attenuation frequency points are at 404.6 kHz and 505.7 kHz, and the 3 dB attenuation frequency points are at 444.3 kHz and 465.5 kHz, both satisfying the desired design specifications. The group delay of the resulting digital IF filter is as shown in Fig. 4.12.

The convergence speed for the above DCGA optimization for various values of the shape coefficient parameter  $0.6 \leq c \leq 0.95$  for a fixed  $\alpha$ -value of 0.4 is as shown in Fig. 4.13, with a best convergence within 373 generations when  $c = 0.8$ . In Fig. 4.14, the convergence speed is shown for various values of the exponent parameter  $0.1 \leq \alpha \leq 0.7$  for a fixed  $c$ -value of 0.8, leading to a best convergence within 328 generations when  $\alpha = 0.3$ .

### 4.7.2 Application example 2:

In this second example, the proposed DCGA optimization is applied to the design of a BIBO stable digital IF filter with its center frequency located at 910 kHz, where the design specifications consist of magnitude frequency-response constraints given in Table 4.10.

In much the same way as discussed in the previous example, the values of  $C_{il_i}$  and  $L_{il_i}$  are obtained as given in Table 4.11. Similarly, the values of the multiplier coefficients  $m_{ik_i}$  for the infinite-precision seed digital IF filter are obtained as shown in Table 4.12 in terms of the values of  $C_{il_i}$  and  $L_{il_i}$  (using Table 4.1 and 4.2).

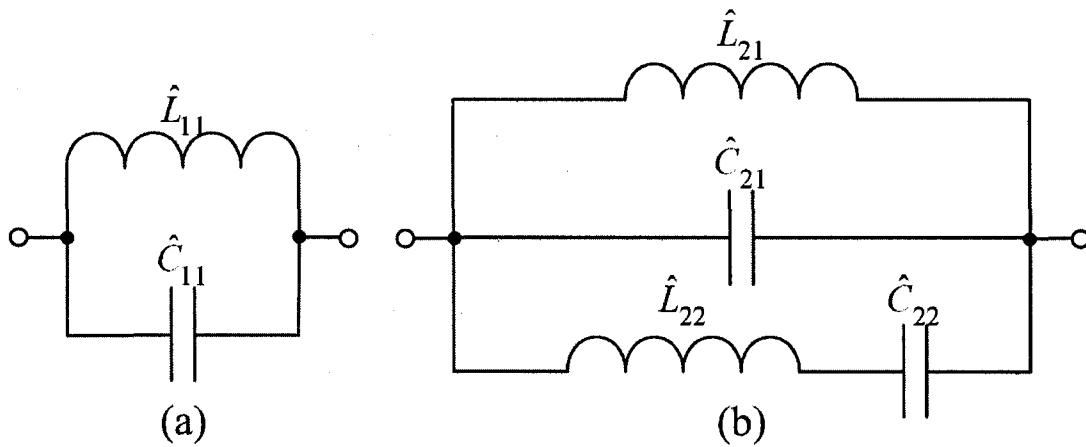


Fig. 4.9. Realization of Back-Transformed Reactance  $\hat{Z}_1(s)$  and  $\hat{Z}_2(s)$

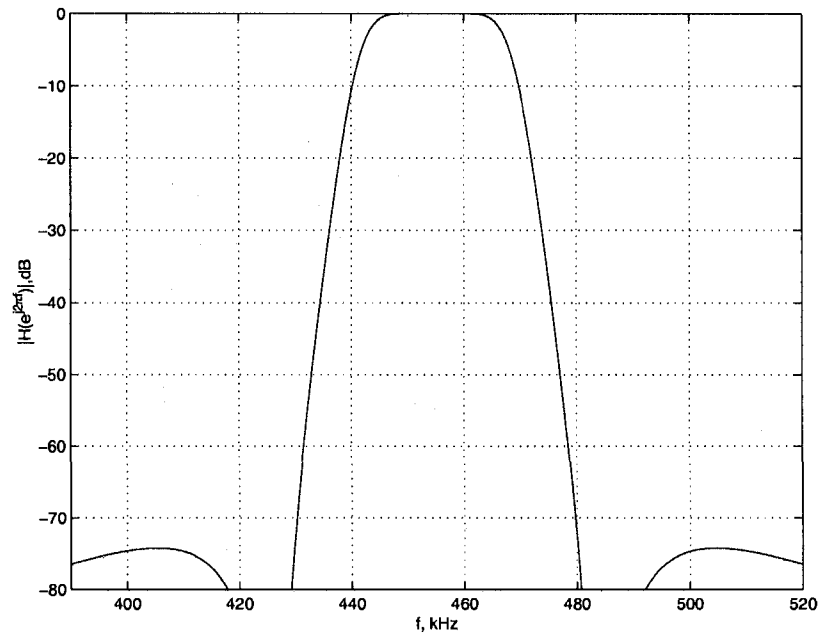


Fig. 4.10. Magnitude Frequency-Response of the Infinite-Precision Digital IF Filter in Example 1

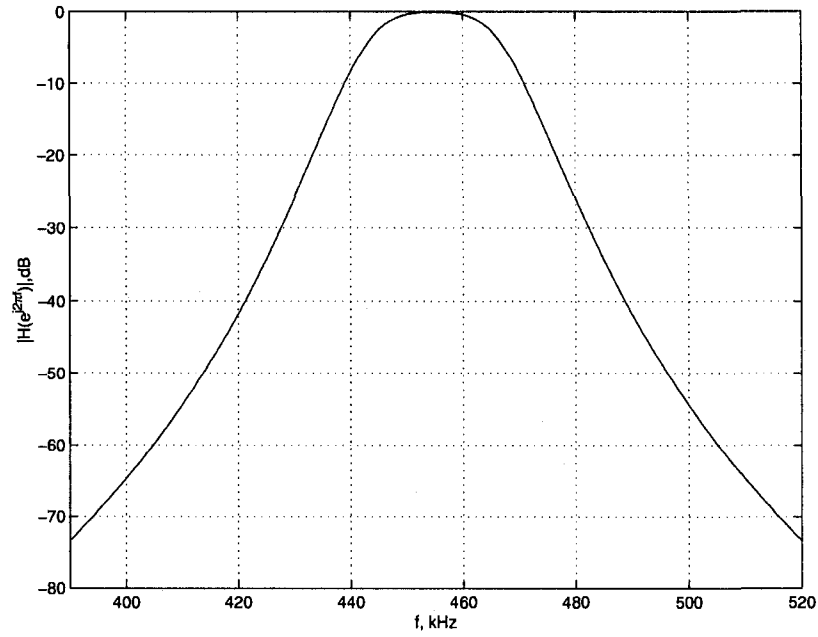


Fig. 4.11. Magnitude Frequency-Response of the Optimized Digital IF Filter for Example 1

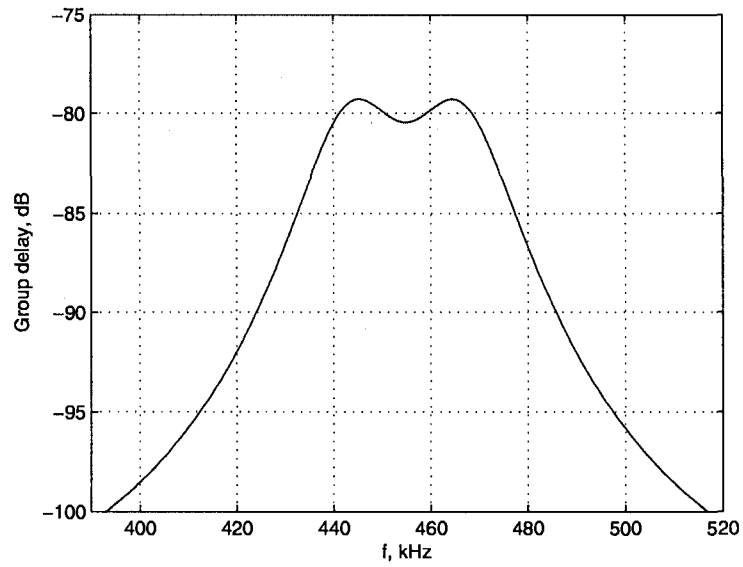


Fig. 4.12. Optimized Digital IF Filter Group Delay after DCGA Application in Example 1

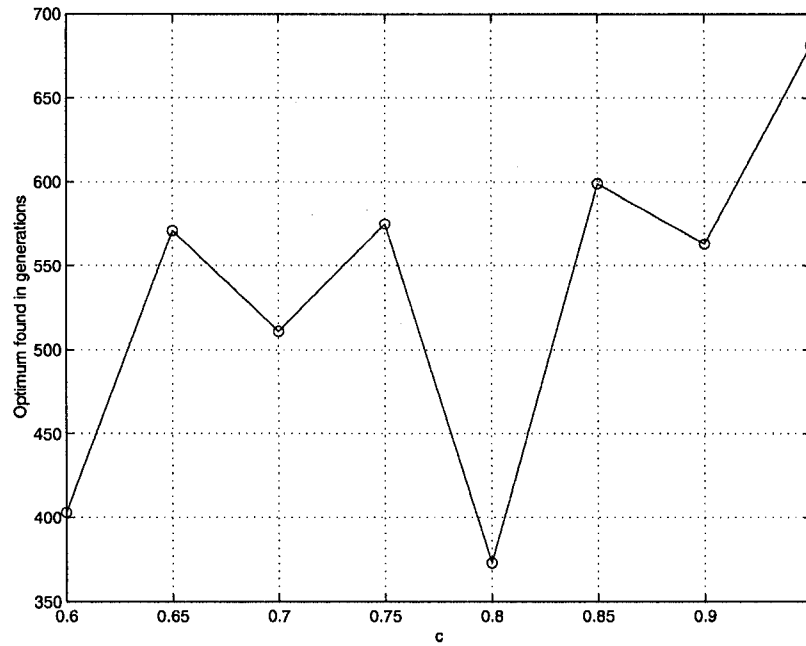


Fig. 4.13. Convergence Speeds for various  $c$ -values in Example 1

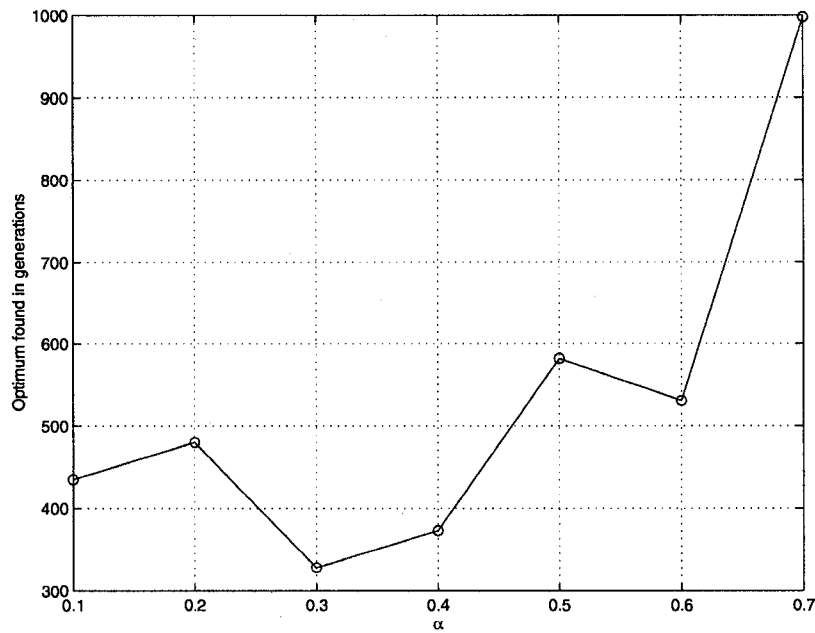


Fig. 4.14. Convergence Speeds for various  $\alpha$ -values in Example 1

The magnitude frequency-response associated with the initial finite-precision seed digital IF filter is as shown in Fig. 4.15. It is observed that the 3dB attenuation frequency point is violated by 2.5 kHz, and that the 60 dB attenuation frequency point is violated by 26 kHz.

Based on the infinite-precision values for the multiplier coefficients  $m_{ik_i}$  (in Table 4.12), the CSD LUTs for the proposed DCGA optimization are constructed by choosing the remaining design parameters as shown in Table 4.13.

By employing the proposed DCGA optimization technique, the values of the quantized multiplier coefficients  $\hat{m}_{ik_i}$  are obtained as given in Table 4.14. The magnitude frequency-response of the resulting digital IF filter is as shown in Fig. 4.16. By inspection of Fig. 4.16, the 60dB attenuation frequency points are at 867 kHz and 956 kHz, and the 3 dB attenuation frequency points are at 899.4 kHz and 920.5 kHz, both satisfying the desired design specifications. The group delay of the resulting digital IF filter is as shown in Fig. 4.17.

The convergence speed for the above DCGA optimization for various values of the shape coefficient parameter  $0.6 \leq c \leq 0.95$  for a fixed  $\alpha$ -value of 0.4 is as shown in Fig. 4.18, with a best convergence within 505 generations when  $c = 0.75$ . In Fig. 4.19, the convergence speed is shown for various values of the exponent parameter  $0.1 \leq \alpha \leq 0.7$  for a fixed  $c$ -value of 0.8, leading to a best convergence within 498 generations when  $\alpha = 0.3$ .

## 4.8 Summary

This chapter has been concerned with DCGA optimization of digital IF filters over the finite-precision CSD multiplier coefficient space. This optimization technique exploits the bilinear-LDI lattice digital filter design approach for the realization of the required initial infinite-precision seed digital IF filter chromosome. However, a direct application of DCGA technique to the digital IF filters may give rise to two separate problems. One is that the operations of crossover and mutation in the course of DCGA optimization may

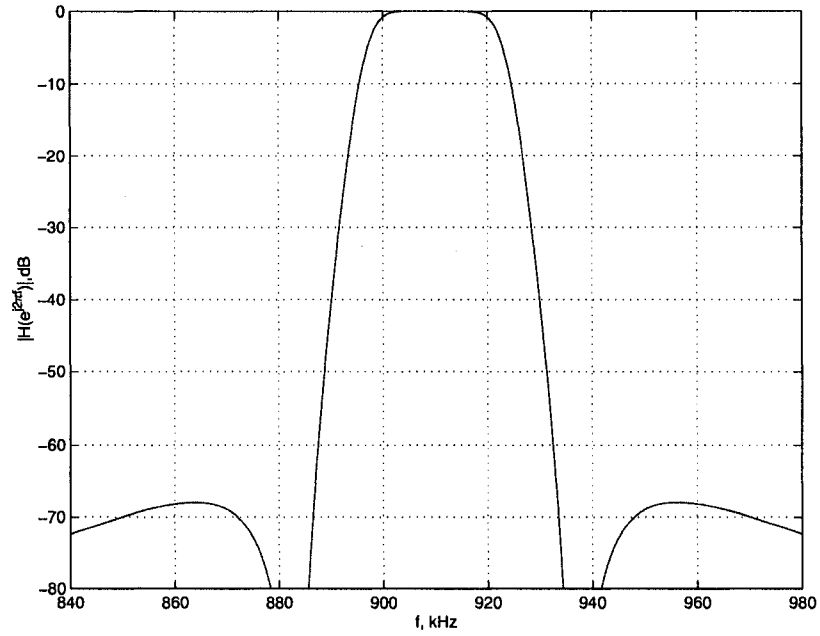


Fig. 4.15. Magnitude Frequency-Response of the Infinite precision Digital IF Filter in Example 2

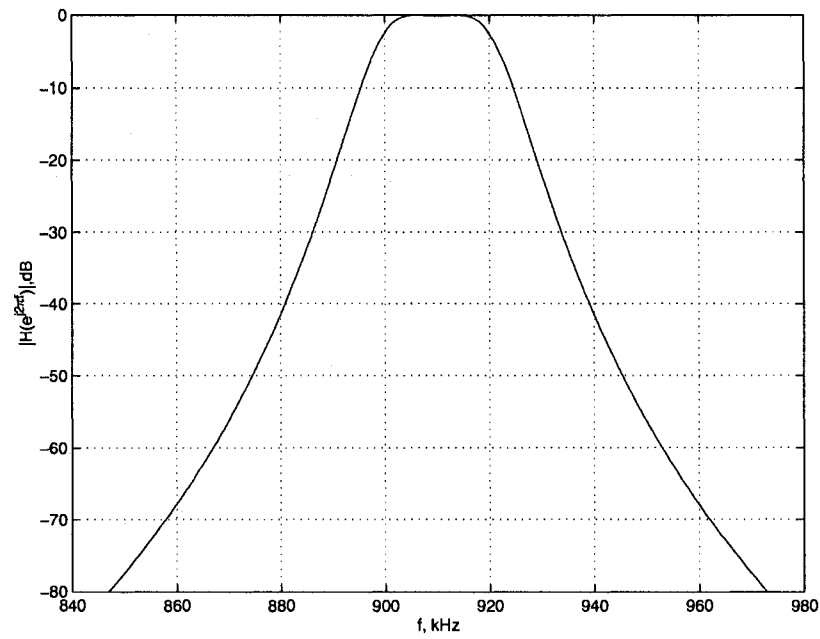


Fig. 4.16. Magnitude Frequency-Response of the Optimized Digital IF Filter in Example 2

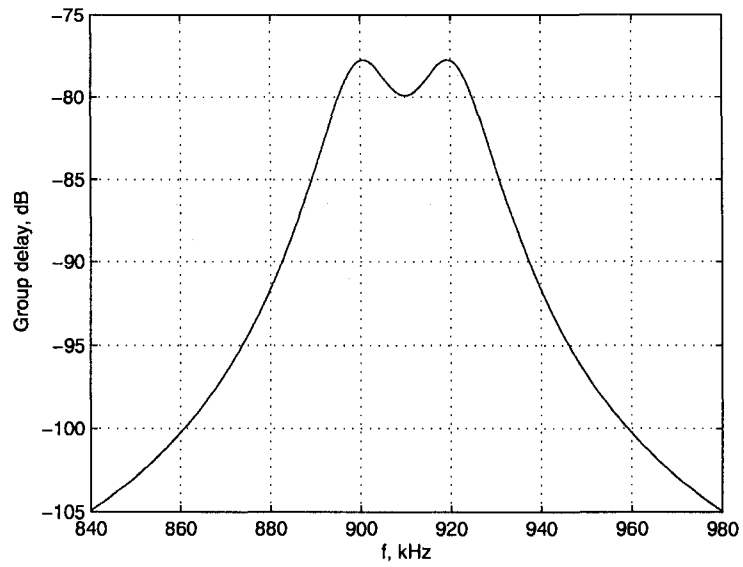


Fig. 4.17. Optimized Digital IF Filter Group Delay after DCGA Application in Example 2

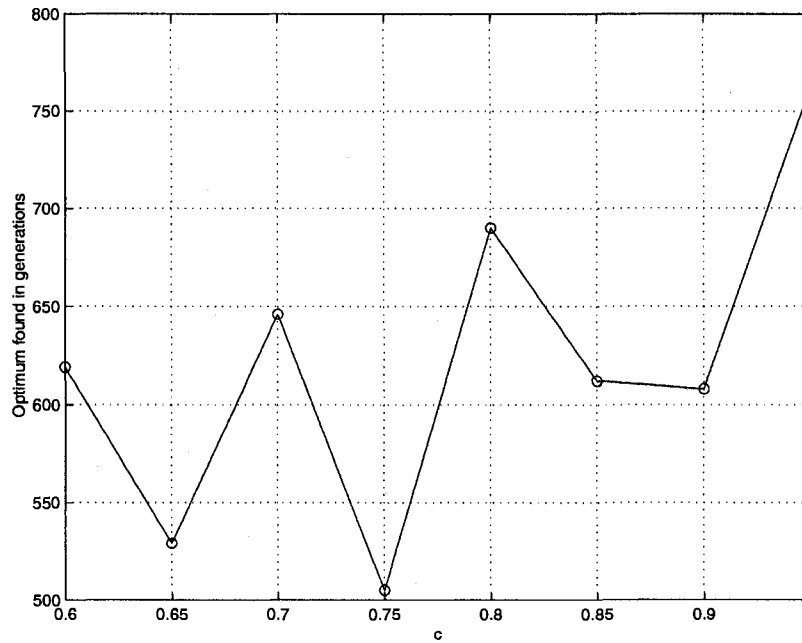


Fig. 4.18. Convergence Speeds with various c-values in Example 2

produce chromosomes which no longer conform to the CSD number format. The other is that DCGA optimization may produce a solution chromosome which leads to a digital IIR IF filter that is not BIBO stable.

Therefore, three separate LUTs have been proposed, which uses the indices of the resulting multiplier coefficient in the LUTs as opposed to their values to represent digital IF filter chromosome. The resulting LUT-based DCGA optimization technique is illustrated through its application to the design of a pair of digital IF filters satisfying different design specifications.

TABLE 4.5  
Digital IF Filter Design Specifications for Example 1

Center frequency	455 kHz
Bandwidth	21 kHz
3 dB attenuation frequency regions	
Lower passband (444 kHz, 445 kHz)	Upper passband (465 kHz, 466 kHz)
60 dB attenuation frequency regions	
Lower stopband (403 kHz, 407 kHz)	Upper stopband (503 kHz, 507 kHz)

TABLE 4.6  
Analog Element Values  $C_{i_l}$  and  $L_{i_l}$  for Example 1

$C_{11}$	$2.4045\mu F$
$L_{11}$	$0.3139nH$
$C_{21}$	$0.4288\mu F$
$L_{21}$	$0.1760\mu H$
$C_{22}$	$17.3120nF$
$L_{22}$	$4.3597\mu H$

TABLE 4.7  
Infinite-Precision Multiplier Coefficient Values for Example 1

$m_{ik_i}$	Decimal Value
$m_{11}$	0.1081
$m_{12}$	17.5044
$m_{21}$	0.0806
$m_{22}$	23.7373
$m_{23}$	31.7382
$m_{24}$	0.0630

TABLE 4.8  
Parameter values for Constructing the CSD LUTs for Example 1

$W_I$	6 bits
$W_F$	6 bits
$w$	5 bits
$\hat{m}_{21}$ table size	$2^{11} \times 12$
$\hat{m}_{11}, \hat{m}_{12}$ table size	$2^{16} \times 24$
$\hat{m}_{23}, \hat{m}_{24}$ table size	$2^{17} \times 24$

TABLE 4.9

Finite-Precision Multiplier Coefficient Values after DCGA Optimization for Example 1

$\hat{m}_{ik_i}$	CSD Representation	Decimal Value
$\hat{m}_{11}$	000000.000101	0.0781
$\hat{m}_{12}$	10 $\hat{1}$ 010. $\hat{1}$ 00010	25.5313
$\hat{m}_{21}$	000000.000101	0.0781
$\hat{m}_{22}$	10 $\hat{1}$ 000. $\hat{1}$ 01000	23.6250
$\hat{m}_{23}$	00100 $\hat{1}$ .00000 $\hat{1}$	6.9844
$\hat{m}_{24}$	000000.00010 $\hat{1}$	0.0469

TABLE 4.10

Digital IF Filter Design Specifications for Application Example 2

Center frequency	910 kHz
Bandwidth	21 kHz
3 dB attenuation frequency regions	
Lower passband (899 kHz, 900 kHz)	Upper passband (920 kHz, 921 kHz)
60 dB attenuation frequency regions	
Lower stopband (858 kHz, 862 kHz)	Upper stopband (958 kHz, 962 kHz)

TABLE 4.11

Analog Element values  $C_{il_i}$  and  $L_{il_i}$  for Example 2

$C_{11}$	$2.3590\mu F$
$L_{11}$	$7.9984nH$
$C_{21}$	$0.5136\mu F$
$L_{21}$	$36.7630nH$
$C_{22}$	$4.4185nF$
$L_{22}$	$4.2703\mu H$

TABLE 4.12

Infinite-Precision Multiplier Coefficient Values for Example 2

$m_{ik_i}$	Decimal Value
$m_{11}$	0.0566
$m_{12}$	34.3476
$m_{21}$	0.0397
$m_{22}$	49.3043
$m_{23}$	62.1765
$m_{24}$	0.0322

TABLE 4.13

Parameter Values for LUTs in Example 2

$W_I$	7 bits
$W_F$	6 bits
$w$	5 bits
$\hat{m}_{21}$ table size	$2^{12} \times 12$
$\hat{m}_{11}, \hat{m}_{12}$ table size	$2^{17} \times 24$
$\hat{m}_{23}, \hat{m}_{24}$ table size	$2^{18} \times 24$

TABLE 4.14

Finite-Precision Multiplier Coefficient Values after DCGA for Example 2

$\hat{m}_{ik_i}$	CSD Representation	Decimal Value
$\hat{m}_{11}$	0000000.000010	0.0313
$\hat{m}_{12}$	1000010.001000	61.8750
$\hat{m}_{21}$	0000000.000010	0.0313
$\hat{m}_{22}$	1000000.001001	64.1090
$\hat{m}_{23}$	1000001.001000	62.8750
$\hat{m}_{24}$	0000000.000001	0.0156

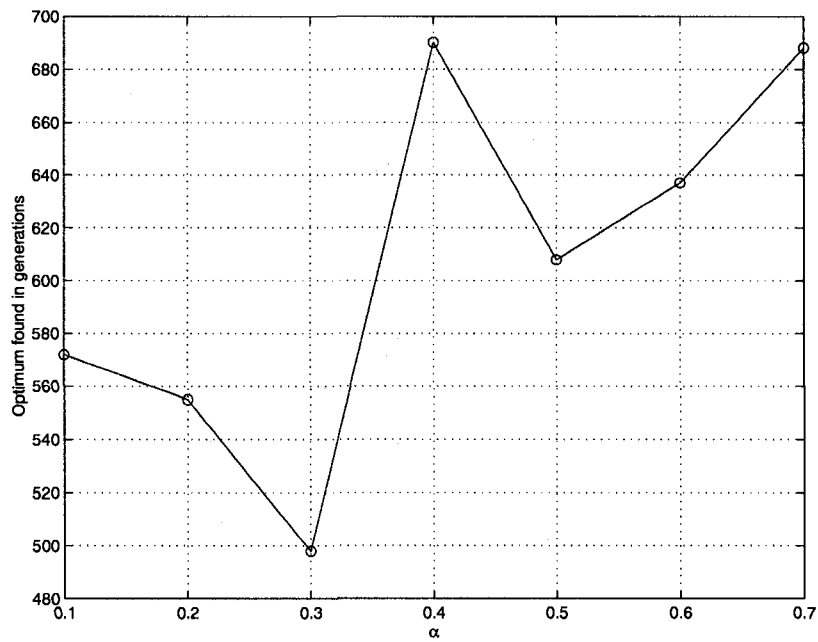


Fig. 4.19. Convergence Speeds with various  $\alpha$ -values in Example 2

# Chapter 5

## Conclusion

### 5.1 Conclusion

This thesis has been concerned with the design and discrete optimization of two different classes of IF filters in current IC fabrication technologies, one being an analog OTA-C IF filter and the other being a digital IF filter. The design of OTA-C IF filter is based on a prototype passive RLC bandpass filter section. By replacing the passive elements (resistors and inductors) with their OTA-C combinations, the corresponding OTA-C bandpass filter has been obtained. A cascaded combination of three such identical OTA-C bandpass filters gives rise to an eighteenth-order OTA-C IF filter consisting of 39 OTAs and 18 capacitors.

The optimization of OTA-C IF filters can be achieved by employing either the existing gradient-based optimization techniques or conventional GAs. The latter approach is well known for its effectiveness and efficiency in solving complex multimodal optimization problems. However, the conventional GAs suffer from low convergence speed problems that usually have a high tendency to converge towards a local optimal point. Therefore, this thesis has applied diversity control in addition to GA for the rapid optimization of OTA-C IF filters. DCGA has the advantage of increasing the diversity of the population pool through the incorporation of additional non-elite chromosomes (chosen based on their hamming distance from the chromosome with the best fitness value).

In OTA-C IF filter optimization, DCGA starts from a seed chromosome obtained from quantizing the constituent 39 OTA transconductance gains to their nearest binary counterparts (the capacitors have been assigned with fixed values). Then, this seed chromosome is randomly flipped to generate an initial population pool. Through evolution from one generation to the next, the desired IF filter satisfying the required design specifications has been obtained.

This thesis has presented an application example for an OTA-C AMPS IF filter operating around a center frequency of 455 kHz. Through investigation over a region of DCGA external control parameters, a fastest convergence of 167 generations has been reached when the shape coefficient is 0.8 and the exponent is 0.5.

In addition, this thesis has presented DCGA optimization of digital IF filters over the finite-precision CSD multiplier coefficient space. This optimization technique exploits the bilinear-LDI lattice digital filter realization approach for the realization of the required initial seed digital IF filter chromosome. Three separate LUTs have been proposed, which use the indices of the resulting multiplier coefficients in the LUTs as opposed to their values to represent digital IF filter chromosome. The reason for the use of such LUTs is because a direct application of DCGA technique to the digital IF filters may give rise to two separate problems. The first problem is that the operations of crossover and mutation in the course of DCGA optimization may produce chromosomes which no longer conform to the CSD number format. The second problem, on the other hand, is that the DCGA optimization may produce a solution chromosome which leads to a digital IIR IF filter that is not BIBO stable.

The resulting LUT-based DCGA optimization is illustrated through its application to the design of a pair of digital IF filters satisfying two different design specifications.

## 5.2 Summary of Contributions

The contributions of this thesis are summarized in the following.

- This thesis has presented a step-by-step procedure to show how to obtain an OTA-

C filter from a corresponding analog prototype passive RLC filter. The resulting analog OTA-C IF filter is guaranteed BIBO stable provided that all the constituent transconductances are positive.

- This thesis has demonstrated the usefulness of DCGA technique to optimize magnitude frequency-response of an OTA-C IF filter. The convergence speed of the proposed DCGA optimization outperforms that of previous optimization using conventional GAs by an order of magnitude.
- This thesis has presented the first discrete optimization of digital IF filter employing DCGA.
- This thesis has demonstrated the use of bilinear-LDI technique for realization of digital IF filters. The resulting digital IF filter preserves the frequency-response characteristics of the corresponding analog prototype passive RLC filter.
- This thesis has proposed the use of an efficient LUT-based technique for representing digital IF filter chromosomes in terms of their LUT indices. The LUTs presented in Chapter 4 not only guarantee the conformance to the CSD number format, but also ensure that the finite-precision CSD digital IF filter chromosomes generated in the course of DCGA optimization are guaranteed to be BIBO stable (without generating intermediate digital IF filter chromosomes which are not BIBO stable).
- This thesis has conducted an empirical investigation on a pair of DCGA control parameters (namely, the shape coefficient and the exponent) in order to find their best suitable values for rapid convergence.
- This thesis has also applied DCGA to optimize frequency-response of FIR digital filters exhibiting sharp transition bands in a related research as discussed in the Appendix.

### 5.3 Suggestions for Future Work

Further work involves the improvement of DCGA convergence speed through dynamic adjustments of the shape coefficient and the exponent. It may be reasonable to encode those two parameters as chromosomes in the process of DCGA optimization. This will increase the length of the chromosome, but may lead to noticeable reduction in the time spent on empirical investigations.

The bilinear-LDI lattice digital filter design approach has been employed in the design of proposed digital IF filters. Future work involves different realization approaches of the digital IF filter (e.g. the wave digital or the bilinear-LDI digital Jaumann filter realization approach).

This thesis has provided three separate LUTs for guaranteed BIBO stable sixth-order IIR bandpass filter. It has been shown that IIR digital filters exhibits much shorter filter length and hardware cost compared to the FIR counterpart. However, the resulting filter may be BIBO unstable due to the presence of feedback loops. Therefore, it is expedient to design higher order IIR filters employing the LUT-based technique (e.g. FRM IIR filters). In the future work, one need to apply similar principles to develop a systematic approach for DCGA optimization of higher order IIR filters.

# Appendix A

## Author's Contribution

### Referred Journal Publications:

- Y. Wu and B. Nowrouzian, "A Novel Approach to the Design of BIBO Stable Digital IF Filters over CSD Multiplier Coefficient Space Employing a Diversity Controlled Genetic Algorithm," *Journal of Circuits, Systems and Signal Processing (CSSP)*, Submitted for review.
- S. Kilambi, B. Nowrouzian, and Y. Wu, "A Novel Diversity Controlled Genetic Algorithm for Rapid Optimization of Bandpass FRM FIR Digital Filters Over CSD Multiplier Coefficient Space," *Journal of Circuits, Systems and Signal Processing (CSSP)*, Accepted for publish.
- S. Kilambi, Y. Wu, and B. Nowrouzian, "Rapid Optimization of FRM FIR Lowpass Digital Filters over CSD Multiplier Coefficients Space Using a Diversity Controlled Genetic Algorithm," *Microelectronics Journal*, Submitted for review.

### Referred Conference Publications:

- Y. Wu and B. Nowrouzian, "Application of Diversity Controlled Genetic Algorithms to the Design and Optimization of OTA-C IF Filters," in *IEEE International Conference on Electronics, Circuits and Systems*, Marrakech, Morocco, December 2007.

- Y. Wu and B. Nowrouzian, "A Novel Technique for the Design and DCGA Optimization of Bilinear-LDI Lattice-Based Digital IF Filters," in *IEEE International Symposium on Circuits and Systems*, Seattle, USA, May 2008.

## Appendix B

### DCGA Optimization of FRM FIR

### Lowpass Digital Filters

Linear-phase FIR digital filters with sharp transition bands have many practical applications in modern digital signal processing systems [34, 35]. These kinds of filters usually lead to a high degree of computational complexity in their hardware implementations since the length of an FIR digital filter is inversely proportional to its transition bandwidth [36, 37]. In general, the multiplication operation is the most cost-intensive part in the digital filter implementation. Therefore, there is every incentive to reduce the number of multiplication operations in the FIR digital filter realization techniques [38].

It is well known that the frequency-response masking (FRM) approach provides one of the most efficient techniques for the design of sharp transition bands linear-phase FIR digital filters. This technique employs lower order digital subfilters with gradual transition bands in such a manner as to realize very narrow transition bandwidths in the overall FRM FIR digital filter. The resulting FIR digital filters turn out to have an inherently large number of zero-valued multiplier coefficients, leading to a substantial reduction in the computational complexity of the resulting digital filter [39] as discussed in Chapter 4. This appendix is concerned with the application of DCGA to the design and rapid optimization of FRM FIR lowpass digital filters incorporating floating radix-point CSD multiplier

coefficients [38].

As discussed in Chapter 4, the multiplier coefficients  $\hat{m}_i$  usually have a general CSD number format in the form:

$$\hat{m}_i = \text{CSD}(W, w) = \sum_{k=1}^W D_{i,k} 2^{R-k} \quad (\text{B.1})$$

where  $W$  represents the common multiplier coefficient wordlength, where  $w$  represents the maximum number of nonzero bits within the coefficient wordlength, and where  $0 < R < W$  represents a floating radix-point. In addition, the CSD number system has the following constraints:

$$\begin{aligned} D_{i,k} &\in \{1, -1, 0\} \\ D_{i,k} \times D_{i,k+1} &= 0 \end{aligned} \quad (\text{B.2})$$

$$\sum_{k=1}^W |D_{i,k}| \leq w, \quad (\text{B.3})$$

## B.1 Overview of FRM FIR Lowpass Digital Filter Design Approach

This section is concerned with the design of linear-phase FIR digital filters which exhibit sharp transition bands using the conventional FRM approach. Let us consider a linear-phase FIR lowpass digital filter having a transfer function  $H_F(z)$ . In the conventional FRM approach [39], the transfer function  $H_F(z)$  is realized by using a configuration as shown in Fig. B.1. In Fig. B.1,  $H_a(z)$  represents a linear-phase lowpass band-edge shaping transfer function, and  $H_b(z)$  represents the complementary highpass band-edge shaping transfer function having a magnitude frequency-response in accordance with

$$H_b(z) = z^{-(N_a-1)/2} - H_a(z) \quad (\text{B.4})$$

where  $N_a$  represents the order of  $H_a(z)$ . Moreover,  $H_a(z^L)$  and  $H_b(z^L)$  are the interpolated band-edge shaping transfer function obtained from  $H_a(z)$  and  $H_b(z)$  by replacing each unit-delay by  $L$  unit-delays (usually called  $L$ -fold interpolation). In addition,  $H_{am}(z)$  and  $H_{mb}(z)$  represent a pair of lowpass masking digital sub-filters with gradual transition bands, responsible for suppressing the unwanted image components generated by  $H_a(z^L)$  and  $H_b(z^L)$ . Finally, the overall FRM FIR lowpass digital filter transfer function is given by

$$H_F(z) = H_a(z^L)H_{ma}(z) + H_b(z^L)H_{mb}(z) \quad (\text{B.5})$$

Let  $\Delta = \omega_s - \omega_p$  represents the transition bandwidth of the lowpass band-edge shaping transfer function  $H_a(z)$ , with  $\omega_p$  representing its passband-edge frequencies, and with  $\omega_s$  representing its stopband-edge frequencies. The transition bandwidth of the resulting FIR digital filter is given by  $\Delta/L$ . In this way, the overall FRM FIR lowpass filter therefore has a  $L$  times narrowed transition bandwidth.

In accordance with the above discussions, the overall FRM FIR digital filter transfer function  $H_F(z)$  involves a total number of multiplications of  $N_{total} = L \times N_a + N_{ma} + N_{mb}$ , where  $N_{ma}$  and  $N_{mb}$  represent the order of the masking transfer functions  $H_{ma}(z)$  and  $H_{mb}(z)$ , respectively [38].

## B.2 Design Methodology

The proposed design methodology is concerned with the optimization of an FRM FIR lowpass digital filter having a transfer function  $H_F(z)$  over the CSD multiplier coefficients  $\hat{m}_i$  space (constructed by the digital subfilters  $H_a(z)$ ,  $H_{ma}(z)$  and  $H_{mb}(z)$ ).

The values of the multiplier coefficients  $\hat{m}_i$  are usually represented as fixed or floating radix-point binary numbers in the conventional GA optimization of FRM FIR digital filters as digital filter chromosome. This facilitates the encoding of the FRM FIR digital filter multiplier coefficients into digital filter chromosomes by concatenating their binary representations [38].

An initial population pool of candidate chromosomes is formed by randomly comple-

menting bits in the FRM FIR seed digital filter chromosome which is usually obtained via the conventional continuous optimization approach (e.g. the Parks-McClellan approach).

Unfortunately, in the case of CSD multiplier coefficient representations, after an operation which would be equivalent to complementing bits in binary representations, one may arrive at a chromosome which violates the CSD number format in Eqn. C.3. Then the offspring chromosome no longer conforms to the CSD number format. Similar problems also arise under the operations of crossover and mutation in the course of GA optimization. This problem can be successfully solved by generating an indexed LUT of permissible CSD multiplier coefficient values as discussed in the following [38].

### B.2.1 Generation of CSD LUT

The CSD LUT is developed as a two-column table consisting of permissible CSD multiplier coefficient values and their binary indices as discussed below.

Let  $W_I$  represents the wordlength associated with the integer part of the multiplier coefficient  $\hat{m}_i$  in floating radix-point CSD format, and  $W_F$  represents that associated with the fractional part of  $\hat{m}_i$  (total wordlength of  $\hat{m}_i$  is  $W = W_I + W_F$ ). In practical situations,  $W_I$  is chosen to accommodate the representation of the maximum integer values of the infinite-precision multiplier coefficients  $m_i$ , and the fractional length  $W_F$  is chosen based on the interplay between satisfying the magnitude frequency-response specifications and the hardware implementation cost. Since all the CSD multiplier coefficients  $\hat{m}_i$  have the same  $W_I$  and  $W_F$ , it is necessary and sufficient to form a single LUT to contain all the permissible CSD multiplier coefficients values. In this way, each CSD multiplier coefficient  $\hat{m}_i$  can be referenced by its index in the LUT [38].

The length of the LUT is restricted to a power of 2 number ( $2^B$ ) so as to enable binary representation of all the indices as B-bit strings. Then, the seed chromosome is obtained by concatenating the binary representation of the indices associated with the CSD multiplier coefficient values as opposed to the values of the multiplier coefficients themselves. Moreover, the set of B-bit indices are chosen in such a manner that they form a closed set

under the operations of crossover, mutation, and bits complementing [16]. In this way, due to the closedness of the index set, the seed chromosome will always result in chromosomes which conform to the original CSD number system in GA operations. Therefore, a CSD FRM digital filter chromosome can be represented by a binary bit-string of length  $B \times M$  bits, where  $M$  represents the total number of multiplier coefficients  $\hat{m}_i$ . It should be pointed out that since the same LUT is used in connection with all the multiplier coefficients  $\hat{m}_i$ , it has a relatively small computer memory requirement [38].

### B.2.2 Generation of Initial Population Pool

Let us constrain the permissible CSD multiplier coefficient values to a pre-specified wordlength of  $W$  bits, and to a pre-specified maximum number of  $w$  non-zero bits within the wordlength.

The starting point in the proposed DCGA optimization is to obtain a corresponding initial infinite-precision seed FRM FIR digital filter, achieved by applying the conventional Parks-McLellan optimization technique to obtain the multiplier coefficients  $m_i$  of the constituent digital subfilters  $H_a(z)$ ,  $H_{ma}(z)$  and  $H_{mb}(z)$ . Then, the initial CSD FRM FIR finite-precision digital filter can be obtained simply by approximating the values of the infinite-precision seed multiplier coefficients  $m_i$  to their closest CSD counterparts in the above LUT. Then, the indices of the finite-precision multiplier coefficients  $\hat{m}_i$  are concatenated to obtain the finite-precision FRM FIR digital filter chromosome.

The initial population pool of  $N$  chromosomes is formed by perturbing the above digital filter chromosome  $B$  bits (i.e. one binary index) at a time, where the  $b^{th}$  bit (with  $1 \leq b \leq B$  from the least significant to the most significant bit) is complemented by using the probabilistic relation  $p_F \times (0.5)^{B+1-b}$ , where  $p_F$  is a fixed probability factor [38].

### B.2.3 Formation of the Next Generation Population pool

The current population pool  $P(t)$  of size  $N$  is replaced by an enlarged population pool  $\hat{P}(t)$  of size  $2N$  by using the crossover and mutation operations.

The chromosomes in the enlarged population pool  $\hat{P}(t)$  are ranked by evaluating their

fitness values, and duplicate chromosomes are eliminated so as to maintain diversity. The next generation population pool of  $P(t+1)$  is formed by using the CPSS scheme (c.f. Eqn 2.3).

#### B.2.4 Fitness evaluation

The fitness of each of the resulting FRM FIR lowpass digital filter chromosomes in the enlarged population pool  $\hat{P}(t)$  is evaluated in accordance with

$$fitness_1 = -20 \log [\max \{ \epsilon_p, \epsilon_s \}] + C, \quad (B.6)$$

where

$$\epsilon_p = \underbrace{\max}_{\omega \in \Omega_p} [W_p |H(e^{j\omega}) - 1|] \quad (B.7)$$

with  $\Omega_p$  representing the passband frequency region, and where

$$\epsilon_s = \underbrace{\max}_{\omega \in \Omega_s} [W_s |H(e^{j\omega})|] \quad (B.8)$$

with  $\Omega_s$  representing the stopband frequency region. Here,  $W_p$  and  $W_s$  are passband and stopband weighting factors, and  $C$  is a constant chosen so as to make  $fitness_1 > 0$ .

Through the course of empirical investigations it has become apparent that the most-fit chromosome inferred by  $fitness_1$  in Eqn. B.6 may not necessarily satisfy all the given magnitude frequency-response specifications [8]. This is mainly due to an inherent tendency of DCGA which amounts to over optimizing the frequency-response over certain frequency points in the stopband region at the expense of drastically under optimizing the magnitude frequency-response over other frequency points in the passband. In order to alleviate this problem,  $fitness_1$  is modified through the addition of a penalty function in accordance with [8]

$$fitness_2 = fitness - \beta \times penalty \quad (B.9)$$

where  $\beta$  is a weighting factor. Eqn. B.9 penalizes the stopband frequency points where the magnitude frequency-response is over-killed by treating such chromosomes as less fit.

The over-optimized frequency points are considered as such points where the stopband magnitude frequency-response falls within a lower limit of  $M_l$  and upper limit of  $M_u$ , where  $M_l$  and  $M_u$  are greater than the specified stopband gain [38]. The penalty function is given by the relation

$$penalty = \frac{\sum_{i=1}^{i=P} |H_F(e^{j\omega})|_{stopband}}{P} \quad (\text{B.10})$$

where  $|H_F(e^{j\omega})|_{stopband}$  represents stopband magnitude frequency-response points falling within the range  $M_l$  to  $M_u$ , and where  $P$  represents the total number of such points.

### B.3 Application Example

This section presents the application of the above DCGA optimization technique to the design of an FRM FIR lowpass digital filter for a passband bandwidth of  $0.4\pi$ . The remaining CSD FRM FIR lowpass digital filter frequency-response design specifications are shown as follows:

Passband region	$0 \leq \omega/2\pi \leq 0.2$	(B.11)
Stopband region	$0.205 \leq \omega/2\pi \leq 0.5$	
Maximum passband ripple	$\pm 0.1$ dB	
Minimum stopband attenuation	40 dB.	

The parameters necessary for the design of the desired FIR lowpass digital filter is summarized in Table B.1. Let us first apply Parks-McClellan optimization approach to the above parameters and design specifications and obtain an initial infinite-precision seed FRM FIR lowpass digital filter.

The magnitude frequency-responses associated with the band-edge shaping subfilter  $H_a(z)$  and the complementary subfilter  $H_b(z)$  are obtained as shown in Figs. B.2 and B.3, and those associated with their  $L$ -interpolated counterparts  $H_a(z^L)$  and  $H_b(z^L)$  (for  $L = 6$ ) are obtained as shown in Figs. B.4 and B.5, respectively. Moreover, the magnitude frequency-responses associated with the masking digital subfilters  $H_{ma}(z)$  and  $H_{mb}(z)$  are obtained as shown in Fig B.6 and Fig B.7. Finally, the magnitude frequency-response associated with the infinite-precision seed FRM FIR digital filter  $H_F(z)$  is obtained as shown in

TABLE B.1

Design Parameters for DCGA Optimization for FRM FIR Lowpass Digital Filter with a Passband Widths of  $0.4\pi$

Design Parameters
$L = 6, N_a = 84, N_{ma} = 24, N_{mb} = 42$
$p_M = 0.05, \beta = 100, M_u = -43dB, M_l = -60dB$
$\omega_p = 0.4\pi, \omega_s = 0.41\pi, k = 1.3/0.9, C = 30$

Fig. B.8. From the frequency-response shown in Fig. B.8, the resulting FIR lowpass digital filter exhibits a maximum passband ripple of 0.08 dB and a minimum stopband attenuation of 44.50 dB.

Let us consider the additional optimization parameters given in Table B.2 for DCGA optimization of the infinite-precision seed FRM FIR digital filter over the CSD multiplier coefficient space. Based on the infinite-precision multiplier coefficient values, the maximum and minimum possible values for the CSD multiplier coefficients can be chosen appropriately as 5.25 and  $-5.25$ , respectively. In this way, the required CSD LUT is formed as consisting of 12-bit binary indices (i.e. a set of 4096 CSD multiplier coefficient values) each having a wordlength of 17 bits.

TABLE B.2

Additional Design Parameters for DCGA Optimization for FRM FIR Lowpass Digital Filter with a Passband Widths of  $0.4\pi$

Design Parameters
$W = 17, W_l = 3, W_F = 14, B = 12$
$p_F = 0.8, N = 500$
$c = 0.6, \alpha = 0.225$

By quantizing the infinite-precision multiplier coefficient values to their nearest CSD counterparts in the LUT, the magnitude frequency-response of the resulting finite-precision FRM FIR seed lowpass digital filter is obtained as shown in Fig B.9. The resulting seed

lowpass digital filter clearly violates the magnitude frequency-response specifications by almost 0.8 dB in the passband region, and by almost 15 dB in the stopband region.

The application of the proposed DCGA technique results in a final CSD FRM FIR lowpass digital filter with a maximum passband ripple of 0.08 dB and a minimum stopband attenuation of 42.80 dB as shown in Fig B.10 (with its passband region characteristics enlarged and as shown in Fig B.11).

The convergence speed for the above DCGA optimization for various values of the shape coefficient parameter  $0.2 \leq c \leq 0.8$  for a fixed  $\alpha$ -value of 0.225 is as shown in Fig B.12, with a best convergence within 202 generations when  $c = 0.6$ . In Fig. B.13, the convergence speed is shown for various values of the exponent parameter  $0.3 \leq \alpha \leq 0.8$  for a fixed  $c$ -value of 0.6, leading to a best convergence within 204 generations when  $\alpha = 0.3$ .

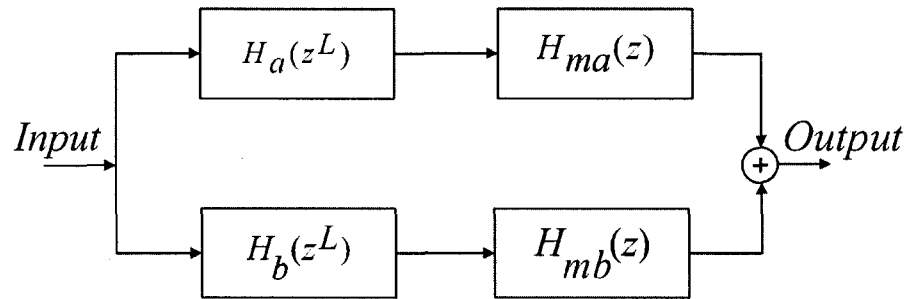


Fig. B.1. Realization of an FIR Lowpass Digital Filter using the FRM Approach

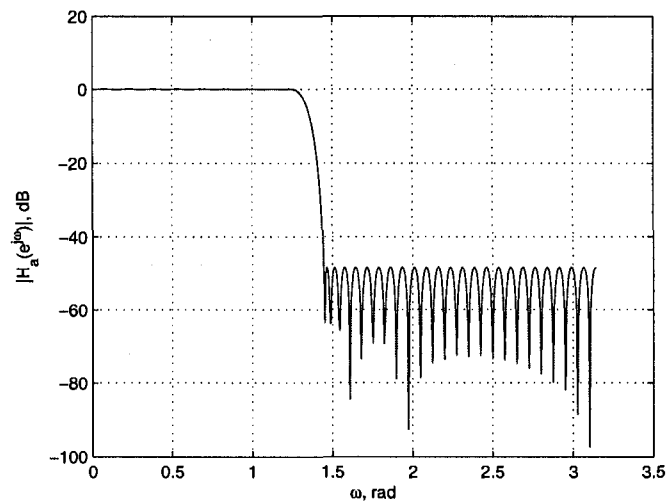


Fig. B.2. Magnitude Frequency-Response of the Bandedge-Shaping Digital Subfilter  $H_a(e^{j\omega})$

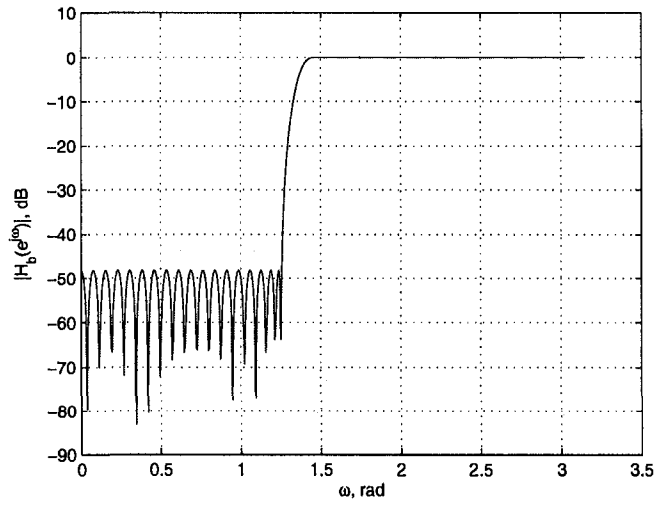


Fig. B.3. Magnitude Frequency-Response of the Complementary Bandedge-Shaping Digital Subfilter  $H_b(e^{j\omega})$

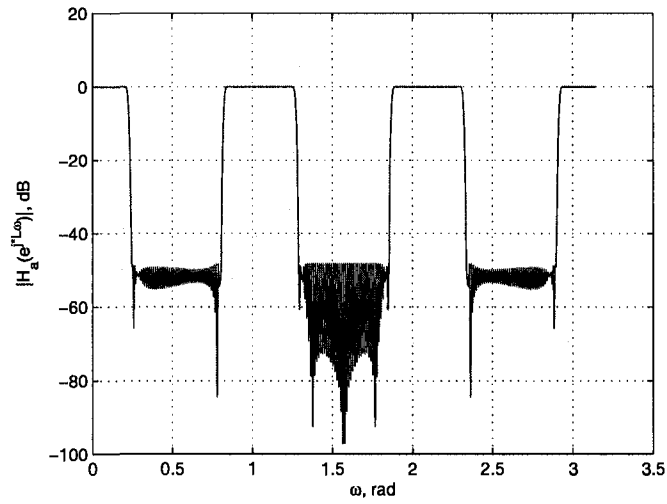


Fig. B.4. Magnitude Frequency-Response of  $L$ -Interpolated Bandedge-Shaping Digital Subfilter  $H_a(e^{jL\omega})$

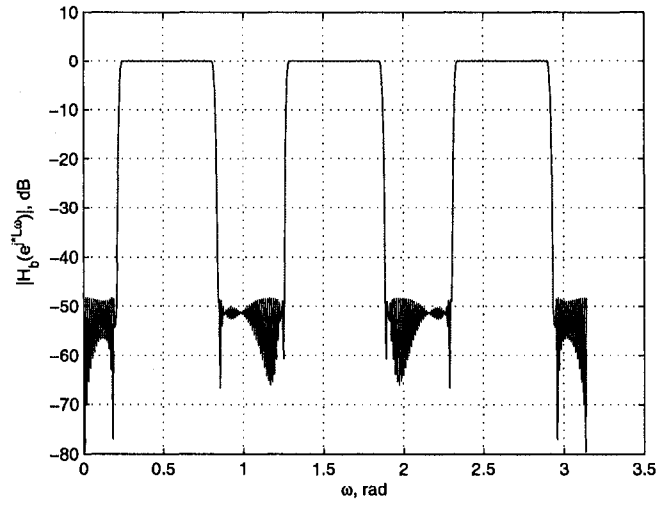


Fig. B.5. Magnitude Frequency-Response of  $L$ -Interpolated Complementary Bandedge-Shaping Digital Subfilter  $H_b(e^{jL\omega})$

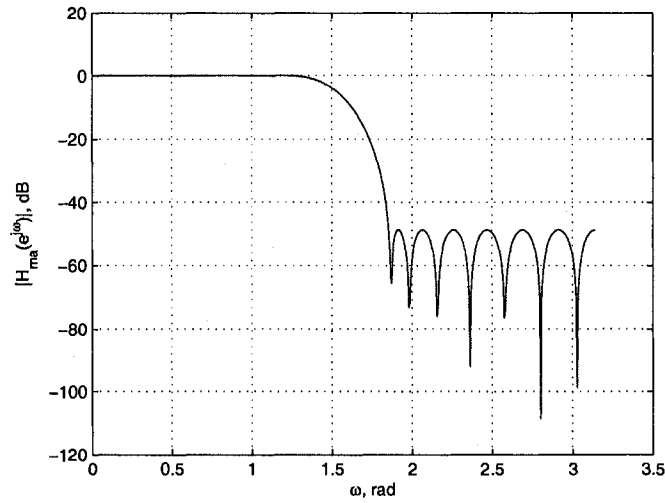


Fig. B.6. Magnitude Frequency-Response of Lowpass Masking Digital Subfilter  $H_{ma}(e^{j\omega})$

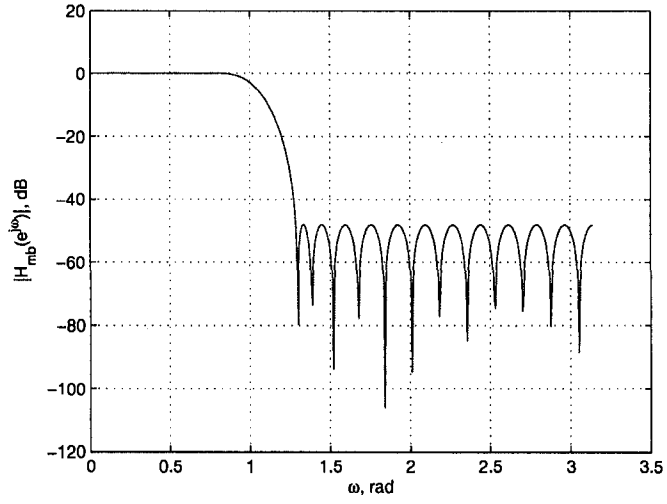


Fig. B.7. Magnitude Frequency-Response of Lowpass Masking Digital Subfilter  $H_{mb}(e^{j\omega})$

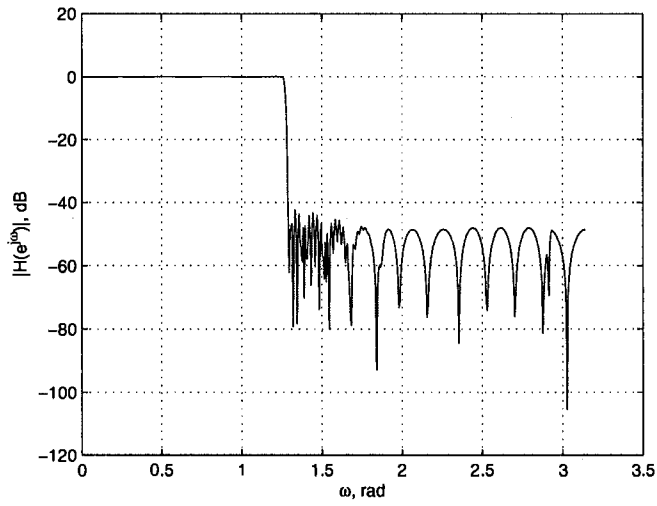


Fig. B.8. Magnitude Frequency-Response of Infinite-Precision FRM FIR Lowpass Digital Filter

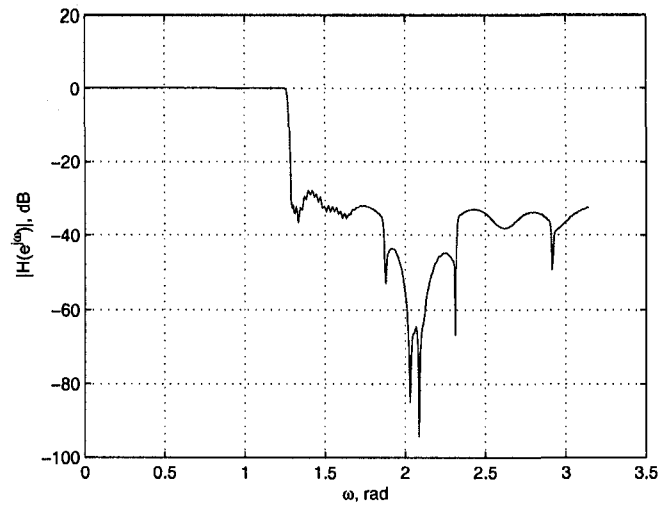


Fig. B.9. Magnitude Frequency-Response of FRM FIR Lowpass Digital Filter after Multiplier Coefficients Quantization

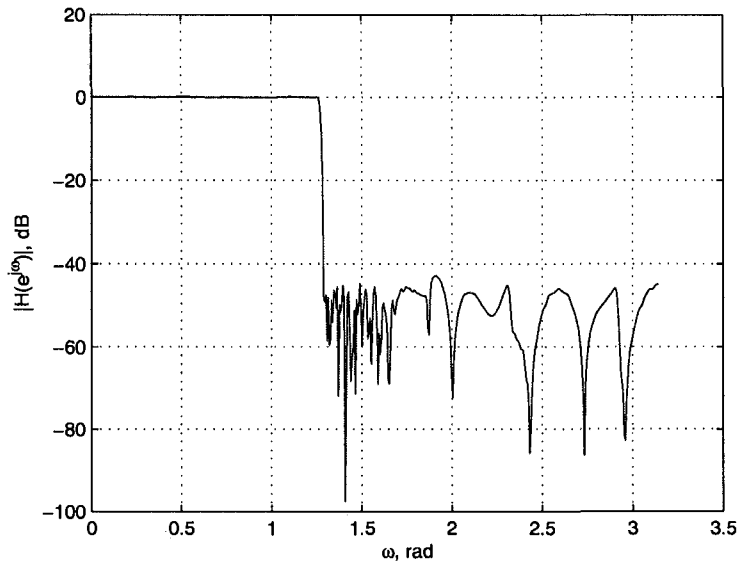


Fig. B.10. Magnitude Frequency-Response of CSD FRM FIR Lowpass Digital Filter after DCGA Optimization

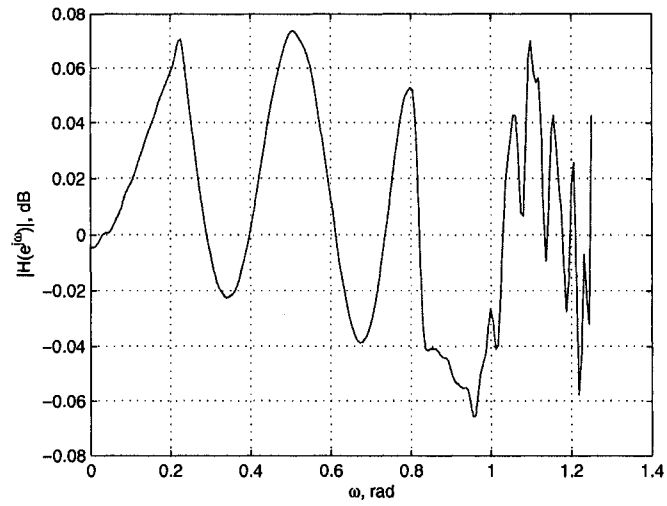


Fig. B.11. Passband Magnitude Frequency-Response of CSD FRM FIR Lowpass Digital Filter after DCGA Optimization

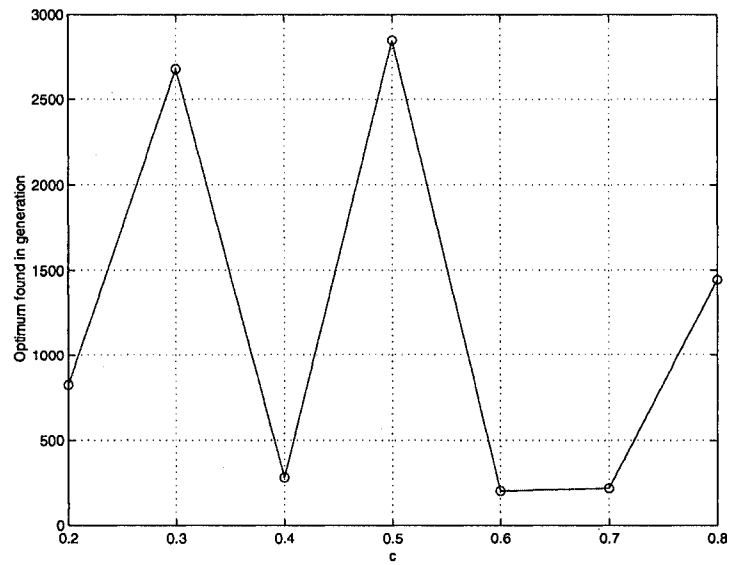


Fig. B.12. DCGA Convergence Speeds for FRM FIR Lowpass Digital Filter for Varying Values of the Shaping Parameter  $c$

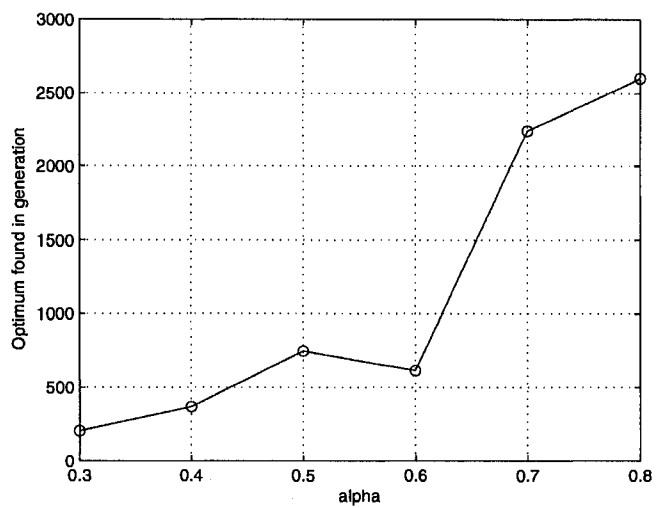


Fig. B.13. DCGA Convergence Speeds for FRM FIR Lowpass Digital Filter for Varying Values of the Exponent Parameter  $\alpha$

# Appendix C

## Generation of the Three LUTs

This appendix is concerned with the construction of the three LUTs for BIBO stable digital IF filter multiplier coefficients. First, let us recall that CSD multiplier coefficient  $\hat{m}_{ik_i}$  can be represented as:

$$\hat{m}_{ik_i} = \sum_{n=1}^W (D_{ik_i})_j 2^{R-j} \quad (\text{C.1})$$

where:

$$\sum_{k=1}^W |(D_{ik_i})_j| \leq w \quad (\text{C.2})$$

$$(D_{ik_i})_j \in \{1, -1, 0\} \quad (\text{C.3})$$

$$(D_{ik_i})_j \times (D_{ik_i})_{j+1} = 0 \quad (\text{C.4})$$

and where  $0 < R < W$  represents a floating radix-point, and  $w$  is the total number of nonzero bits within a wordlength of  $W$  bits.

In order to make the multiplier coefficients satisfy the CSD number system requirements, let us construct a single LUT  $L_0$  to enumerate all the possible combinations of bits representing  $\hat{m}_{ik_i} \in \text{CSD}(W, w)$ . The LUT  $L_0$  is of size  $n \times 2$ . The first column contains CSD numbers of wordlength  $W$  and the second column contains the decimal equivalent of the multiplier  $\hat{m}_{ik_i}$ .  $n$  is the total number of multipliers coefficients in  $\hat{m}_{ik_i} \in \text{CSD}(W, w)$ .

Based on  $L_0$ , the following steps summarize the generation of three LUTs required for BIBO stable digital IF filter:

- The first LUT  $L_1$  is constructed jointly for multiplier coefficients  $\hat{m}_{11}$  and  $\hat{m}_{12}$ . Recall that these multiplier coefficients must be positive and satisfy the following inequality:

$$\hat{m}_{11}\hat{m}_{12} + 2\hat{m}_{11} - 4 < 0 \quad (\text{C.5})$$

The dark area in Fig. C.1 shows the possible values of  $\hat{m}_{11}$  and  $\hat{m}_{12}$  where  $0 \leq \hat{m}_{12} < 32$ . In this example, all the discrete sets of CSD points in the marked area in Fig. C.1 need to be included in LUT  $L_1$ .

In accordance with the above discussion,  $L_1$  is of size  $n_1 \times 2$ , where the first column of  $L_1$  contains CSD numbers of wordlength  $W$  for multiplier coefficient  $\hat{m}_{11}$  and the second column contains CSD numbers of wordlength  $W$  for multiplier coefficient  $\hat{m}_{12}$ .  $n_1$  is the number of possible multiplier coefficient combinations that satisfy inequality constraint (C.5).

- The second LUT  $L_2$  is formed the same way as  $L_1$ , but with the inequality condition:

$$\hat{m}_{23}\hat{m}_{24} - 4 < 0 \quad (\text{C.6})$$

Same as  $L_1$ , it contains CSD numbers of wordlength  $2W$  for multiplier coefficient pairs  $\hat{m}_{23}$  and  $\hat{m}_{24}$  that satisfy the inequality (C.6).

- The third LUT  $L_3$  contains CSD numbers of wordlength  $W$  for single multiplier coefficient  $\hat{m}_{21}$ . It is almost identical to LUT  $L_0$ .

In this way, multiplier coefficient  $\hat{m}_{21}$  from LUT  $L_3$  and multiplier coefficients  $\hat{m}_{23}$  and  $\hat{m}_{24}$  from LUT  $L_2$  can be substituted into the following equation to obtain the value of the infinite-precision multiplier coefficient  $\tilde{m}_{22}$ :

$$\tilde{m}_{22} = -\varepsilon + \frac{4\hat{m}_{24}}{\hat{m}_{23}\hat{m}_{24} - 4} + \frac{4}{\hat{m}_{21}} - 2 \quad (\text{C.7})$$

where  $\varepsilon$  is a positive slack variable. This guarantees the satisfaction of the following constraint:

$$\tilde{m}_{22} + 2 - \frac{4}{\hat{m}_{21}} - \frac{4\hat{m}_{24}}{\hat{m}_{23}\hat{m}_{24} - 4} = -\varepsilon < 0 \quad (\text{C.8})$$

Finally,  $\hat{m}_{22}$  is determined by truncating the infinite-precision multiplier coefficient  $\tilde{m}_{22}$  to its nearest CSD counterpart in the LUT  $L_3$ .

In accordance with the above discussion, the three LUTs  $L_1$ ,  $L_2$ , and  $L_3$  are constructed and their indices can be subsequently used to represent the multiplier coefficients. This permits the multiplier coefficients to conform to the CSD number system, and the digital IF filter to be always BIBO stable.

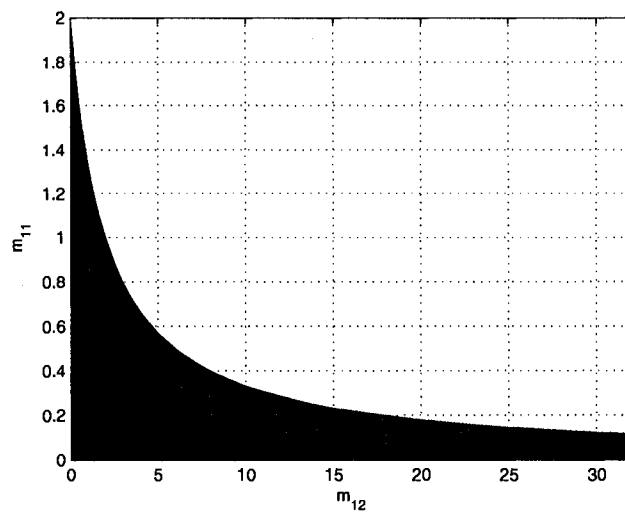


Fig. C.1. Example of Possible Values for Multipliers  $\hat{m}_{11}$  and  $\hat{m}_{12}$

## References

- [1] M. Murakawa *et al.*, “An AI-Calibrated IF Filter: A Yield Enhancement Method With Area and Power Dissipation Reduction,” *IEEE J. Solid-State Circuits*, vol. 38, no. 3, pp. 495–501, March. 2003.
- [2] T. Adachi, A. Ishikawa, and K. Tomioka, “A Low Noise Integrated AMPS IF Filter,” in *Proc. IEEE Custom Integrated Circuits Conf*, 1994, pp. 159–162.
- [3] S. Ichkawa, S. Mitobe, M. Koshino, and Y. Ebata, “A Low Loss CDMA-IF Filter Based on RSPUDT on LBO Substrate,” in *IEEE ULTRASONICS SYMPOSIUM*, October 1999.
- [4] “The wiki Website for Superheterodyne Receiver.” [Online]. Available: [wikipedia.org/wiki/Superheterodyne](http://wikipedia.org/wiki/Superheterodyne)
- [5] “The Qrpedia of Superheterodyne Receiver.” [Online]. Available: [cite-seer.ist.psu.edu/busetti01genetic.html](http://cite-seer.ist.psu.edu/busetti01genetic.html)
- [6] P. Nilsson and M. Torkelson, “A Custom Digital Intermediate Frequency Filter for the American Mobile Telephone System,” *IEEE J. Solid-State Circuits*, vol. 32, no. 6, pp. 806–815, June. 1997.
- [7] D. E. Goldberg, *Genetic Algorithms in Search, Optimizaito, and Maching Learning*. Reading, MA: Addison-Wesley, 1989.
- [8] S. Kilambi, B. Nowrouzian, and Y. Wu, “A Novel Diversity Controlled Genetic Algorithm for Rapid Optimization of Bandpass FRM FIR Digital Filters Over CSD Multi-

plier Coefficient Space,” *Journal of Circuits, Systems and Signal Processing (CSSP)*, Accepted for publish.

- [9] S. Kilambi and B. Nowrouzian, “A Diversity Controlled Genetic Algorithm for Optimization of FRM Digital Filters over DBNS Multiplier Coefficient Space,” in *IEEE International Symposium on Circuits and Systems (ISCAS’07)*, Lafayette, NO, May 2007, pp. 2331–2334.
- [10] H. Shimodaira, “A Diversity-Control-Oriented Genetic Algorithm (DCGA): Performance in Function Optimization,” *Proceedings of 2001 Congress on Evolutionary Computation*, vol. 1, pp. 44–51, May 2001.
- [11] Y. Wu and B. Nowrouzian, “A Novel Approach to the Design of BIBO Stable Digital IF Filters Over CSD Multiplier Coefficient Space Employing A Diversity Controlled Genetic Algorithm,” *Journal of Circuits, Systems and Signal Processing (CSSP)*, Submitted for review.
- [12] F. Buseti, “Genetic Algorithms Overview.” [Online]. Available: [cite-seer.ist.psu.edu/buseti01genetic.html](http://cite-seer.ist.psu.edu/buseti01genetic.html)
- [13] J. H. Yu and Y. Lian, “Design Equations for jointly Optimized Frequency-Response Masking Filters,” *Circuits Systems and Signal Processing*, vol. 26, no. 1, pp. 27–42, Jan. 2007.
- [14] Y. J. Yu and Y. C. Lim, “Genetic Algorithm Approach for the Optimization of Multiplierless Sub-filters Generated by the Frequency Response Masking Technique,” *IEEE International Conference on Electronics, Circuits and Systems*, vol. 3, pp. 1163–1166, 2002.
- [15] S. Kilambi, “Design and Optimization of FRM FIR Digital Filters using Genetic Algorithms over the CSD and DBNS Multiplier Coefficient Spaces,” Master’s thesis, University of Alberta, Alberta, Canada, 2007.

- [16] P. Mercier, S. Kilambi, and B. Nowrouzian, "Optimization of FRM FIR Digital Filters Over CSD and DBNS Multiplier Coefficient Spaces Employing a Novel Genetic Algorithm," *Journal of Computers*, vol. 2, no. 7, pp. 20-31, 2007.
- [17] M. Srinivas *et al.*, "Adaptive Probabilities of Crossover and Mutation in Genetic Algorithms," *IEEE Transactions on Systems, Man and Cybernetics*, vol. 24, no. 4, pp. 656-657, 1994.
- [18] L. Cen and Y. Lian, "Hybrid Genetic Algorithm for the Design of Modified Frequency-response Masking Filters in a Discrete Space," *Circuits Systems and Signal Processing*, vol. 25, no. 2, pp. 153-174, Apr. 2006.
- [19] Y. Wu and B. Nowrouzian, "Application of Diversity Controlled Genetic Algorithms to the Design and Optimization of OTA-C IF Filters," in *IEEE International Conference on Electronics, Circuits and Systems*, Marrakech, Morocco, December 2007.
- [20] W. Chen, *Passive, Active and Digital Filters*. Taylor and Francis Group, 2006.
- [21] J. E. Kardontchik, *Introduction to the Design of Transconductor Capacitor Filters*. Norwell, MA: Kluwer Academic Publishers, 1992.
- [22] F. Krummenacher and G. V. Ruymbeke, "Integrated Selectivity for Narrow-Band FM IF Systems," *IEEE J. Solid-State Circuits*, vol. 25, no. 3, pp. 757-760, June. 1990.
- [23] "The wiki Website for Routh-Hurwitz stability criterion." [Online]. Available: [http://en.wikipedia.org/wiki/Routh\\_Hurwitz\\_stability\\_criterion](http://en.wikipedia.org/wiki/Routh_Hurwitz_stability_criterion)
- [24] L. E. Turner, E. S. K. Liu, and L. T. Bruton, "Digital LDI Ladder Filter Design using the Bilinear Transform," in *IEEE International Symposium on Circuits and Systems*, vol. 3, May 1984, pp. 1017-1020.
- [25] A. I. Zverev, *Handbook of Filter Synthesis*. John Wiley and Sons, Inc., 1967.

- [26] Y. C. Lim, R. Yang, D. Li, and J. Song, "Signed Power-of-Two Term Allocation Scheme for the Design of Digital Filters," *IEEE Transactions on Circuits and Systems - Analog and Digital Signal Processing*, vol. II, pp. 577–584, May 1999.
- [27] A. T. G. Fuller, B. Nowrouzian, and F. Ashrafzadeh, "Optimization of FIR Digital Filters Over the Canonical Signed-Digit Coefficient Space Using Genetic Algorithms," *IEEE International Midwest Symposium on Circuits and Systems*, pp. 456–469, Aug. 1998.
- [28] B. Nowrouzian, N. Bartley, and L. Bruton, "Design and DSP-Chip Implementation of a Novel Bilinear-LDI Digital Jaumann Filter," *IEEE J. Circuits and Systems*, vol. 37, no. 6, pp. 695–706, June. 1990.
- [29] B. Green and L. Turner, "Digital LDI Ladder Filters Using Lattice Equivalent and Wave Concepts," *IEEE J. Circuits and Systems*, vol. 37, no. 1, pp. 133–135, January. 1990.
- [30] Y. Wu and B. Nowrouzian, "A Novel Technique for the Design and DCGA Optimization of Bilinear-LDI Lattice-Based Digital IF Filters," in *IEEE International Symposium on Circuits and Systems*, Seattle, USA, May 2008.
- [31] L. S. Lee, "Design Techniques for Bilinear-LDI Digital Allpass Networks," Master's thesis, University of Calgary, Calgary, Canada, 1988.
- [32] R. Hashemian, "A New Method for Conversion of a 2s Complement to Canonic Signed Digit Number System and Its Representation," in *Conf. on Signals, Systems and Computers*, Asilomar, USA, 1997, pp. 904–907.
- [33] A. Antoniou, *Digital Filters, Analysis, Design and Applications*. McGraw-Hill, Inc., 1993.
- [34] T. Sarmaki and A. T. Fam, "Subfilter Approach for Designing Efficient FIR Filters," *IEEE International Symposium on Circuits and Systems*, vol. 3, pp. 2903 – 2915, June 1998.

- [35] Y. C. Lim, "A Digital Filter Bank for Digital Audio Systems," *IEEE Transactions on Circuits and Systems*, vol. 33-8, pp. 848 – 849, 1986.
- [36] S. K. Mitra, *Digital Signal Processing - A Computer-Based Approach*. New York, NY: McGraw Hill, 2006.
- [37] O. Hermann, L. R. Rabiner, and D. S. K. Chan, "Practical Design Rules for Optimum Finite Impulse Response Lowpass Digital Filter," *Bell System Tech. J.*, vol. 52, pp. 769–799, 1981.
- [38] S. Kilambi, Y. Wu, and B. Nowrouzian, "Rapid Optimization Of FRM FIR Lowpass Digital Filters Over CSD Multiplier Coefficients Space Using A Diversity Controlled Genetic Algorithm," *Microelectronics Journal*, Submitted for review.
- [39] Y. C. Lim, "Frequency-Response Masking Approach for the Synthesis of Sharp Linear Phase Digital Filters," *IEEE Transactions on Circuits and Systems*, vol. CAS-33, pp. 357–364, 1986.